GSISH

Technische Universität München

ANNUAL REPORT
2012 / 2013

TUM Graduate School of Information Science in Health (GSISH)

http://gsish.tum.edu/

GSISH

Technische Universität München

ANNUAL REPORT
2012 / 2013

TUM Graduate School of Information Science in Health (GSISH)

http://gsish.tum.edu/

CONTENT

PROF. DR.-ING. ALOIS C. KNOLL

“By offering a tailor-made doctoral education, the GSISH´s vision is to educate a new generation of uniquely trained scientists.”

MESSAGE FROM THE DIRECTOR

Revolutionizing doctoral education is the very ambitious aim of the TUM Graduate School of Information Science in Health (GSISH). To attain this, GSISH has established a new concept for training doctoral candidates, who come from such diverse disciplines as computer science, engineering, physics or chemistry, and whose goal is to develop applications for the medical field.

GSISH’s central theme is that the school will provide as much guidance to the doctoral candidates as necessary – however, the main purpose is to provide challenging opportunities, which will aid and encourage them to develop their individual scientific profile. To meet this aim, the GSISH provides high level scientific and interdisciplinary skills training, international exchange, a large variety of transferable skills courses as well as social activities.

On behalf of all members of the GSISH, Axel Haase and I are pleased to present the GSISH Annual Report of 2013. The report gives an overview of the research activities of the international graduate school for the scientific year 2012/2013.

Alois C. Knoll
GSISH Director

PROF. DR. RER. NAT. AXEL HAASE

“A multidisciplinary and international setting can only be as good as the people involved.”

MESSAGE FROM THE CO-DIRECTOR

The world is changing, and so is edcuation. To realize our vision of uniquely trained scientists, who will be able to understand the scientific culture of other disciplines beside their own, coordinated efforts have been put into place. We have been looking for highly motivated doctoral candidates, who are willing to take the challenge of working interdisciplinary. The TUM Graduate School of Information Science in Health (GSISH) has profited greatly from the support of the TUM Executive Board of Management, the TUM Graduate School as well as the Deans of the Departments of Medicine and Computer Science.

The GSISH would not be where it is today without the generous support of the Bavarian State Ministry of Sciences, Research and the Arts; and it has also benefited significantly from other partners such as the General Electric Research Center Europe, or the Helmholtz Center Munich.

I would like to take the occasion to thank all those who contributed to the success of the school - our supporters, our cooperation partners, our national and international faculty, our management office and of course our doctoral candidates for their continuous input.

Axel Haase
GSISH Co-Director

REFLECTION ON THE PAST AND FUTURE OUTLOOK

REVOLUTIONIZING DOCTORAL EDUCATION

is the very ambitious aim of the TUM Graduate School of Information Science in Health (GSISH). Traditionally, doctoral candidates work with one professor for several years, during which time they contribute to the chair's scientific work and also teach, and in return, they are given the opportunity to write a doctoral thesis. This approach still works well within highly specialized disciplines. However, it does not meet the requirements of the GSISH, which aims to advance medical progress by information science and medicine. Here, we want to achieve an active, cross-discipline exchange.

To attain this, GSISH has established a new concept for training doctoral candidates, who come from such diverse disciplines as computer science, engineering, physics or chemistry, and whose goal is to develop applications for the medical field. GSISH's central theme is that the school will provide as much guidance to the doctoral candidates as necessary – however, the main purpose is to provide challenging opportunities, which will aid and encourage them to develop their individual scientific profile. To meet this aim, the GSISH provides high level scientific and interdisciplinary skills training, international exchange, a large variety of transferable skills courses as well as social activities.

GSISH organizes all doctoral candidates into interdisciplinary project groups. The groups' supervisors include both physicians and computer scientists, natural scientists or engineers, and this pool of diversified experts focuses on and solve problems from different perspectives. Together with the doctoral candidates they agree on a training schedule and on a thesis plan and the GSISH Management consults and supports them in doing so. Outstanding international researchers are invited to become members of the GSISH International Faculty. They visit the school on a regular basis and give lectures at our symposia or summer schools. They also serve as additional mentors for our doctoral candidates.

To realize our vision, coordinated efforts have been put into place. The GSISH has profited greatly from the support of the TUM Executive Board of Management, the TUM Graduate School as well as the Deans of the Departments of Medicine and Computer Science. The GSISH would not be where it is today without the generous support of the Bavarian State Ministry of Sciences, Research and the Arts; and it has also benefited significantly from other partners such as the General Electric Research Center Europe, or the Helmholtz Center Munich.

OUR MISSION: A NEW GENERATION OF EXPERTS

The importance of biomedical informatics and biomedical engineering for the healthcare sector has risen continuously during the last years. The fast scientific progress achieved in biomedical science has to be translated back to the medical field so that high quality and effective health care can be assured. In order to handle the massive complexity that on the one hand comes along with new possibilities of processing medical data and that on the other hand highly affects the clinical decision-making process, we need multidisciplinary collaboration of a broad spectrum of disciplines. We believe, that it is only through experts in information science that have a profound understanding of the biomedical disciplines' terminology and scientific culture, that true multidisciplinarity can arise and, at the end, progress in clinical applications can be achieved.

GSISH' mission is therefore to train a new generation of researchers, who have a profound background in information science but at the end will be both: experts in information science and the medical field. We believe that especially the information science related disciplines such as informatics or medical engineering will be the most important drivers and mediators for innovation in all health-related scientific disciplines. They are the ones, which embrace and support those fields, and also facilitate the pioneering of new services – with even more significant impact than previously witnessed in other areas such as the automotive industry, traffic control or global logistics.

To accomplish our ambitious goal, GSISH has developed a new approach and overall concept for education and research for doctoral candidates working on the interface of information science and healthcare thereby placing strong emphasis on the scientific training. For realizing our approach, GSISH can draw upon an innovative scientific community with a longstanding research tradition. As an interdisciplinary graduate school, we provide excellent opportunities for conducting doctoral research and qualify for the best jobs available, both in academia and university hospitals, and industry.

OUR PERSPECTIVES

GSISH has the long term objective of training new experts in information science in health both for the Technische Universität München and beyond. Inherently, GSISH is highly multidisciplinary, as defined by our four large research areas encompassing medicine, informatics, bioinformatics and system biology, engineering, physics and chemistry, as well as public health. Each of these disciplines has developed its own domestic culture and language, which can make communication difficult, and, which in the past, sometimes even restrained collaboration.

Within the last five years, GSISH has already made significant contributions to facilitate this much needed collaboration over disciplines. We have realized this due to our bottom-up approach: By setting up multidisciplinary research groups and assisting them with funding, structure, contacts, and other adequate means whenever it is needed, we successfully support different researchers from different cultures in working together on a continuous basis. While the scientific core of each discipline remains stable, this multidisciplinary environment provides a highly encouraging structure for permanent and compulsory exchange of people and ideas. This environment successfully enforces the networking of scientists, and, in a very natural way, also allows the integration of industry into the activities of the school at various levels of commitment.

The fact that at GSISH senior researchers and doctoral candidates are supported to work together across disciplines is already by today opening up new pathways for finding new solutions to old and new problems. While excelling in their "home disciplines", the members of the school serve as "boundary-breaking" agents to other research areas. In the future, they will deliver solutions to challenges in clinical applications and thus, on the long run, empower true innovation.

GSISH ENVIRONMENT

OUR APPROACH: A MULTIDISCIPLINARY ENVIRONMENT FOR EXCELLENT MEMBERS

A multidisciplinary and international setting can only be as good as are the people involved. The GSISH is very proud to lean on highly motivated pioneers, who are pursuing a multidisciplinary approach within their own research strategy and thus are the true drivers of GSISH. Most important to name are our two directors, Prof. Alois C. Knoll (Chair for Robotics and Embedded Systems, Department of Informatics) and Prof. Axel Haase (TUM Institute for Medical Engineering) who both believe that without multidisciplinary collaboration, innovation in the medical field will not be possible. The school is moreover strongly driven by the TUM Departments of Informatics and Medicine, which are represented by the Deans who are part of the GSISH Executive Board (Prof. Dr. Hans-Joachim Bungartz, Dean Informatics; Prof. Dr. Peter Henningsen, Dean Dean Medicine; Prof. Dr. Markus Schwaiger, former Dean Medicine). Heavily involved in driving the GSISH are also Prof. Klaus A. Kuhn (Further Representative Medicine), Prof. Tim Lüth (Representative Me-chanical Engineering) and Prof. Franz Pfeiffer (Department of Physics, Biomedical Physics). Further relevant partners include the Helmholtz Zentrum München (Prof. Dr. Werner Mewes, Representative Life Sciences and Prof. Dr. Vasilis Ntziachristos, Electrical Engineering and Information Technology), the TUM University Medical Center rechts der Isar, the German Heart Center Munich, selected researchers of the Ludwig-Maximilians-Universität München, as well as industry partners such as General Electric Global Research Europe.

STAFF & NETWORK

GSISH´s quality is defined by both our talented doctoral candidates and by our senior researcher. In particular, it is our Principal Investigators from informatics, medicine and science who lay the foundation for our multidisciplinary doctoral education.

The GSISH network consists of our Director and Co-Director, our Executive Board Members, GSISH Faculty and International Faculty, the GSISH Management Office and last but not least our Doctoral Candidates.

Executive Board

Prof. Dr.-Ing. Alois Knoll
Director
TUM, Informatics

Prof. Dr. rer. nat. Axel Haase
Co-Director
TUM, IMETUM

Prof. Dr. med. Peter Henningsen
Dean Medicine
TUM, Medicine

Prof. Dr. Hans-Joachim Bungartz
Dean Informatics
TUM, Informatics

Prof. Dr. med. Klaus A. Kuhn
Representative Medicine
TUM, Medicine

Prof. Dr. rer. nat. Tim C. Lüth
Representative Mechanical Engineering
TUM, MiMed

Prof. Dr. rer. nat. Hans-Werner Mewes
Representative Life Sciences
Helmholtz Zentrum München

Prof. Dr. rer. nat. Franz Pfeiffer
Representative Physics
TUM, Physics

Prof. Dr. med. Markus Schwaiger
Representative of outstanding interdisciplinary Research Projects
TUM, Medicine

Core Faculty

Prof. Dr. rer. nat Dr.-Ing. habil. Arndt Bode, TUM, Informatics
Prof. Dr. rer. nat. Dr. h.c. Manfred Broy, TUM, Informatics
Prof. Dr.-Ing. Darius Burschka, TUM, Informatics
Prof. Dr. oec. troph. Hannelore Daniel, TUM, Molecular Nutrition Unit
Prof. Dr. med. Hans Hauner, TUM, Nutritional Medicine / Else Kröner-Fresenius Center
Prof. Dr. med. Heinz Höfler, TUM, Medicine
Prof. Alfons Kemper, PhD, TUM, Informatics
Prof. Dr. med. Rüdiger Lange, TUM, Medicine / German Heart Center Munich (DHM)
Prof. Dr. rer. nat. Ernst Mayr, TUM, Informatics
Prof. Dr. med. Thomas Meitinger, TUM, Medicine / Helmholtz Zentrum München
Prof. Dr. Nassir Navab, TUM, Informatics
Prof. Dr. Vasilis Ntziachristos, TUM, Electrical Engineering and Information Technology / Helmholtz Zentrum
Prof. Dr. med. Christian Peschel, TUM, Medicine
Prof. Dr. med. Dr. h.c. Maximilian Reiser, LMU, Medicine
Prof. Dr. med. Dr. phil. Johannes Ring, TUM, Medicine
Prof. Dr. med. Ernst Rummeny, TUM, Medicine
Prof. Dr. med. Albert Schömig, TUM, Medicine
Prof. Dr. rer. nat. Dr. med. Heinz-Erich Wichmann, LMU, Epidemiology / Helmholtz Zentrum München

Faculty

Prof. Dr. med. Robert Bauernschmitt, Isarherzzentrum München
Prof. Dr. Bernd Brügge, TUM, Informatics
Prof. Dr. Claudia Eckert, TUM, Informatics / Fraunhofer Institution AISEC
Prof. Dr. med. Hubertus Feußner, TUM, Medicine
Prof. Dr. rer. nat. Brigitte Forster-Heinlein, TUM, Mathematics / Helmholtz Zemtrum München
Prof. Dr. rer. nat. Steffen Glaser, TUM, Chemistry
Prof. Dr. med. Reiner Gradinger, TUM, Medicine
Prof. Dr. med. Bernhard Hemmer, TUM, Medicine / Neuro-Kopf-Zentrum
Prof. Dr. med. Bernhard Holzmann, TUM, Medicine
Prof. Dr. rer. nat. Alexander Horsch, TUM, Medicine
Prof. Dr. med. Eberhard Friedrich Kochs, TUM, Medicine
Prof. Dr. med. Arthur Konnerth, TUM, Medicine
Prof. Dr. techn. Stefan Kramer, Johannes Gutenberg Universität Mainz, Informatics
Prof. Dr. Hans-Peter Kriegel, LMU, Informatics
Prof. Dr. Reiner Leidl, LMU, Economics / Helmholz Zentrum München
Prof. Dr. rer. nat. Ulrich Mansmann, LMU, Medicine
Prof. Dr. med. Alexander Meining, TUM, Medicine
Prof. Dr. med. Michael Molls, TUM, Medicine
Prof. Dr. rer. nat. Fridtjof Nüsslin, TUM, Biomedical Physics
Prof. Dr. med. Markus Ollert, TUM, Medicine
Prof. Dr. rer. nat. Burkhard Rost, TUM, Informatics
Prof. Dr. rer. nat. Johann Schlichter, TUM, Informatics
Prof. Dr. med. Roland M. Schmid, TUM, Medicine
Prof. Dr. med. Kurt Ulm, TUM, Medicine
Prof. Dr. oec. publ. Stefan Wagenpfeil, Universität des Saarlandes, Medicine
Prof. Dr. rer. nat. Sibylle Ziegler, TUM, Medicine
Prof. Dr. med. Claus Zimmer, TUM, Medicine / Neuro-Kopf-Zentrum

GSISH International Faculty

GSISH's Principle Investigators and faculty members are involved in numerous national and international collaborative research activities, as the research within the Graduate School addresses fundamental problems. This provides the basis for successful application of Information Science in the whole health care domain. Flourishing co-operations with a variety of academic and industry partners are already in place such as with Harvard, Cambridge, Johns Hopkins University, Vanderbilt University, Mount Sinai School of Medicine and many more.

Our current international faculty includes:

Basia Belza
Professor at the Departement of Biobehavioral Nursing and Health Systems
Adjunct Professor, Department of Health Services / School of Public Health and Community Medicine
The University of Washington, *USA*

Peter Elkin
Professor of Medicine
Mount Sinai School of Medicine / Center for Biomedical Informatics
New York, *USA*

Gregory D. Hager
Professor at the Department of Computer Science
Director of the Computational Interactions and Robotics Laboratory
Johns Hopkins University, Baltimore, *USA*

Kanako Harada
Project Assistant Professor
The University of Tokyo Global COE Program
Tokyo, *Japan*

Paul Harris
Research Associate Professor
Department of Biomedical Informatics
Vanderbilt University, Nashville, *USA*

Stanley M. Huff
Professor (Clinical)
Department of Biomedical Informatics
University of Utah, *USA*

Casimir A. Kulikowski
Professor of Computer Science
Department of Computer Science
Rutgers - The State University of New Jersey, *USA*

Blackford Middleton
Partners HealthCare
Harvard Medical School
Harvard School of Public Health, Boston, *USA*

Mamoru Mitsuishi
Professor at the Department of Engineering Synthesis
University of Tokyo, *Japan*

Shu Takagi
Professor at the Department of Mechanical Engineering
University of Tokyo, *Japan*

Russell H. Taylor
Professor at the Department of Computer Science / Whiting School of Engineering
The Johns Hopkins University / Director Engineering Research Center for Computer-Integrated Surgical Systems and Technology (CISST ERC), Baltimore, *USA*

Guang-Zhong Yang
Professor at the Institute of Biomedical Engineering
Imperial College London, *Great Britain*

GSISH Management

The management staff of GSISH supports the GSISH directors and the GSISH Executive Board in reaching decisions and implementing these into practice. Moreover, they support the GSISH faculty and doctoral candidates and coordinate the development of the school. They also consult GSISH faculty members in setting up new projects, which includes not only organizing the projects' review process but also recruiting new doctoral candidates. Another important part of their work is to consult the doctoral candidates in planning their doctoral work (including support on curriculum and finances).

They offer event organization (GSISH symposia, colloquia and social events) and editing of information material to trigger the public's understanding of science. Last but not least, they sustain the existence of the school, for instance by raising new funds from industry, foundations, or public funding agencies such as the BMBF or the DFG.

The management staff consists of two permanent staff members, Dr. Petra Dorfner (Managing Director) and Katharina Lang (Project Manager) and is continuously supported by student assistants and interns.

GSISH - FACTS & FIGURES

Within the scope of four research areas in October 2013, the school is supporting 40 Doctoral Candidates who are working with 54 professors:

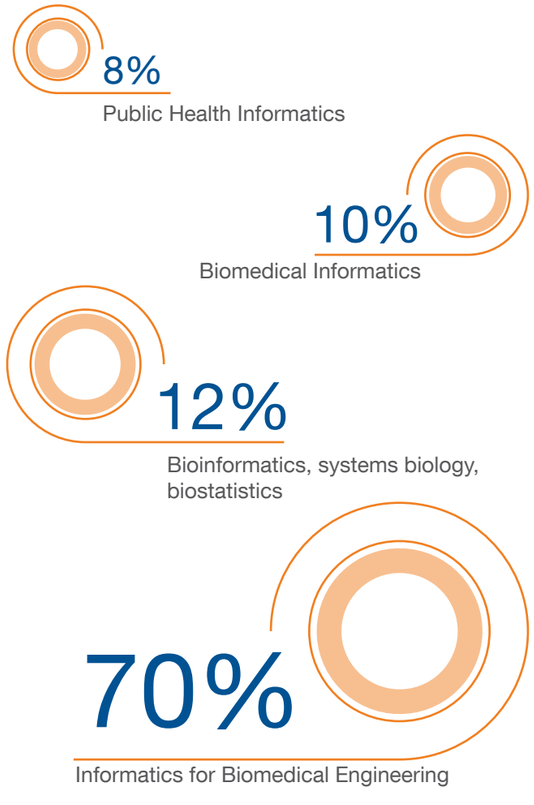

GSISH has from the very beginning on installed several measures to attract highly talented woman.

By October 2013 28% of all GSISH doctoral candidates were female, which is a highly satisfactory number, especially when compared to TUM female doctoral graduates in our core disciplines informatics (17 percent), engineering (13 percent) and physics (17 percent).*

*Based on TUM statistics on finished doctoral thesis in 2008/2009.

The age of GSISH doctoral candidates ranges from 25 to 43 years. By October 2013, most doctoral candidates were 30 years old.

GERMANY 23 (57%)

OTHERS 17 (43%)

GSISH Doctoral Candidates do not only work within multidisciplinary research groups, they themselves have a very diversified background with 40% of them coming from one of the 13 foreign countries represented in GSISH.

TUM GRADUATE SCHOOL

The TUM-GSISH is part of TUM Graduate School (TUM-GS), which is the umbrella organization that embraces all TUM graduate centers, set up by TUM´s 13 departments and interdisciplinary research centers. By being affiliated to the umbrella organization of TUM Graduate School, GSISH ensures its members the highest quality possible in doctoral education, as the entire diversity of TUM´s excellent scientific qualification program. Together with TUM-GS, GSISH provides high-level answers to the increasing complexity of research matters and today´s expectations of labor markets. The integration of GSISH into TUM Gradate School will, moreover, guarantee its long-term operation and its ongoing development.

Executive bodies of the TUM Graduate School include, among others, the Management Board, the Committee of Graduate Center Spokespersons or the Graduate Council. Most important for our doctoral candidates, the Graduate Council provides the doctoral candidates with a voice in deciding matters across the university campus. With the elected spokesperson, it obtains a seat in the TUM Senate, consequently representing the body of TUM doctoral candidates, and thus also GSISH doctoral candidates with their own identity.

DOCTORAL CANDIDATES´ PROJECTS

DENSE GENOTYPING OF SIX ATOPIC DERMATITIS AND 180 AUTOIMMUNE RISK LOCI IN 2,425 ATOPIC DERMATITIS PATIENTS

H. Baurecht (GSISH Member)
Technische Universität München / University Hospital Schleswig-Holstein

S. Weidinger* (Advisor), S. Wagenpfeil** (Co-Advisor)

* Department of Dermatology, Allergology and Venereology, University Hospital Schleswig-Holstein, Schittenhelmstr. 7, 24105 Kiel.
** Institut für Medizinische Biometrie, Epidemiologie und Medizinische Informatik, Universitätsklinikum des Saarlandes, 66421 Homburg.

Atopic dermatitis (AD) is a strongly genetic inflammatory skin disease characterized by skin barrier deficiency and immunoregulatory abnormalities. To better define susceptibility variants and to evaluate susceptibility loci previously implicated in immune-mediated diseases, we genotyped 2,425 German AD cases and 5,449 German population controls using the custom Immunochip array, followed by independent replication in a German, Japanese and Irish case control collection.

Testing 128,830 single nucleotide variants, we identified six loci newly associated with AD in Europeans (P<5×10-8), increasing the number of known susceptibility loci to eleven, which together account for approximately 14.4% of the estimated heritability of AD.

The strongest association was seen for a variant in the CLEC16A gene (rs2041733, P=1.34×10-14, OR=1.25) at 16p13.13. Our data provide evidence for a substantial contribution of immune-mediated disease loci in AD, which are shared with other immune-mediated diseases.

1 INTRODUCTION

Atopic dermatitis (AD) is a common inflammatory skin disease characterized by a strong hereditary basis and environmental factors which precipate susceptibility into manifestation. AD has an enormous morbidity with a lifetime prevalence of more than 20% and shows a remarkably high clinical heterogeneity. Integrated pathogenetic models consider both keratinocyte differentiation defects and immune alterations as scaffolds1. A total of six linkage studies for AD were conducted in the past, which identified several putative disease susceptibility regions. However, with the exception of the filaggrin (FLG) gene, which partly explains the linkage signal observed on chromosome 1q21.3, no disease gene could be unambitiously assigned to these regions so far. An emerging theme from genome-wide association studies (GWAS) is the remarkable overlap in genetic susceptibility identified across a range of chronic immune-mediated (IM) diseases. Two European-origin GWAS on AD have established a total of five additional susceptibility loci, all of which also confer risk to other immune-mediated diseases (e.g. Crohn's disease, asthma, and psoriasis). All these loci were confirmed in a recent Japanese GWAS, which in addition reported 8 new susceptibility loci. However, the causal variants at all loci apart from FLG are yet unknown. To better define susceptibility variants and to evaluate susceptibility loci previously implicated in other IM diseases, we performed a study on 2,425 German AD cases and 5,449 German population controls using the Immunochip array, followed by genotyping the most strongly associated SNPs with P<10-4 from each associated locus for replication analysis in two independent case-control collections.

2 MATERIALS AND METHODS

2,424 AD cases and 4,449 controls of German decent were genotyped on the Immunochip, a custom array designed for the Immunochip Consortium in order to finemap established GWAS loci for IM diseases. It covers 186 distinct IM risk loci and contains all European variants from the 1000 Genomes Project and SNPs from disease specific resequencing projects. After extensive and stringent data quality control, 128,830 SNPs were available for association testing. Second stage replication was carried out in a German cohort of 794 cases and 3,338 controls and followed by a third stage in a Irish cohort of 1,157 cases and 1,261 controls, a Japanese cohort of 2,397 cases and 7,937 controls and a Chinese cohort of 2,848 cases and 2,944 controls. Replication genotyping was carried out using Sequenom® iPlex or TaqMan® technology followed by stringent quality control for each population separately. Allele-based association tests were performed for each cohort and subsequently meta-analyzed using PLINK software. Heritability was estimated by the method described by So et al.2.

Chr	dbSNP id	Key genes	Discovery Immunochip (2,425/5,449) P	Discovery Immunochip (2,425/5,449) OR (95% CI)	Replication Germany (794/3,338) P	Replication Germany (794/3,338) OR (95% CI)	Immunochip+Replication (3,219/8,787) $P_{combined}$	Immunochip+Replication (3,219/8,787) OR (95% CI)
(a) Known AD loci on Immunochip* meeting genome-wide significance ($P_{combined} < 5\times10^{-8}$)								
1q21.3	rs72702813	*FLG*	4.51×10^{-22}	1.91(1.66-2.19)	1.90×10^{-16}	2.46(1.98 -3.04)	1.49×10^{-33}	2.06(1.83-2.31)
5q31.1	rs848	*IL13*	1.99×10^{-14}	1.36(1.25-1.47)	3.47×10^{-9}	1.46(1.29-1.65)	7.01×10^{-22}	1.39(1.30-1.48)
11q13.5	rs7110818	*C11orf30*	5.22×10^{-11}	1.25(1.17-1.34)	7.20×10^{-7}	1.35(1.20-1.53)	3.33×10^{-16}	1.28(1.21-1.36)
(b) Novel AD loci on Immunochip meeting genome-wide significance ($P_{combined} < 5\times10^{-8}$)								
2q12.1	rs759382	*SLC9A4*	1.40×10^{-6}	1.21(1.12-1.30)	1.23×10^{-5}	1.32(1.16-1.49)	1.49×10^{-10}	1.24(1.16-1.32)
4q27	rs17389644	*IL2/IL21*	1.16×10^{-6}	1.21(1.12-1.30)	5.72×10^{-4}	1.25(1.10-1.41)	2.95×10^{-9}	1.22(1.14-1.30)
11p13	rs12295535	*PRR5L*	2.71×10^{-7}	1.63(1.35-1.96)	3.55×10^{-6}	2.01(1.49-2.69)	1.12×10^{-11}	1.73(1.48-2.03)
16p13.13	rs2041733	*CLEC16A/DEXI*	1.00×10^{-11}	1.26(1.18-1.35)	2.64×10^{-4}	1.23(1.10-1.37)	1.34×10^{-14}	1.25(1.18-1.33)
17q21.32	rs16948048	*ZNF652*	6.46×10^{-5}	1.15(1.07-1.23)	6.03×10^{-5}	1.25(1.12-1.40)	3.37×10^{-8}	1.18(1.11-1.25)
20q13.33	rs909341	*TNFRSF6B*	7.73×10^{-10}	0.76(0.70-0.83)	6.70×10^{-3}	0.75(0.66-0.87)	2.50×10^{-11}	0.76(0.71-0.82)

Table 1: Susceptibility loci associated with AD at genome-wide significance level.

3 RESULTS

Of the five established European-origin AD susceptibility loci, three (1q21.3, 5q31.1 and 11q13.5) reached conservative genome-wide significance (GWS) with P<5×10-8 (Table 1, Figure 1). For the remaining established loci, we observed a significant association for 11q13.1 (P=3.60×10-6), but no association for 19p13.2, which was sparsely covered on the Immunochip. For the locus 2q12.1 of the recently reported Japanese loci we observed a significant association (P=1.49×10-10), which maps to a ~400 kb linkage disequilibrium block that encompasses four genes (IL1RL1, IL18R1, IL18RAP and SLC9A4). The IL1RL1 gene encodes a receptor for IL33, which promotes Th2-type immune response. Furthermore, we could confirm the Chinese-origin AD locus 20q13.33 at TNFRSF6B (P=2.50×10-13) with GWS as a new susceptibility locus for Europeans. The most significant association, not previously known for AD, was observed at 16p13.13 (CLEC16A; P=1.34×10-14). Several CLEC16A SNPs have been associated with autoimmune disorders such as multiple sclerosis and type 1 diabetes, as well as alopecia areata, a disease that is a frequent comorbidity of AD. At 11p13, a significant association was observed for a SNP in PRR5L (P=1.12×10-11). PRR5L encodes a protein that has been shown to promote apoptosis. Further significant associations were observed at 17q21.32 (ZNF652, P=3.37×10-8) and at 4q27 (IL2/IL21, P=2.95×10-9). ZNF652 has been described as suppressor of various epithelial cancers and IL2 has pleiotropic immunoregulatory functions and variants have been associated with multiple IM diseases. Except for rs17389644 (IL2/IL21) in the Japanese and rs759382 (SLC9A4) as well as rs16948048 (ZNF652) in the Irish, all identified loci (Table 1, Figure 1) replicated in these two studies.

4 DISCUSSION

In summary, our dense genotyping approach across loci associated with immune-mediated diseases AD identified six new AD risk loci in Europeans (SLC9A4/IL1RL1/IL18R1, IL2/IL21, PRR5L, CLEC16A, ZNF652 and TNFRSF6B) reaching genome-wide significance, bringing the number of known loci in Europeans to eleven. Our results not only expand the catalog of genetic loci implicated in AD susceptibility, but also provide evidence for a substantial contribution of loci shared with other immune-mediated and autoimmune diseases, which might represent common therapeutic targets. Together with established AD risk loci, the newly discovered loci meeting genome-wide significance collectively account for approximately 14.4% of AD heritability, indicating that further genetic studies, including fine mapping studies and searches for uncommon susceptibility variants are needed.

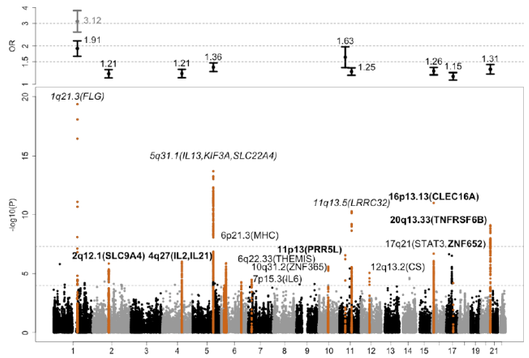

Figure 1: Manhattan plot and odds ratio + 95% confidence interval of the identified susceptibility loci.

5 REFERENCES

1 Bieber, T. Atopic dermatitis. N Engl J Med 358, 1483-94 (2008)..

2 So, H.C. & Sham, P.C. Multiple testing and power calculations in genetic association studies. Cold Spring Harb Protoc 2011, pdb top95 (2011).

3 Ellinghaus D., Baurecht H. & Esparza-Gordillo J.. et al. High-density genotyping study identifies four new susceptibility loci for atopic dermatitis. Nat Genet 45, 808-12 (2013).

AN ATOPY-ASSOCIATED VARIANT IN THE TH2 CYTOKINE LOCUS IMPACTS THE FUNCTION

A. Kleinschmidt (GSISH Stipend Holder)
Technische Universität München / University Hospital Schleswig-Holstein

S. Weidinger* (Advisor), S. Wagenpfeil** (Co-Advisor)

* Department of Dermatology, Allergology and Venereology, University Hospital Schleswig-Holstein, Schittenhelmstr. 7, 24105 Kiel.
** Institut für Medizinische Biometrie, Epidemiologie und Medizinische Informatik, Universitätsklinikum des Saarlandes, 66421 Homburg.

Type 2 immune responses directed by Th2 cells and characterized by the signature cytokines IL4, IL5 and IL13 play major pathogenic roles in atopic diseases.

Single nucleotide polymorphisms in the human Th2 cytokine locus and in particular variants in an intronic locus control region inside the DNA-repair gene RAD50, have been robustly associated with atopic traits in genome-wide association studies (GWAS).

This study aimed to characterize the functional impact of one common atopy associated polymorphism located in the human RAD50 gene on regulatory function. Using electrophoretic mobility shift assays, mass spectrometry (LC-MS/MS) comparisons and reporter gene assays we show that the variant impacts transcriptional activity and allele-specific binding of SMAD3, SP1 and other specific transcription factors.

1 INTRODUCTION

Atopic diseases (atopic dermatitis, asthma, rhinitis) are strongly heritable and closely related traits which are associated with Th2 mediated adaptive responses. One of the disease-specific susceptibility loci identified is 5q31, where the genes encoding the Th2 cytokines interleukin 4, 5 and 13 (IL4, IL5, IL13) are clustered with the constitutively expressed DNA repair gene *RAD50* (Fig. 1). Genome-wide association studies (GWAS) for asthma, total IgE, and atopic dermatitis identified signals from variants within the *RAD50* locus [1,2], although no functions have been described for the *RAD50* protein for the development of atopic diseases. Results from mouse models have shown the existence of a locus control region (LCR) which resides 3´ of Rad50, the core of which is constituted by four Rad50 hypersensitive sites (RHS4-7) [3]. This LCR coordinates the expression of the neighboring genes *Il4* and *Il13* in Th2 cells. The robust atopy-association of the human variant investigated here and its localization within the well described murine *cis*-acting regulatory element RHS7 prompted us to functionally investigate this variant.

2 MATERIALS AND METHODS

The prediction of gained or lost transcription factor binding sites at the here investigated variant was performed by using the Genomatix SNPInspector and MatInspector software. DNaseI hypersensitive sites and sequence similarity between species were analyzed by using the “ENCyclopedia of DNA Elements” (ENCODE) database and the UCSC Genome Browser. For the experimental identification of differential transcription factor binding due to the variant within RHS7 nuclear protein extracts were prepared from Jurkat- and HeLa cells and used in electrophoretic mobility shift assays (EMSA). Additional supershift EMSAs were performed by using specific antibodies for the candidate transcription factors.

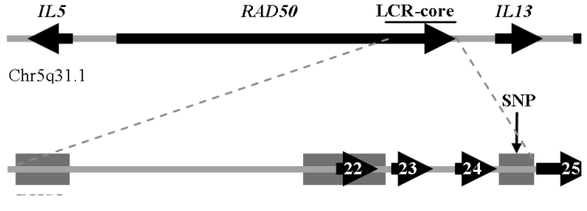

Figure 1: Schematic overview of the human Th2 cytokine locus and a zoom-in of the core of the LCR at the 3’ end of RAD50 containing the atopy-associated SNP within the RHS7.
Numbered arrows = exon with exon number, grey boxes = human conserved RHS sites.

To validate results obtained by EMSA mass spectrometry was applied. Proteins were purified by DNA-affinity. The obtained purified proteins were used in non-targeted liquid chromatography-mass spectrometry (LC-MS/MS). Spectra were searched against the Ensembl human database and relative quantification was performed. To identify variant-dependent changes in transcriptional activity plasmids for luciferase assays were constructed and tested in luciferase assays.

3 RESULTS

For the study the human Jurkat T cell line was used to investigate T cell specific effects at the Th2 cytokine locus. Additionally, HeLa epithelial cells were used, because T cell specific effects were not expected for this cell line.

The variant within RHS7 modulates binding of a protein complex containing SMAD3 and SP1

Protein-DNA interactions were investigated by EMSA. In Jurkat cells, but not in HeLa cells, the non-risk allele of the variant showed a higher affinity for one protein-DNA complex as compared to the risk allele. By supershift experiments and mass-spectrometry SP1, SMAD3 and further proteins were shown to be involved in the protein-DNA complex.

The risk allele of the variant influences human RHS7 regulatory function

After having shown that the variant affects the formation of a protein-DNA complex which includes SMAD3, SP1 and additional proteins, we next analyzed if this variant also modifies the transcriptional activity mediated by the SNP-surrounding RHS7 genomic sequence. Minimal promoter luciferase assays were carried out with different RHS7 constructs containing either the non-risk or the risk allele of the variant. In Jurkat cells, but not in HeLa cells, the risk allele led to increased transcription activity.

IL4 expression is increased when the risk-allele is present

Results of whole blood expression profile analysis of 740 German individuals from the KORA F4 population-based study analyzed on the Illumina HumanHT-12 v3 BeadChip, show increased IL4 expression levels for the risk allele genotype.

4 DISCUSSION

In summary, our study shows that RHS7 exerts a cell type specific regulatory function in humans, and demonstrates that the common allergy-associated variant has a regulatory function on transcriptional activity and alters binding of SMAD3 and SP1. In humans, SMAD3/4 mRNA expression levels are increased in the skin of healthy controls as compared to atopic dermatitis lesional skin. Further, Smad3-knockout mice express elevated levels of Il4, Il5, and Il13 and are susceptible to asthma [4]. The interaction of SMADs with a variety of SMAD-binding cofactors, e.g. SP1, is essential for high affinity and specificity of target gene regulation. Our results indicate that due to a loss of SMAD3 binding at the associated risk allele IL4 expression is elevated. This provides valuable insights into mechanisms contributing to the regulation of Th2 cytokine expression by identification of one causative variant.

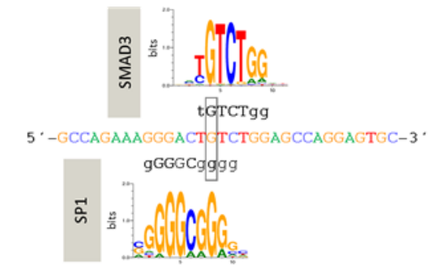

Figure 2: : Binding motifs for SMAD3 and SP1 at the variant (C-->T) are located inside the human RHS7. The reverse complementary DNA sequence containing the non-risk allele used for EMSA is depicted. Grey boxed nucleotides = variant-position.

5 ACKNOWLEDGEMENTS

The authors thank Nadine Lindemann and Viola Maag for technical support.

6 REFERENCES

[1] Moffatt MF, Gut IG, Demenais F, Strachan DP, Bouzigon E, Heath S, et al. A large-scale, consortium-based genomewide association study of asthma. N Engl J Med 2010;363(13):1211-1221.

[2] Weidinger S, Gieger C, Rodriguez E, Baurecht H, Mempel M, Klopp N, et al. Genome-wide scan on total serum IgE levels identifies FCER1A as novel susceptibility locus. PLoS Genet 2008;4(8):e1000166.

[3] Lee GR, Spilianakis CG, Flavell RA. Hypersensitive site 7 of the TH2 locus control region is essential for expressing TH2 cytokine genes and for long-range intrachromosomal interactions. Nat Immunol 2005;6(1):42-48.

[4] Anthoni M, Wang G, Leino MS, Lauerma AI, Alenius HT, Wolff HJ. Smad3 -signalling and Th2 cytokines in normal mouse airways and in a mouse model of asthma. Int J Biol Sci 2007;3(7):477-485.

from markerless optical surface imaging based on deformable mesh registration. Phys Med Biol 57(2) (2012).

[7] McClelland, J., et al.: Respiratory motion models: A review. Med Image Anal 17(1) (2013).

EFFICIENT REDUNDANCY REDUCED SUBGROUP DISCOVERY VIA QUADRATIC PROGRAMMING

R. Li (GSISH Stipend Holder)
Technische Universität München

R. Perneczky* (Co-Advisor), A. Drzezga** (Co-Advisor), S. Kramer*** (Advisor)

* Imperial College London, Faculty of Medicine, St Dunstant's Road, London, W6 8RP, UK.
** University of Cologne, Klinik und Poliklinik für Nuklearmedizin, Kerpener Straße 62, 50937 Köln.
*** University of Mainz, Institute of Computer Science, Staudingerweg 9, 55128 Mainz.

Subgroup discovery is a task at the intersection of predictive and descriptive induction, aiming at identifying subgroups that have the most unusual statistical (distributional) characteristics with respect to a property of interest.

Although a great deal of work has been devoted to the topic, one remaining problem concerns the redundancy of subgroup descriptions, which often effectively convey very similar information. In this study, we propose a quadratic programming based approach to reduce the amount of redundancy in the subgroup rules.

Experimental results on 12 datasets show that the resulting subgroups are in fact less redundant compared to standard methods. In addition, our experiments show that the computational costs are significantly lower than the costs of other methods compared in the work.

1 INTRODUCTION

The task of subgroup discovery (SD) is to find population subgroups described by conjunctions of attribute-value conditions that are statistically most interesting (e.g., large, but at the same time distributionally unusual) with respect to a property of interest. The motivation of this study is mainly two-fold: runtime is a critical issue when we cope with high-dimensional datasets. Conventional methods, like beam search and the optimistic estimate, may be computationally very expensive in such a case. Thus, we resort to an optimization technique to alleviate the hard combinatorial problem. Secondly, too many similar patterns would be too redundant and also laborious for end-users to comprehend. The proposed approach can identify correlated variables such that the resulting patterns can be less redundant but still be predictive.

2 MATERIALS AND METHODS

We propose a subgroup discovery via quadratic programming (SDVQP) approach [3]. This method effectively selects promising feature candidates for subgroup discovery. The feature interaction (mutual information) as well as individual feature importance can be taken into account at the same time. The formalized optimization problem can be solved efficiently as a quadratic programming approach. The compared methods are the beam search and a tight optimistic estimate (TOE), which are used to deal with subgroup discovery application. Beam search with beam width 5, 10 and 15 was tested.

The different methods are performed on a set of benchmark UCI datasets [1] as well as a real-world medical dataset (Alzheimer's disease, AD). The UCI datasets are commonly used as benchmark in data mining and machine learning community. The Alzheimer's disease dataset is provided by the psychiatry and nuclear medicine departments of TUM Klinikum rechts der Isar.

class	sex (female, male)	education (1, 2, 3, 4)	age	CDT	MMSE	APOE (23,24,33,34,44)
AD (23)	12, 11	9, 13, 1, 0	69	3.4	21	0,1,12,7,3
Non-AD(47)	26, 21	18, 25, 2, 2	67	2.1	26	5,1,16,22,3

Table 1: Description of Alzheimer's disease dataset.Education is divided into four categories, "Realschule": 1, "Hauptschule": 2, "Gymnasium": 3, "Hochschule": 4. APOE is of five types and their respective numbers are numerated in the third and fourth row. APOE, 23: APOE E2/E3, etc.

It comprises both imaging and non-imaging data. The imaging data is in the form of positron emission tomography (PET) scans, which reflects the metabolic activity of the human brain and is an established biomarker of AD. We build on the data by Schmidt et al. [2] to evaluate our and competing methods. On the other hand, the non-imaging data consist of demographic (e.g., gender, education, age) and clinical data. The clinical variables encompass two different psychometric tests, which are routinely used to assess a patient's overall cognitive performance, including the Clock Drawing Test (CDT), Mini-Mental State Examination (MMSE). In addition, the main AD genetic risk factor APOE is also considered in the work.

3 RESULTS

We briefly show the runtime, accuracy (acc) and cover redundancy (CR) on the benchmark UCI datasets. Then some selected rules are shown to present the interesting rules discovered by the proposed SDVQP using AD dataset.

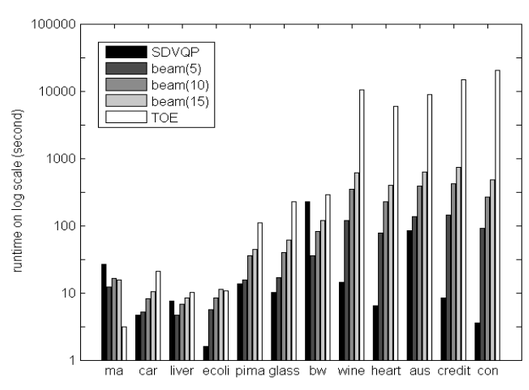

Figure 1: Runtime comparison on 12 UCI datasets.

		b5	b10	b15	TOE
acc	win	4	4	4	5
	tie	8	7	7	7
	loss	0	1	1	0
CR	win	11	11	11	11
	tie	1	1	1	1
	loss	0	0	0	0

Table 2: Results summary of the comparison of SDVQP versus compared methods of 12 UCI datasets. Times of win, tie and loss.

Rule 1: IF MMSE <= 25 THEN AD

Rule 2: IF MMSE <= 25 AND APOE = E3/E3 THEN AD

Rule 3: IF CDT = 5 THEN AD

Rule 4: IF APOE =E3/E3 THEN AD

Rule 5: IF MMSE > 25 THEN non-AD

Rule 6: IF CDT = 1 THEN non-AD

Table 3: Selected subgroup descriptions (rules) using SDVQP on AD dataset.

4 CONCLUSIONS

The study presented a subgroup discovery approach based on quadratic programming, aiming at reduced redundancy and improved computational efficiency. Instead of evaluating the subgroups individually, we utilize the mutual information matrix to explore the interaction between attributes. As a result, the degree of redundancy is reduced, which in turn avoids overfitting and thus makes classification more reliable, if used also in a predictive setting. Last, but not least, the proposed method runs much faster than other methods compared in this paper, which is a crucial factor when applied to high dimensional data. As such, it offers an interesting alternative to beam search and the optimistic estimates, which have difficulty already on data of medium dimensionality. However, it should be kept in mind that the focus of this study was just on redundancy, computational efficiency, predictive power and rule complexity, whereas subgroups can be evaluated also along other dimensions.

5 ACKNOWLEDGEMENTS

The first author acknowledges the support of the TUM-Graduate School of Information Science in Health (GSISH), Technical University of Munich.

6 REFERENCES

[1] Frank, A., Asuncion, A.: UCI machine learning repository (2010). URL http://archive.ics.uci.edu/ml

[2] Schmidt, J., Hapfelmeier, A., Müller,M., Perneczky, R., Drzezga, A., Kurz, A., Kramer, S.: Interpreting pet scans by structured patient data: A data mining case study in dementia research. Journal of Knowledge and Information Systems (KAIS) 24, 149–170 (2010)

[3] Li, R and Kramer.: Efficient Redundancy Reduced Subgroup Discovery via Quadratic Programming, The 15th International Conference on Discovery Science, pp. 125–138, Lyon, France, Springer-Verlag. Lecture Notes in Artificial Intelligence (LNAI).

ENVIRONMENTAL PRESSURE IMPRINTED UPON GENOMES THROUGH PROTEIN DISORDER

E. Vicedo (GSISH Member)
Technische Universität München

B. Rost* (Advisor), J. Buchner** (Co-Advisor), B. Müller-Myhsok*** (Co-Advisor)

* TUM Department of Informatics, Bioinformatics & Computational Biology - i12, Boltzmannstr. 3, 85748 Garching.
** Technische Universität München, Department of Chemistry, Lichtenbergstr. 4, 85747 Garching.
*** Max-Planck Institute of Psychiatry, Statistical Genetics, Kraepelinstr. 2-10, 80804 München.

Many prokaryotic organisms have adapted to incredibly extreme habitats. Such extremophiles change their genome with respect to their non-extremophile relatives in order to survive. Some proteins in high-temperature surviving thermophiles increase their heat-resistance by becoming more compact than their homologs in other species. Conversely, some proteins have increased volumes to compensate for freezing effects in psychrophiles that survive in cold climates.

We ran various prediction methods on 46 entirely sequenced genomes representing organisms from diverse habitats and found a correlation between protein disorder and the extremity of the environment. In fact, the overall percentage of proteins with long disordered regions was more similar between organisms of similar habitats than between organisms of similar taxonomy. More generally, our finding that a microscopic feature as coarse-grained as the overall content in proteins with disordered regions correlates with such a complex macroscopic variable such as the environment remains surprising and will have to be investigated through future case-by-case studies of the underlying molecular mechanisms.

1 INTRODUCTION

Here, we zoom into protein disorder abundance across prokaryotes. Specifically, our first question was whether the abundance of protein disorder is associated with organism habitat, or alternatively, with taxonomic distance. For example, is a halophilic bacterium more similar in its disorder level to a mesophilic bacterium or to a halophilic archaean? The second question ultimately aims at finding the "origins" of disorder abundance. In particular, do these differences arise from the use of organism-specific proteins that are disordered? We ran disordered predictions methods on about 46 different proteomes representing organisms from a variety of animal kingdoms (archaea and bacteria) and that thrive in different habitats.

2 MATERIALS AND METHODS

The UniProt database [1] provided the complete proteome sequence data at the base of our study. We removed all duplicates always giving priority to longer proteins. We applied no other filtering step. Our analysis considered 46 organisms (from extreme habitats, their closest relatives and model Eukaryotes) with a total of 225.550 proteins annotated.

We used prediction methods that were developed based on different concepts and capture different "flavors" of protein disorder [2] IUPred uses pairwise statistical potentials of residue contacts [3] MD (Meta-Disorder) [4] and NORSnet [5] are neural network-based methods that use evolutionary information and other predicted features. MD combines several original prediction methods including NORSnet, with the evolutionary profiles and sequence features that correlate with the protein disorder such as predicted solvent accessibility and protein flexibility. NORSnet is focused on the identification of long disordered loops (no regular secondary structure); it is optimized without using any experimental data on disorder.

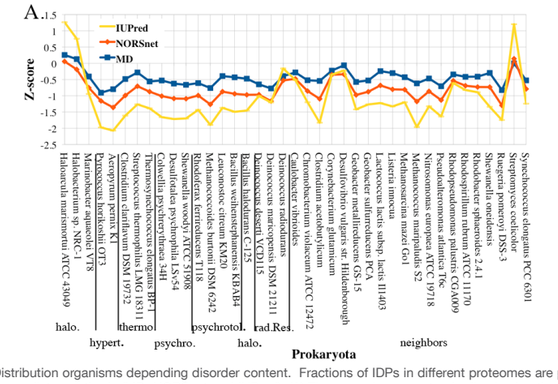

Figure 1: Distribution organisms depending disorder content. Fractions of IDPs in different proteomes are predicted by three disorder predictor methods (MD, NORSnet and IUPred). (A) The raw values are standardized using the Z-score and the mean and standard deviation (sd) obtained from a population of 1910 prokaryotes calculated for the three predictor methods.

In order to identify phylogenetic relations, e.g. proteins as homologues between the thermophile Pyrococcus horikoshii OT3 and the model organism for the study of life in permanently cold environments Colwellia psychrerythraea 34H, we applied the following ad hoc procedure: We ran all protein sequences from one organism against all from the other using BLAST. Subsequently, for each alignment we calculated the HSSP-value (HVAL) [5], which measures sequence similarity by combining alignment length and percentage pairwise sequence identity. For instance, HVAL=0 corresponds to about 22% pairwise sequence identity for alignments over 250 residues. As a result of our procedure, proteins can have multiple homologues. Due to technical concerns, we did not distinguish between paralogs and orthologs.

3 RESULTS

Halophiles higher protein disorder than taxonomic relatives. Halophiles thrive in hostile salt-saturated habitats. The percentages of proteins predicted with long disorder in the two halophile archaea Halobacterium sp. NRC-1 and Haloarcula marismortui ATCC 43049 both reached levels around 20-23% (>30 consecutive residues by MD and IUPred, Z-score [0.1, 1.2], Fig. 1). This was much higher than the values for their closest taxonomic relatives Methanococcus maripaludis S2 (2-11%, Z-score [-0.6, -0.8], Fig 1) that do not survive in high salt.

Protein disorder may proportion an optimal tool for the freeze. Colwellia psychrerythraea 34H is considered as a marine psychrophile obligate bacterium, i.e. it needs very low temperatures (-1°C-10°C) to grow; it can support high pressures in the deep sea. Its predicted disorder ranged from 3-12% (Z-score [-0.5, -0.6], Fig. 2B). Leuconostoc citreum KM20 is considered to be a psychrotolerant antimicrobial producer (used for fermentation of kimchi). However, it can also be cultivated at significantly higher temperatures (optimal growth at 30°C). The predicted disorder ranged from 5-14% (Z-score [-0.4, -0.5], Fig. 1).

Corresponding homologues confirm whole-proteome results. We calculated disorder abundance in organism specific and homologues of two model organisms representing two extreme temperature environments, using various cutoffs to define "homologues proteins". Overall, it seems likely that the difference of disorder across these two species mainly originated from homologous proteins that kept their overall shape with some modifications to adapt to extreme climates.

4 CONCLUSIONS

We found that the levels of protein disorder appeared to depend on the environment more than on the evolutionary relation. This suggests that disordered regions can assist in the adaption to diverse habitats. Furthermore, we show that the differences in the disorder abundance among organisms from different habitats are independent of their corresponding taxonomic branch. Finally, we found also how related are the habitat factors such as temperature, pH, oxygen requirements to the protein disorder. Clearly, protein disorder is an important building block of evolution, and clearly the story that remains yet to be understood is much more complex that we have suspected so far.

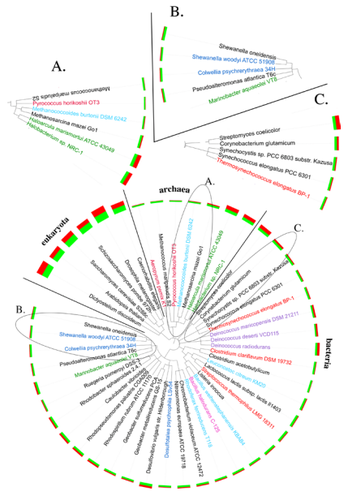

Figure 2: Protein disorder is linked to habitat. Fractions of IDPs in different proteomes are predicted by two disorder predictor methods (MD, IUPred). Variability in disorder abundance also appears within kingdoms and extreme organisms groups. In general we can mark that there are more differences in IDPs content for the different extreme groups than to the taxonomic distance of their genomes. (A) Hyperthermophile (dark red), archaeas are more ordered than their neighbors and the opposite for the salt living organisms (green). (B) The bacteria halophile contains also more disordered proteins as its mesophile relatives the same for the psychrophile (blue) relative. (C) The bacterial thermophile (red) presents also less disorder protein content than its relatives.

5 ACKNOWLEDGEMENTS

Thanks to Tim Karl and Laszlo Kajan (TUM) for invaluable help with hardware and software; to Christian Schaefner and Arthur Dong for helpful comments on the manuscript. This work was supported by a grant from the Alexander von Humboldt foundation through the German Ministry for Research and Education (BMBF: Bundesministerium für Bildung und Forschung).

6 REFERENCES

[1] Consortium, T.U. (2011) Reorganizing the protein space at the Universal Protein Resource (UniProt), Nucleic Acids Res, 40, D71-75.

[2] Schlessinger, A., Liu, J. and Rost, B. (2007) Natively unstructured loops differ from other loops, PLoS Comput Biol, 3, e140.

[3] Dosztanyi, Z., Csizmok, V., Tompa, P. and Simon, I. (2005) IUPred: web server for the prediction of intrinsically unstructured regions of proteins based on estimated energy content, Bioinformatics, 21, 3433-3434

[4] Schlessinger, A., Punta, M., Yachdav, G., Kajan, L. and Rost, B. (2009) Improved disorder prediction by combination of orthogonal approaches, PLoS One, 4, e4433.

[5] Sander, C. and Schneider, R. (1991) Database of homology-derived protein structures and the structural meaning of sequence alignment, Proteins, 9, 56-68.

HEMATOPOIETIC STEM CELLS AND THEIR MICRO-ENVIRONMENT

B. Vilne (GSISH Stipend Holder)
Technische Universität München / Deutsches Herzzentrum München

H.-W. Mewes* (Advisor), C. Peschel** (Co-Advisor)

* Technische Universität München, Lehrstuhl für Genomorientierte Bioinformatik, Maximus-von-Imhof-Forum 3, 85354 Freising.
** Technische Universität München, Klinikum rechts der Isar, Ismaninger Str. 22, 81675 München.

Hematopoietic stem cell (HSC) fate decisions (self-renewal vs. differentiation) are thought to be regulated by extracellular cues from the ‚niche', however, precise regulatory networks have remained largely elusive.

Here, time-course gene expression analysis of co-cultured Lin-Sca1+cKit+ (LSK) and HSC-supportive UG26-1B6 stromal cells and candidate gene prioritization followed by dynamic network analysis using Boolean logic identified Connective tissue growth factor (Ctgf) as a putative regulator of HSC cell cycle progression through the AKT/GSK3-ß pathway.

Experimental validation using Ctgf defficient UG26-1B6 showed higher percentage of progenitors, accompanied with decreased engraftment potential in peripheral blood, 16 wks after transplantation. In line with the prediction, a decrease in Cyclin D1 protein, p21Cip1 and Ctgf mRNA and protein, as well as an increase in p27Kip1 protein levels could be observed.

We could also confirm diminished phospho-Gsk3-ß (Ser9), whereas its target, ß-catenin phosphorylated at Ser33/Ser37/Thr41, was more abundant.

1 INTRODUCTION

Efforts to examine the interactions between HSCs and their micro-environmental cells have led to the generation of in vitro culture systems. We have previously established two midgestation-derived stromal clones--UG26-1B6 (urogenital ridge-derived) and EL08-1D2 (embryonic liver-derived), which are able to preserve the maintenance of repopulating HSCs (Oostendorp et al 2002). In this study, we combine experimental and computational analyses in order to explore the two-way cell-cell communication of LSK and UG26-1B6 stromal cells within a co-culture and identify Connective tissue growth factor (Ctgf) as a putative novel regulator of hematopoiesis.

2 MATERIALS AND METHODS

UG26-1B6 stromal cell and hematopoietic stem cell co-cultures. The stromal cell line UG26-1B6 was cultured as described in (Oostendorp et al 2002). Stable knockdown for Ctgf were made using lentiviral shRNAmir (Open Biosystems, USA). As a control, stromal cells transformed with empty (pLKO.1) vector were used. Bone marrow (BM) cells were depleted of lineage-positive cells using the Lineage Cell Depletion Kit (Miltenyi Biotec, Germany) according to manufacturer's instructions. Lin- were then used to set up a 1 week co-culture or further purified by flow cytometry to obtain Lin-Sca-1+c-Kit+ cells (LSKs). UG26-1B6 were grown to confluence and irradiated (30 Gy) prior to seeding with hematopoietic cells.

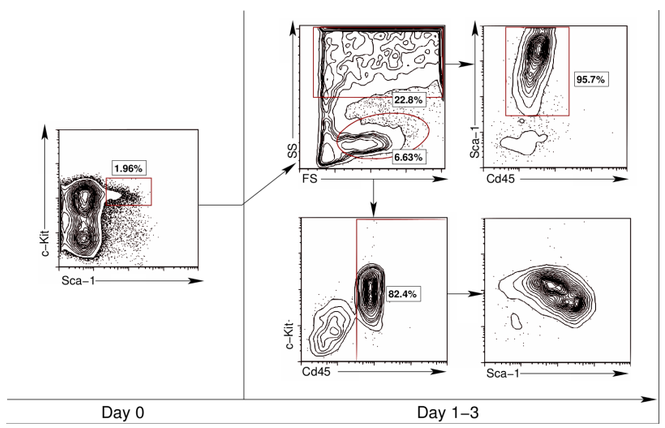

Figure 1: FACS gating strategy demonstrating the selection of LSK cells on Day 0 and the separation of co-culture into Cd45+LSK cells and Cd45-Sca1+ stromal cells on Day1, 2 and 3.

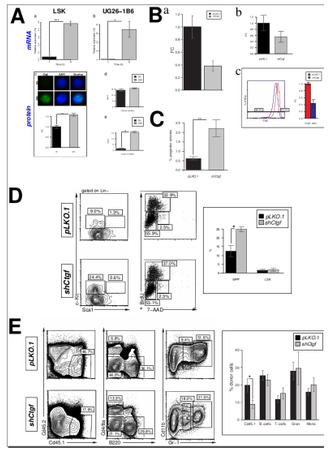

Figure 2: Connective tissue growth factor (Ctgf) is a putative novel regulator of hematopoiesis.

Ctgf network construction and analysis. Literature mining using EXCERBT The text-mining system EXCERBT http://mips.helmholtz-muenchen.de/excerbt/ (Barnickel et al , 2009) was used for automated extraction and inference of relations between entities of interest such as protein-protein interactions or regulatory interrelations i.e.,"CTGF enhanced the expression of cyclin D1" --> "CTGF" + "activates" + "Cyclin D1". Co-occurrence search was employed in order to retrieve as much associations as possible. Thereafter, false positives were discarded by manual curation. Thereafter, a Boolean model of Ctgf signaling network was defined and analyzed using the R/BoolNet package htto://cran.rproject.org/web/packages/BoolNet/.

3 RESULTS

To gain insight on the reciprocal influence of HSCs and their ‚niche' cells and to study the integration of molecular players during initial activation events, we performed time-course gene expression analysis, in which sorted Lin-Sca1+c-Kit+ (LSK, stem cells) were co-cultured together with HSC-supportive UG26-1B6 stromal cells (as previously described by (Oostendorp et al 2002) (Fig. 1).

Well-known regulators of hematopoiesis were used to prioritize genes differentially expressed after the co-culture. Connective tissue growth factor (Ctgf), one of the genes induced in both cells, was among the highest ranked genes and was selected for further experimental studies. Phenotypic and functional assays using siCtgf UG26-1B6 demonstrated that a decrease of microenvironmental Ctgf promotes hematopoietic progenitor activity in vitro, leading to exhaustion of the long-term stem cell pool in vivo (Fig. 2).

To elucidate possible underlying mechanisms, we constructed a literature-based Boolean network connecting Ctgf to the HSC cell cycle progression (Fig. 3), which was then validated experimentally. In line with the prediction, a decrease in Cyclin D1, p21Cip1 and Ctgf , as well as an increase in p27Kip1 protein levels could be observed. We could also confirm diminished phospho-Gsk3- b (Ser9) and phospho-Akt.

4 DISCUSSION OR CONCLUSIONS

Hematopoietic stem cells (HSC) are present in activated and dormant states which differ in their cell cycle status which is thought to be precisely coordinated by a specific combination of ‚niche' signals. In the present study, we sought to study the genome-wide changes in gene expression during the initial activation events of HSC in culture, under conditions that we have previously shown to maintain stem cell activity (Oostendorp et. al. 2002, Oostendorp et. al. 2005). For this purpose, we co-cultured Lin-Sca1+cKit+ (LSK) and HSC-supportive UG26-1B6 stromal cells and studied changes in their gene expression patterns in a dynamic fashion (Fig. 1).

We here show that Ctgf is a novel regulator of normal HSC quality (Fig. 2), since microenvironmental loss of Ctgf contributed to increased hematopoietic progenitor activity in vitro (C,D) and dicreased overall engraftment potential in vivo (E), suggesting that Ctgf is required for maintenance of HSC quality.

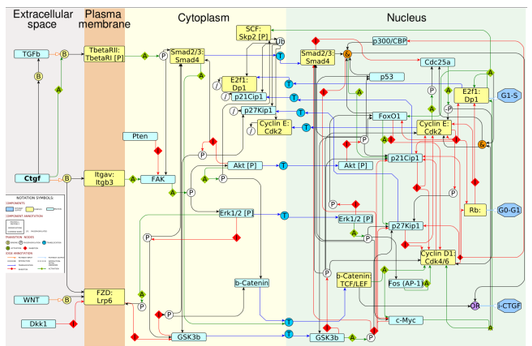

Figure 3: The graphical network map depicting Ctgf regulated G0-to-G1 transition, G1/S block, as well as its auto-induction derived from published data using the modified Edinburgh Pathway Notation (mEPN) scheme http://www.mepn-pathway.org/.

5 ACKNOWLEDGEMENTS

This project was kindly supported by the TUM Graduate School of Information Science in Health (GSISH) .

6 REFERENCES

[1] Oostendorp RAJ, Harvey KN, Kusadasi N, de Bruijn MFTR, Saris C, Ploemacher RE, Medvinsky AL, Dzierzak EA (2002) Stromal cell lines from mouse aorta-gonads-mesonephros subregions are potent supporters of hematopoietic stem cell activity. Blood 99: 1183–1189.

[2] Barnickel T, Weston J, Collobert R, Mewes HW, Stümpflen V (2009) Large scale application of neural network based semantic role labeling for automated relation extraction from biomedical texts. PLoS One 4: e6393.

DOCTORAL CANDIDATES´ PROJECTS

ARX: A TOOL FOR THE EFFICIENT ANONYMIZATION OF PERSONAL HEALTH DATA

F. Kohlmayer+** (GSISH Stipend Holder), **F. Prasser**+** (GSISH Alumnus), **R. Lautenschläger*** (GSISH Member)
Technische Universität München

K. A. Kuhn* (Advisor), C. Eckert** (Advisor), A. Kemper** (Advisor)

* Technische Universität München, Klinikum rechts der Isar, Ismaninger Str. 22, 81675 München.
** Technische Universität München, Department of Computer Science, Boltzmannstr. 3, 85748 Garching.

+ Equal contributors

Sensitive personal health information is an important resource for biomedical research. Public awareness of privacy threats has lead to national and international laws and regulations that mandate preventing the misuse of such data. In this project, we focus on data anonymization, which plays an important role for the re-use of clinical data and for the sharing of research data.

Data anonymization is commonly implemented by transforming a dataset in such a way that it fulfills a given set of privacy criteria. Different such criteria (e.g., *k*-Anonymity, *l*-Diversity, *t*-Closeness and δ-Presence) exist that allow protecting datasets from different types of threats. Data anonymization is computationally complex and only few data anonymization tools exists. Moreover, these can not easily be handled by non-experts.

In this work, we have developed a flexible and intuitive high-performance data anonymization tool. It is the first to implement a wide variety of common privacy criteria and therefore allows protecting a dataset from a multitude of privacy threats.

1 INTRODUCTION

Biomedical research requires releasing and sharing of sensitive personal health information. Public awareness of privacy threats has lead to high social and political pressure to prevent the misuse of personal data. To this end, frequently used methods are de-identification according to the HIPAA privacy rule [1], restriction to HIPAA's limited data set, and data anonymization. The latter is an important building block for balancing the individual's privacy and the need for fine-grained data collections. Data is commonly anonymized by transforming it in such a way that it fulfills a given set of privacy criteria.

Different such criteria, the most important ones being *k*-Anonymity [2], *l*-Diversity [3], *t*-Closeness [4] and δ-Presence [5], exist that allow protecting a dataset from different types of threats. Anonymizing data with minimal information loss is computationally complex, because it requires evaluating a large set of transformations (i.e., solution candidates) to find an optimal solution. As a result, efficient algorithms are required to incorporate anonymization procedures into day-to-day data processing. From a usability perspective, there is a lack of intuitive tools that can be handled by non-experts.

2 METHODS

Firstly, we developed a data management framework that implements dedicated optimizations for anonymization algorithms [6]. The basic idea is to encode the data in a way that allows evaluating transformations efficiently. Moreover, similarities between elements in the search space are leveraged to additionally reduce the complexity of evaluating individual solution candidates. Secondly, we proposed a new algorithm that exploits these optimizations and guarantees optimality (i.e., minimal information loss) for all major privacy criteria [7]. The basic idea is to traverse the search space greedily while exploiting the optimizations implemented in the framework. Thirdly, we developed a graphical anonymization tool that allows non-experts to specify privacy guarantees in an intuitive manner and to explore potentially large solution spaces efficiently [8].

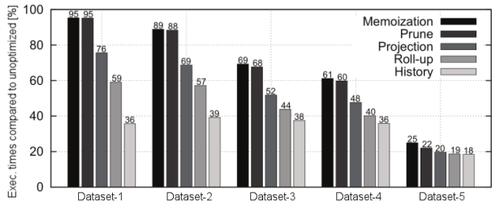

Figure 1: Comparison of the effectiveness of different optimizations in our data management framework for different datasets. Optimizations are enabled incrementally.

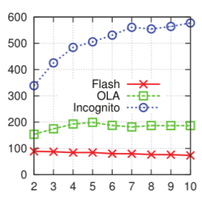

Figure 2: Comparison of our algorithm with the current state-of-the-art approaches.

3 RESULTS

We evaluated our data management framework and our algorithm with five real-world datasets, which are commonly used for comparing anonymization algorithms. Figure 1 shows a comparison of execution times when different optimizations are incrementally enabled in our framework. It can be seen that all of them effectively reduce execution times. Figure 2 presents a comparison of our novel algorithm – Flash – with previous state-of-the-art approaches, i.e., Incognito [9] and OLA [10]. The plot shows the execution times when enforcing the *k-Anonymity* criterion for a large dataset (Dataset-1 with 1.2M data items) for increasing values of k. It can be seen that Flash consistently outperforms the other algorithms by up to a factor of six.

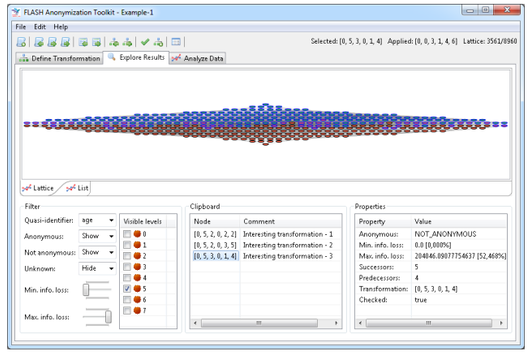

Figure 3: ARX Anonymization Tool: Exploring the solution space.

Screenshots of our graphical anonymization tool are presented in Figures 3 and 4. The tool is divided into three perspectives. The first perspective allows defining the required privacy guarantees. The second perspective, which is shown in Figure 3, allows exploring the solution space, which has been consistently characterized during the anonymization phase. As can be seen, the space is visualized by means of a large network of interconnected transformations. Transformations that fulfill the criteria as well as the optimal solution determined by the algorithm are highlighted. The perspective shown in Figure 4 allows comparing interesting transformations to the original dataset. To this end, a multitude of statistical metrics is visually presented to the user.

4 DISCUSSION

Our data anonymization framework provides a runtime that leads to unprecedentedly high performance for all state-of-the-art anonymization algorithms.

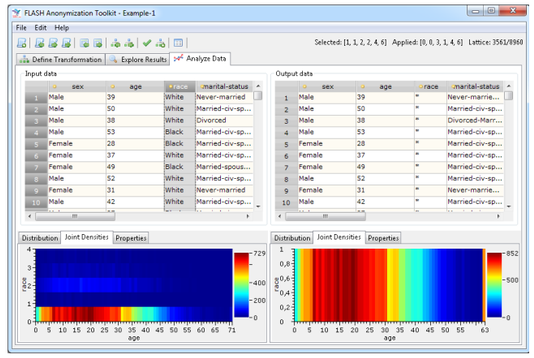

Figure 4: ARX Anonymization Tool: Comparing data transformations.

Our novel algorithm achieves outstanding performance by optimally exploiting this framework. In contrast to previous solutions, our algorithm is the first to support and guarantee optimality for (in terms of minimal information loss) all major privacy criteria and their combinations. Currently, *k*-Anonymity [2], *l*-Diversity [3], *t*-Closeness [4] and δ-Presence [5] are implemented. Moreover, our algorithm is the first to provide algorithmic stability with execution times being independent of the actual representation of the input dataset.

Our anonymization tool is the most comprehensive open source solution for anonymizing sensitive personal datasets. A flexible API enables software developers to integrate powerful anonymization capabilities into their products. Developed as a cross-platform solution, our project addresses data anonymization needs in a multitude of application domains. Our graphical tool, the software library and the source code are available at [8]. In future investigations, we will focus on pseudonymization, which allows mitigating privacy threats on storage level by separating identifying attributes from other data.

5 REFERENCES

[1] "Health insurance portability and accountability act of 1996," Public Law Gazette, 1–349, 1996.
[2] L. Sweeney, "k-anonymity: A model for protecting privacy," IJUFKS, 10, 5, 557 – 570, 2002.
[3] A. Machanavajjhala et al., "l-diversity: privacy beyond k-anonymity," TKDD, 1, 1, 3, 2007.
[4] N. Li et al., "t-closeness: privacy beyond k-anonymity and l-diversity," ICDE, 2007.
[5] M. Nergiz et al., "Hiding the presence of individuals from shared databases," SIGMOD, 2007.
[6] F. Kohlmayer, F. Prasser et. al., "Highly efficient optimal k-anonymity for biomedical datasets," CBMS, 2012.
[7] F. Kohlmayer, F. Prasser et al., "Flash: efficient, stable and optimal k-anonymity," PASSAT, 2012.
[8] ARX – Powerful Data Anonymization. http://arx.deidentifier.org
[9] K. LeFevre et al. "Incognito: efficient full-domain k-anonymity," SIGMOD, 2005.
[10]K. El Emam et al., "A globally optimal k-anonymity method for the de-identification of health data," JAMIA, 16, 5, 670–682, 2009.

IDENTITY MANAGEMENT IN DISTRIBUTED ENVIRONMENTS IN SUPPORT OF TRANSLATIONAL MEDICAL RESEARCH

G. Lamla (GSISH Member)
Technische Universität München

K. A. Kuhn* (Advisor), A. Knoll** (Advisor)

* Technische Universität München, Klinikum rechts der Isar, Ismaninger Str. 22, 81675 München.
** Technische Universität München, Department of Computer Science, Boltzmannstr. 3, 85748 Garching.

Today, personal data of patients and probands are identified and managed differently and redundantly in different information systems. A specific divide exists between research and clinical environments. In this dissertation, a concept for managing identities across different information systems has been developed. Identities are not only referring to actors (physicians and researchers with roles and rights) but also to subjects (patients, probands) and to biosamples. Data protection, security, and privacy, are of central importance in this context. This work presents a software architecture which has been developed to handle identities in research environments and to access data from clinical systems if informed consent has been given.

PROCESS INTEGRATION IN MEDICAL RESEARCH

D. Schmelcher (GSISH Member)
Technische Universität München

K. A. Kuhn* (Advisor), A. Knoll** (Advisor)

* Technische Universität München, Klinikum rechts der Isar, Ismaninger Str. 22, 81675 München.
** Technische Universität München, Department of Computer Science, Boltzmannstr. 3, 85748 Garching.

Currently many IT systems and databases are in use for foundational research, for clinical trials, and for clinical processes. Effective process integration of these information systems and databases is needed to improve cooperation of different research units and research disciplines, and to bring phenotype and genotype data together. This thesis is concerned with the development of concepts and solutions for process support of translational research. It is based at the Chair of Medical Informatics, TUM medical center rechts der Isar, and at the Chair of Database Systems at TUM.

Data integration is playing a major role in medical research, especially when genotype and phenotype associations are being investigated, and when clinical trial data, bio-banks, image data and the results of ‚omics' analyses (genomics, proteomics, metabolomics, etc.) have to be managed. Intra-, inter-institutional and international collaboration is necessary in order to gain sufficient power for statistical analyses and for a broader picture of co-morbidities. In this context, complex collaborative processes have to be supported by information technology, and concepts are needed to support cooperation and to manage distribution, heterogeneity and complexity. Research data have to fulfill high quality standards based on well defined, to some degree formalized processes for generation, capture, and management of data.

Consistent approaches to annotation, documentation of provenance, and usage of metadata are needed. The process of translating results from bench to bedside and back is highly complex, multifaceted, and in constant need of integrating newly developed methods and technology platforms. Projects like BRIDG indicate that there is a lack of shared understanding of semantics of medical research. Typically, separate information systems are used for clinical documentation and for clinical trial data management which have evolved separately in clinical and in research environments. Often, within one organization, similar data are entered multiple times, different identifiers are used, and the semantics of similar data items in different systems is not controlled by a common vocabulary.

The idea of reducing complexity, and, e.g., accessing clinical data repositories and registers for research purposes is obvious, but legal constraints have to be observed, pseudonymization concepts are needed, and use cases have to be chosen carefully. As translational research processes are not sufficiently supported by information technology, concepts, tools, and systems have been developed by a number of large-scale initiatives. CaBIG is aiming at the development of a network of tools, data, and researchers in order to support translational and clinical research in oncology. MIMM, the Molecular Medicine Informatics Model is a *virtual* research repository of clinical, laboratory and genetic data sets. The RFD profile of IHE/CDISC is addressing the question of using point-of-care data capture for both the medical record and clinical research in the setting of a clinical trial. The project is based at the Chair of Medical Informatics, TUM Medical Center "Rechts der Isar", and the Chair of Database Systems at TUM.

DOCTORAL CANDIDATES´ PROJECTS

SURFACE REGISTRATION FOR RANGE IMAGING APPLICATIONS IN MEDICINE

S. Bauer (GSISH Member)
Friedrich-Alexander-Universität Erlangen-Nürnberg

J. Hornegger* (Advisor), H. Feußner** (Co-Advisor), A. Knoll*** (Co-Advisor)

* Friedrich-Alexander-Universität Erlangen-Nürnberg, Lehrstuhl für Mustererkennung, Martensstr. 3, 91058 Erlangen.
** Technische Universität München, Klinikum rechts der Isar, MITI, Trogerstr. 26, 81675 München.
*** Technische Universität München, Department of Informatics, Boltzmannstr. 3, 85748 Garching.

The intra-procedural tracking of respiratory motion has the potential to substantially improve image-guided diagnosis and interventions.

We have developed a sparse-to-dense non-rigid registration approach that is capable of recovering the patient's external 3D body surface and estimating a dense 4D (3D+time) surface motion field from sparse range imaging measurements and patient-specific prior shape knowledge.

In combination with 4D tomographic planning data, these surface motion fields can be used in radiation therapy to establish patient-specific motion models that correlate the external body deformation with the internal tumor motion. These models can then be applied for non-radiographic motion-compensated dose delivery.

1 INTRODUCTION

Real-time monitoring of the patient body holds great potential for the management of respiratory motion and is a rapidly evolving field in modern medicine. Motion management is of particular interest in image-guided radiation therapy (RT) for abdominal and thoracic targets where motion induces a substantial source of error. To account for potential targeting errors and to assure adequate dosimetric coverage of the tumor-bearing tissue, large safety margins are typically applied today. However, this comes at the cost of irradiating surrounding radio-sensitive structures. To reduce the tolerances between the planned and actually delivered dose distribution, a multitude of techniques for respiratory motion management have been developed over the past decades [1].

Early strategies in range imaging (RI) based motion management were restricted to low-dimensional respiration surrogates. In contrast, recent RT motion tracking solutions target dense non-rigid surface deformation tracking [2] that better reflects the complexity of respiratory motion [3]. We have developed a marker-less system based on a non-moving active laser triangulation (AT) sensor that delivers sparse but highly accurate 3D data in real-time. Using prior shape knowledge from tomographic planning data, a variational model is introduced to recover a dense and accurate 4D (3D+time) displacement field that provides a high-dimensional breathing surrogate, and to reconstruct a reliable and complete patient surface model at the instantaneous respiration phase.

2 MATERIALS AND METHODS

The system utilizes an emerging marker-less and laser-based active triangulation (AT) sensor that delivers sparse but highly accurate 3D measurements in real-time. These sparse position measurements are registered with a dense reference surface extracted from tomographic planning data. Thereby, along the lines of inverse-consistent registration, in a joint manner, a dense displacement field is recovered, which describes the spatio-temporal 4D deformation of the patient body surface, depending on the type and state of respiration4,5. It yields both a reconstruction of the instantaneous patient shape and a high-dimensional respiratory surrogate for respiratory motion tracking, cf. Fig. 1. The method is validated on a 4D computed tomography (CT) respiration phantom and evaluated on both real data from an AT prototype and synthetic data sampled from dense surface scans acquired with a structured-light scanner.

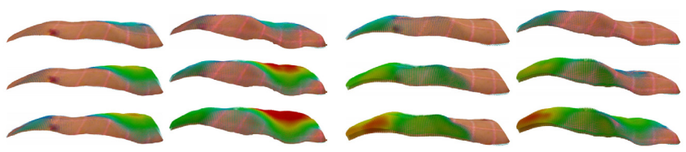

Figure 1: Results on real AT data from two healthy subjects, for abdominal respiration (left two columns) and thoracic respiration (right two columns). The individual rows show the estimated non-rigid surface motion fields for different phases throughout the respiration cycle. The local magnitude of the displacement is color coded.

3 RESULTS

We have investigated the performance of the proposed method on synthetic, realistic and real data [4]. On 256 datasets from 16 subjects with an average initial mismatch of 5.66 mm, the mean reconstruction error was ±0.23 mm and the 95th percentile did not exceed 1.17 mm for any subject, cf. Table 1. In the experi-ments, it was shown that a proper initialization of the displace-ment fields with previous estimates and an improved variational formulation compared to our first approach [5] reduce the runtime by 19.2% and 48.2%, respectively. Overall, the CPU implemen-tation of the proposed surface registration approach outperforms related work [6] substantially in terms of runtime perfor-mance (two orders of magnitude).

4 DISCUSSION

Let us distinguish the proposed system from commercially available RI-based solutions in RT. First and foremost, available solutions do not support dense sampling in real-time or at the cost of a limited field of view. For instance, both the Sentinel system (C-RAD AB, Uppsala, Sweden) and the Galaxy system (LAP GmbH, Lüneburg, Germany) take several seconds for a complete scan of the torso, and the real-time mode of the VisionRT stereo system (VisionRT Ltd., London, UK) is limited to interactive frame-rates of 1.5-7.5 Hz, depending on the size of the surface of interest. The temporal resolution of these solutions may be insufficient to characterize respiratory motion.
Beside its limitations in terms of sampling density and speed, respectively, commercially available solutions often imply high costs in terms of hardware and are subject to measurement uncertainties due to the underlying sampling principles, e.g., active stereo photogrammetry or consecutive light-sectioning using mechanically swept lasers. Third and last, the general focus of these systems is on patient positioning and none of them features dense and non-rigid respiratory motion tracking.

5 CONCLUSION

We have introduced a variational approach to marker-less reconstruction of dense non-rigid 4D surface motion fields from sparse but accurate AT sampling data. In a study on 16 subjects, we demonstrated the capability of the algorithm to precisely reconstruct the dense respiratory displacement field using prior shape knowledge from planning data. In the field of radiation therapy, the 4D surface motion fields can be used as biologically reasonable high-dimensional respiration surro-gates for gated RT, as input for accurate external-internal motion correlation models in respiration-synchronized RT [7], for motion compensated patient positioning, and to reconstruct the intra-fractional body shape for patient setup monitoring during dose delivery. The analysis of dense displacement fields also allows for a computer-aided distinction between abdominal and thoracic respiration.

Beyond its application in RT, the method holds great potential for diagnostic and therapeutic applications, e.g. deformation tracking with 3D endoscopy in minimally invasive procedures.

	Initial Mismatch [mm]		Residual Mismatch [mm]	
	A	T	A	T
Mean	5.09	6.24	0.21	0.25
Median	3.95	4.66	0.13	0.15
95th Percentile	14.0	17.1	0.69	0.82

Table 1: Results over all subjects, respiration types and phases. Given are the mean, median, and 95th percentile of the initial and residual mismatch in [mm], for both abdominal (A) and thoracic respiration (T).

6 REFERENCES

[1] Keall, P.J., et al.: The management of respiratory motion in radiation oncology, AAPM task group 76. Med Phys 33(10) (2006).
[2] Bauer, S., et al.: Joint ToF image denoising and registration with a CT surface in radiation therapy. SSVM, LNCS 6667, Springer (2012).
[3] Fayad, H., et al.: Correlation of respiratory motion between external patient surface and internal anatomical landmarks. Med Phys 38(6) (2011).
[4] Berkels, B., et al.: Joint Surface Reconstruction and 4-D Deformation Estimation from Sparse Data and Prior Knowledge for Marker-Less Respiratory Motion Tracking. Med Phys 40(9) (2013).
[5] Bauer, S., et al.: Marker-less reconstruction of dense 4-D surface motion fields using active laser triangulation for respiratory motion management. In: MICCAI, Part I. LNCS 7511, Springer (2012).
[6] Schaerer, J., et al.: Multi-dimensional respiratory motion tracking from markerless optical surface imaging based on deformable mesh registration. Phys Med Biol 57(2) (2012).
[7] McClelland, J., et al.: Respiratory motion models: A review. Med Image Anal 17(1) (2013).

AUTOMATION OF A PORTABLE HEART-LUNG MACHINE

B. Baumgartner (GSISH Member)
Technische Universität München / Deutsches Herzzentrum München

Prof. A. Knoll* (Advisor), Prof. R. Bauernschmitt** (Co-Advisor)

* Technische Universität München, Department of Informatics, Boltzmannstr. 3, 85748 Garching.
** Isar Heart Center, Department of Cardiology and Intensive Care Medicine, Sonnenstr. 24-26, 80331 München.

A cardiogenic shock is associated with a high mortality rate. Often, patients suffer from irreversible organ damage before they reach a hospital for professional therapy. In recent years miniaturized extracorporeal circulatory support systems increased the survivor rate by providing primary care for the patient at the emergency site and during transportation. Nevertheless, the limited space in ambulances, the lack of trained staff and financial considerations constrain an area-wide employment of such systems.
An automatically regulated support system could provide optimal perfusion, increasing patient safety and reducing the workload of the emergency team. This work examines two aspects of the automation of a portable heart-lung machine (HLM): The design of robust controllers for the regulation of the heart-lung machine, and the application of Data Mining methods for intelligent patient monitoring [1]. Animal experiments allowed to collect vital patient parameters and their interaction with the heart-lung machine in distinct scenarios. Based on this data a simulation model and a hydraulic circulatory model are established. The hydraulic model replicates the cardio- vascular system and is used to design robust controllers, regulating the pump speed of the heart-lung machine dependent on blood pressure and flow. Four concurrent control strategies were implemented: a PI Controller, a H∞-Controller, a Fuzzy Controller and a Model Reference Adaptive Controller. The controllers are tuned robustly and evaluated in several scenarios. Autonomous circulatory support systems require continuous and failure-safe patient monitoring. Usually, the medical practitioner decides on the choice of treatment, based on current patient parameters and his experience. Only in recent years Data Mining and Knowledge Discovery methods found their way into medical research. In this work Data Mining methods for the online assessment of the patient's condition are reviewed. In a benchmark study it is shown how such algorithms are able to reduce the false alarm rate of patient monitors. This increases the quality of care and supports the application of autonomous medical devices such as the controlled heart-lung machine.

1 PROJECT SUMMARY

Preclinical applications of medical devices, such as HLMs or defibrillators, on patients with severe cardiac insufficiencies, have proved to increase the survivor rate. The use of a HLM in emergency situations, however, is still sporadic, since sufficient knowledge for cannulation and additional staff for operating the device is needed (see Figure 1). An automated device would increase the patient safety, quality of care and, at the same time, reduce the workload of the staff.

Figure 1: The Lifebridge B2T HLM during a surgery at the German Heart Center Munich and during transportation.

To investigate the potentials of an automated device, different approaches were followed in this work. In animal experiments, patient and machine parameters were collected, and a prototype controller was tested with good results. Based on the acquired data and an extensive literature research, both a hydraulic and a virtual model of a patient under Extracorporeal Circulation was developed. In this work the focus was on the hydraulic model and its control. The model followed the three-element Windkessel model, which was found to give the best trade-off between accuracy and complexity. It comprises a cylindrical air chamber as a compliance element and two adjustable resistor elements, that change the tube diameter (see Figure 2). A centrifugal pump with a static outlet resistance represents the HLM. A complete mathematical description was derived and transferred to a linear state space representation.

Based on the mathematical model, several pump speed controllers for flow and pressure control were implemented. As a classical feedback controller a Proportional-Integral Controller (PIC) was chosen. From the field of Adaptive Control a Model Reference Adaptive Controller (MRAC) was designed. The H∞-Controller (HINFC) represents the Robust Control family and, finally, a Fuzzy Controller (FUZZYC) was selected from Intelligent Control approaches.

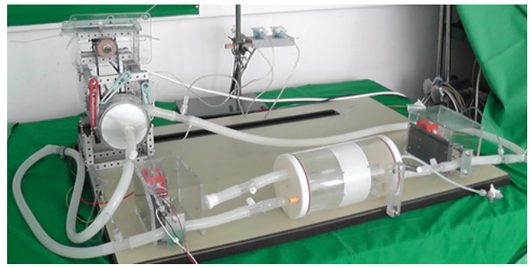

Figure 2: Hydraulic Mockup, representing a Cardiovascular System Model (three-element Windkessel) under Extracorporeal Circulation.

The controllers were tuned robustly and tested in three scenarios, including step changes of the target values, external perturbations and variations of the peripheral resistance.
In scenario 1 all controllers were able to follow step changes in the target values with slight advantages for the PIC. In scenario 2, with additional noise, the MRAC outperformed its competitors in terms of the Integral of Absolute Error (IAE) (see Figure 3). In experiment 3, the peripheral resistance was altered. The PIC achieved the lowest IAE for flow control, while the FUZZYC was ranked first in pressure control.

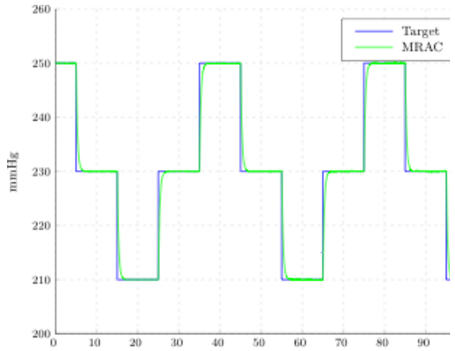

Figure 3: Pressure Control under External Perturbations. The MRAC Controller smoothly follows a given target value.

In general, all controllers lead to stable control and were able to solve the given tasks. It was demonstrated, that pump speed control of a HLM is feasible with high accuracy. However, qualitative factors such as design complexity and user acceptance should also be considered in the evaluation. Compared to its competitors, both the FUZZYC and the PIC are rather easy to design and to maintain.

While the PIC design process requires an analytical system description, the FUZZYC is independent of a mathematical system model. This facilitates maintenance, because a redesign of the controller would not be necessary, if system components change. Also the natural language rulebase differentiates the FUZZYC from the other approaches. As long as the size of the rulebase is limited, the control behavior is transparent, even for untrained users. Furthermore, expert knowledge (from surgeons etc.) can be implemented directly. This increases the user acceptance, so that the FUZZYC is particularly suited for medical control applications.
As a major limitation, the hydraulic mock model is not able to replicate oxygen delivery or hypothermia, so that the control of the machine's gas blender or temperature regulation was not studied in the physical setup. Those tasks were evaluated in the simulation model (see [2]). In both the animal experiments and the tests with the hydraulic model it was observed, that the HLM was not always able to reach an appropriate blood flow. This is due to the femoral cannulation, which requires rather small cannulas. The small cannula diameters create a large resistance for the pump. A major advantage of the presented control approach is, that it is sufficient to measure the produced pump flow and the pressure difference between the pump outlet and inlet. Those parameters are obtained at the HLM. Data collection at the patient is therefore not required for pump speed control, even more, the patient can be considered as a black-box.

2 REFERENCES

[1] This work summarizes major parts of B. Baumgartner, "Automation of a Portable Heart-Lung Machine and Patient Monitoring with Data Mining Methods", Dissertation, Technical University of Munich, 2013, to be published.

[2] A. Mendoza, "Automation of an extracorporeal support system with the use of adaptive fuzzy controllers", Dissertation, Technical University of Munich, 2013.

3D MULTISPECTRAL RECONSTRUCTION AND VISUALIZATION FOR SKIN CANCER DETECTION

A. O. Duliu (GSISH Stipend Holder)
Technische Universität München

Nassir Navab* (Advisor), Johannes Ring** (Co-Advisor), Rüdiger Hein** (Co-Advisor)

* Technische Universität München, Chair for Computer Aided Medical Procedures and Augmented Reality, Boltzmannstr. 3, 85748 Garching.
** Technische Universität München, Clinic und Policlinic for Dermatology und Allergology, Klinikum rechts der Isar, Biedersteinerstr. 29, 80802 München.

Photographic imagery is acquired in large numbers in dermatology for the purpose of monitoring disease progression. Matching a nevi from a documented image to the patient is a cumbersome and time consuming task, performed one-by-one and only for the most suspicious ones.

This work introduces a method for largely automatic and simultaneous identification of nevi in different images, which allows tracking single features over time. The method involves acquiring macroscopic multispectral-images while at the same time capturing the geometry of the skin. After compensating for changes in camera pose and surface changes between examinations, a rotation-invariant feature descriptor is used to match nevi visible in both images and to track their evolution.

1 INTRODUCTION

Multi-spectral imaging is an emerging modality for use in dermatological diagnosis which has the potential to offer quantitative measurements of the skin tissue [1], thus providing a more accurate diagnosis tool for a wide range of afflictions. In dermatology it is mostly applied to imaging nevi during epiluminescence screening for malignant melanoma, which involves taking highly magnified images of the nevi. There are several methodologies to differentiate a benign nevus from a melanoma, including the ABCDE test (Asymmetry, Border, Color, Diameter and Evolution). The ABCD conditions can be evaluated manually or automatically, but to check the evolution of a nevus, the physician needs to compare it with a previously acquired image of the same nevus.

The main motivation of this work is to provide dermatologists with a multispectral imaging system that allows quantification of skin lesions as well as tracking of disease progression in an automated fashion. To this end, both multi-spectral and range images are being acquired simultaneously, providing quantitative metrics about the spectral reflectance of the skin, as well the size and geometry of the lesions. As the imaging data is registered between several examinations over the course of time, it enables tracking and also quantifying the disease progression, yielding important diagnostic information. This also allows to apply automatic methods to detect or classify suspicious lesions, aiding the treating physician.

In the past twelve months most of the work has focused on re-locating nevi from images with unknown surface geometry, improving the photometric calibration and the inter channel registration of the multispectral camera and on segmenting nevi from macroscopic multispectral images. The reminder of this report will focus on nevi re-localization and on registering the channels of multi-spectral images.

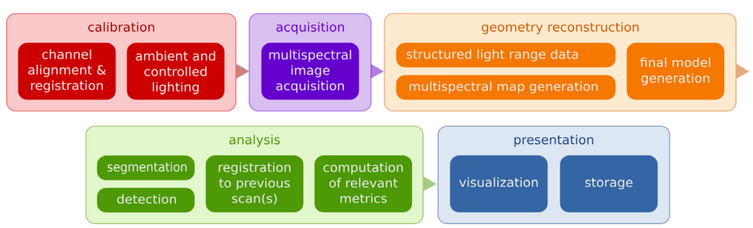

Figure 1: Overview 3D multi-spectral imaging pipeline.

2 MATERIALS AND METHODS

The multi-spectral cameras (figure 2) used in this work consist of 10 band-pass filters mounted on a rotating gantry between the lens and the sensor. A software controlled stepper motor is used to change the channels. Because this set-up involves moving parts, the acquisition times range from 7 to 15 seconds, depending on lighting conditions. As this can lead to a loss of overlap between the channels, intensity based registration using mutual information is used to compensate. For additional mechanical stability during acquisition, a cart was designed to both hold the camera with its processing unit and to enable flexible positioning all around a patient.

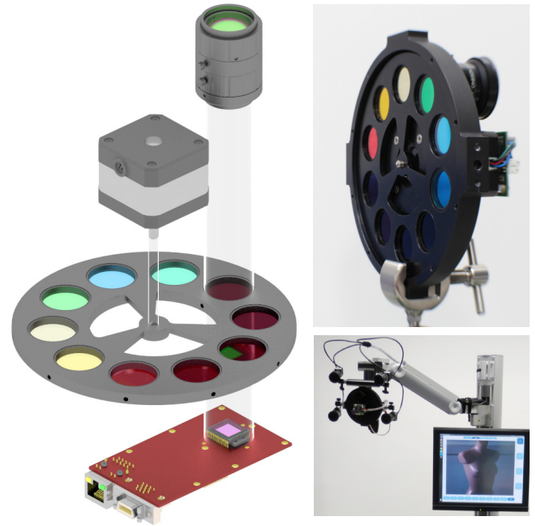

Figure 2: Schematic of the main components of the multi-spectral camera (left, from top to bottom): lens, stepper motor, filter-wheel and camera board; opened camera with filter-wheel visible (top right); multi-spectral camera mounted on cart.

For nevi re-localization a rotation-invariant feature descriptor was developed, that uses the local neighborhood of a nevus to describe it. The texture, size and shape of the nevus are not considered, as these can change over time, especially in the case of a malignancy. The Random Walks framework is used to compute the correspondences based on the probabilities derived from comparing the feature vectors. Outlier rejection is performed using thin-plate-splines and the remaining matches are further improved iteratively.

3 RESULTS

The matching performance was evaluated using synthetic data of random nevi, and subsequently deforming the datasets. Deformation parameters were chosen to realistically reproduce situations observable in clinical practice (table 1).

Deformation	Perspective	Curved	Non-linear
PPV	94.51 ±16.86%	99.18 ±2.08%	96.35 ± 8.85%
PPV (norm)	96.29 ±10.54%	99.36 ±1.94%	95.92 ± 8.30%

Table 1: Matching for nevi re-localization using synthetic data under perspective/ non-linear deformations, or by mapping them onto a curved surface. The descriptors were computed by either using the distances between the nevi, or by normalizing them to the current furthest neighbor.

Real data was acquired at our university dermatology clinic of six patients and representative cases were selected (table 2).

Deformation	Breathing	View Change1	View Change2
PPV	94.85 ±4.99%	84.65 ±3.84%	75.82 ±16.41%

Table 2: Matching for nevi re-localization using patient data: six image pairs for each view change case, and four image pairs for the breathing case.

4 DISCUSSION

When deformably registering the channels of the multispectral images, the relative intensity values are similar to the ones observe in multimodal registration. The multi-resolution framework used here is also robust to channels being partially out-of-focus.
Although the feature descriptor was developed to be robust only to non-linear deformation, is has surpassed expectations also on images that have not been corrected for perspective distortions or taking into account the skin surface geometry.

5 ACKNOWLEDGEMENTS

We would like to thank our colleagues from the CAMP optical group: José Gardiazabal, Jakob Vogel and Tobias Lasser and to our clinical partners from the group of Professor Hein.

6 REFERENCES

[1] M Yamaguchi et al.: Multispectral color imaging for dermatology: application in inflammatory and immunologic diseases, Color and Imaging [2005]
[2] AP Dhawan et al.: Multispectral optical imaging of skin-lesions for detection of malignant melanomas [EMBC 2009]
[3] B Glocker et al.: Deformable Medical Image Registration: Setting the State of the Art with Discrete Methods [Annual review of biomedical engineering, 2011]

REDUCING MOTION AND ATTENUATION ARTEFACTS IN HYBRID PET/MR IMAGING

S. Fürst (GSISH Stipend Holder)
Technische Universität München

Prof. Dr. S. Ziegler* (Advisor), Prof. Dr. A. Haase** (Co-Advisor)

* Technische Universität München, Klinikum rechts der Isar, Ismaninger Str. 22, 81675 München.
** Technische Universität München, IMETUM, Boltzmannstr. 11, 85748 Garching.

The integration of PET and MR imaging is very promising, yet challenges remain. The MR surface coils of the Biograph mMR integrated PET/MR system are unaccounted for during attenuation correction and have instead been optimised specifically for the use with PET. Patient motion degrades PET image quality, leading to inaccurate quantification and diagnoses. Novel physiological monitoring and correction methods were facilitated by the introduction of PET/MR to the clinical routine.

The goals were to quantify the effect of surface coils on quantification and count statistics, as well as to implement and evaluate a respiratory motion compensation technique for PET utilising a radial self-gating MR sequence.

The additional attenuation introduced by MR coils can have a significant effect on PET quantification with its extend highly variable. Initial results suggest that MR-based motion compensation of PET data is feasible without other sensors of physiological signals.

1 INTRODUCTION

Similar to the already established and for both the patient and the clinician highly advantageous technology that combines positron emission tomography (PET) and computed tomography (CT) sequentially in one scanner, integrated positron emission tomography/magnetic resonance imaging (PET/MR) is a multimodal medical-imaging concept, providing functional information of the patient in the anatomic context of the human body. Dedicated radiofrequency (RF) coils are necessary in MRI and have to be positioned near the body region of interest to optimise the signal and hence the image quality. In integrated PET/MR, these coils are also located in the field of view of the PET component and therefore add to the attenuation and scattering of gamma rays, deteriorating PET image quality. Moreover, PET images contain information summed over many breathing cycles, because data are acquired for several minutes during an examination. The according motion of inner structures combined with external patient motion results in image artefacts as well as inaccurate definition of tumour volumes and quantification.
The goals were to quantify the effect of surface coils on quantification and count statistics, as well as to implement and evaluate a respiratory motion compensation technique for PET utilising a radial self-gating MR sequence.

2 MATERIALS AND METHODS

All studies were performed on a fully integrated PET/MR system (Biograph mMR, Siemens Healthcare, Germany), which comprises a 3 T magnet and APD-LSO block detectors[1] (Figure 1). The RF coil under investigation was the standard surface coil that is shipped with the scanner (Body Matrix Coil, Siemens Healthcare, Germany). Its design and materials were optimised for the use with PET, but it is unaccounted for during attenuation correction of PET data. For the evaluation of its effect on quantification, data of 11 oncological patients were acquired on the PET/MR with and then without the surface coil attached (1 bed position, 4 min/bed position). In order to eliminate artefacts due to the truncation of arms in the attenuation maps, patients were scanned with their arms up. Images were reconstructed using the clinical standard[2] (OSEM 3D, 3 iterations, 21 subsets, matrix size: 172, 4.0 mm Gaussian post-reconstruction filter).

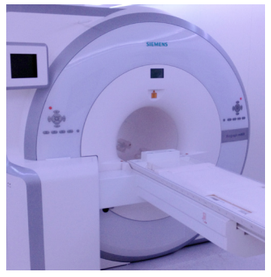

Figure 1: The Biograph mMR integrated PET/MR system.

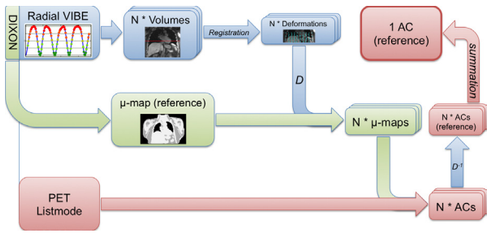

Figure 2: Scan and processing protocol for MR-based PET motion correction.

Towards the establishment of an MR-based method for motion correction, PET and MR data were simultaneously acquired (10 minutes) and processed for three oncological patients (Figure 2). The applied MR sequence was a radial stack-of-stars GRE sequence with golden-angle sampling (3D, spatial resolution: 1.6 x 1.6 x 1.7 mm^3). MR raw data were subsequently binned (n_B = 5) and reconstructed according to a self-gating signal extracted from k-space data. A non-rigid registration algorithm (FastSymmetricForcesDemons) was applied to the MR images to estimate motion fields. Using the same clinical algorithm as described above, respiratory-gated PET images were reconstructed for each bin in addition to static images reconstructed from all available PET data and analysed by means of calculation of the standard uptake value (SUV).

3 RESULTS

By removing the MR surface coils, the SUV increased on average by (6 ± 2) %, (6 ± 4) % and (3 ± 4) % in transaxial volumes of interest (VOI) in livers, lungs and spleens (Figure 3A). In coronal VOIs in the anterior of the lung, the average SUV increase was slightly higher than in the posterior. The average effect was similar in lesions, but exceeded 20 % in almost a fifth of them (Figure 3B). The global number of trues was (6 ± 1) % higher without coils.

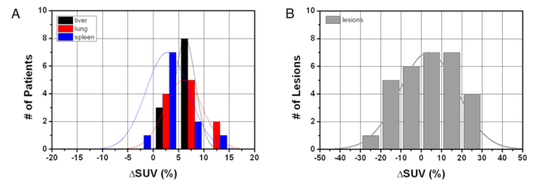

Figure 3: The distribution of average SUV changes related to the removal of MR surface coils in transaxial organ VOIs (A) and in lesions (B). The curves are the respective normal distributions.

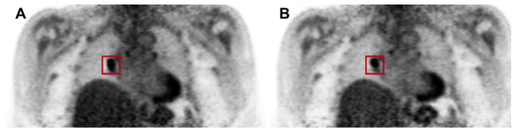

Figure 4: Uncorrected (A) and motion-compensated (B) PET images. The edge of the liver dome appears sharper in (B) and the lesion smaller.

Regarding motion correction, PET and MR acquisitions were successfully synchronized. Locations of morphological structures appeared consistent. Displacement of the edge of the liver dome between exhale and inhale ranged from 11 mm to 14 mm. Compared to the uncorrected images, the SUVs in the lesions of the three patients increased by 2 %, 8 % and 29 %, if motion compensation was applied. The size of the lesions changed by +6 %, -7 % and -16 %, respectively. The edges of morphological structures appear sharper as well (Figure 4).

4 DISCUSSION

The global effect of MRI surface coils is mostly in the order of magnitude of statistical SUV fluctuations. The application of surface coils leads to a larger SUV decrease in anterior body regions. In lesions, the effect is more pronounced and can be significant with its extent highly variable. Therefore, surface coils should be accounted for in attenuation correction.
Furthermore, these first results suggest that compensation of respiratory motion with a radial self-gating MR sequence in integrated PET/MR is feasible without applying additional sensors of physiological signals.

5 ACKNOWLEDGEMENTS

The PET/MR system used for this project was funded through the Deutsche Forschungsgemeinschaft (DFG) Großgeräteinitiative 2010. This research was also supported by the Sonderforschungsbereich (SFB) 824.

6 REFERENCES

[1] Delso G, Fürst S, et al. Performance Measurements of the Siemens mMR Integrated Whole-Body PET/MR Scanner. J. Nucl. Med. 2011;52:1914-22.

[2] Drzezga A, et al. First Clinical Experience with Integrated Whole-Body PET/MR: Comparison to PET/CT in Patients with Oncologic Diagnoses. J. Nucl. Med. 2012;53:845-55.

ITERATIVE RECONSTRUCTION FOR FEW-VIEW PHASE-CONTRAST CT

T. Gaaß (GSISH Member)
Technische Universität München

A. Haase* (Advisor), F. Pfeiffer** (Co-Advisor)

* Technische Universität München, IMETUM, Boltzmannstr. 11, 85748 Garching.
** Technische Universität München, Department of Physics, James-Franck-Str. 1, 85748 Garching.

The aim of this work is to investigate the improvement of image quality in few-view grating-based phase-contrast computed tomography (PCCT) applications via compressed sensing (CS) inspired iterative reconstruction on an *in vitro* mouse model.

PCCT measurements are performed on a grating-based PCCT setup using a high-brilliance synchrotron source and a conventional tube source. The sampling density of the data is reduced by a factor of up to 20 and iteratively reconstructed.

It is demonstrated that grating-based PCCT intrinsically meets the major conditions for a successful application of CS. Contrast fidelity and the reproduction of details is presented in all reconstructed objects.

The feasibility of the iterative reconstruction on data generated with a conventional X-ray source is illustrated on a fluid phantom and a mouse specimen, undersampled by a factor of up to 20.

1 INTRODUCTION

X-ray phase-contrast computed tomography (PCCT) techniques acquire information about the real part of the refractive index corresponding to an X-ray phase shift. While precise dose optimization has yet to be performed when using PCCT, the ALARA principle suggests maximal dose reduction prior to clinical applications. The straightforward way to save measurement time, as well as dose is to reduce the number of projection images per gantry rotation. However, conventional FBP reconstruction of such undersampled data sets results in images impaired by aliasing artifacts. Donoho et al. demonstrated that, by using compressed sensing (CS), under certain conditions it is possible to recover artifact-free images from a drastically smaller number of measurements [1]. Employing a priori information about the reconstructed PCCT image in a non-linear iterative reconstruction framework poses a very effective way to accomplish an artifact-free reconstruction of few-view, thus dose-reduced PCCT acquisitions.

2 MATERIALS AND METHODS

The transformation of sinograms into real space is conventionally realized using filtered backprojection. A different approach, called regridding, was initially adapted to medical imaging by O'Sullivan [2] and further developed by Fessler et al. under the acronym NUFFT (non uniform fast Fourier transform) [3]. The NUFFT algorithm interpolates a radially acquired k-space data set onto a Cartesian grid in order to apply a fast Fourier transform. Utilizing NUFFT rather than filtered backprojections simplifies the implementation of different reconstruction filters as well as sampling schemes and provides the possibility of fast forward and backward transformation during the iteration process.

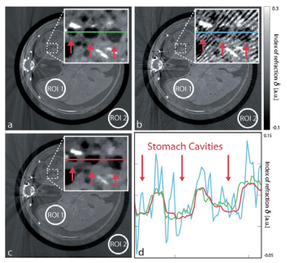

Figure 1: (a) Reconstruction based on a PCCT sinogram with 901 projections, including the used regions of interest (ROI); (b) Image reconstructed from 151 projections; (c) Reconstruction from 151 projections using the iterative algorithm. The windowing was chosen for best visual appearance.

	FS		US		IR	
	Mean δ	STD	Mean δ	STD	Mean δ	STD
ROI 1	0.061	0.006	0.082	0.025	0.061	0.007
ROI 2	-0.005	0.004	0.004	0.019	-0.003	0.003

Table 1: Mean pixel values and standard deviation within the regions of interest, depicted in figure \ref{fig:Jerry_VGL} for the fully sampled (FS), the undersampled (US) and the iterative reconstruction (IR) case.

Subsequently, this image is subject to an optimization process, approaching the sparsest solution in the certain transformation domains.
Equation 1 summarizes the penalized minimization based reconstruction.

$$\mathrm{Im} = \arg\min_f \left[\left\| FT(f) - y \right\|_2 + \lambda_{WL} \left\| WL(f) \right\|_1 + \lambda_{TV} TV(f) \right] \quad (1)$$

The first term of equation 1 denotes the data fidelity of the reconstruction by comparing the raw k-space data y with the Fourier Transform (FT) of the resulting reconstruction f. The minimization of data fidelity is constrained with both the l1-norm in the wavelet domain (WL) weighted by the penalty parameter WL and the l1-norm in the finite difference domain (or Total Variation - TV) weighted by TV.

3 RESULTS

To evaluate the performance of the implemented algorithm on experimental data, we reconstructed a formaline fixated mouse specimen acquired using a synchrotron source at the European Synchrotron Radiation Facility (ESRF, beamline ID19, Grenoble, France). The fully sampled reconstruction in fig. 1(a) exclusively shows phase wrapping artifacts from bone structures, while fig. 1(b) displays the zero-filling reconstruction impaired by additional aliasing artifacts. Figure 1(c) depicts the result of the iterative reconstruction with almost completely suppressed aliasing artifacts. In addition to the visual comparison, the synchrotron data set was quantitatively evaluated on the basis of a region of interest (ROI) analysis (cf. Table 1).

The sensitivity of artifact reduction on solely soft tissue PCCT was evaluated on a tomographic data set of a formalin embedded, decalcified mouse specimen.
The undersampled data set was reconstructed using zero-filling (fig. 2(a)) and via re-binning (fig. 2(b)). Figure 2(c) displays the resulting application of the proposed algorithm, while figure 2(d) comprises the reconstruction of the fully sampled acquisition. The application of the iterative reconstruction lead to a considerable reduction of not only aliasing artifacts, but also noise and apparent ring artifacts caused by the interpolation during NUFFT reconstruction. Line profiles along the dashed black line clearly show that detailed information in fig. 2(a), as well as fig. 2(b) is almost completely lost due to aliasing and loss of resolution, respectively.

4 CONCLUSIONS

In summary we have demonstrated, both numerically and with experimental data, that the proposed iterative reconstruction effectively suppresses undersampling artifacts in phase-contrast CT. Therefore it is possible to reduce the number of projection images far below what the Nyquist/Shannon-theorem conventionally postulates, while maintaining resolution, contrast and visibility of details. Even if no undersampling is performed the introduced algorithm offers the possibility to suppress noise, resulting in an image with improved SNR, when compared to the fully sampled reconstruction.
Current and future work comprises a detailed quantitative evaluation of the achievable resolution with the proposed reconstruction algorithm. Additionally the assessment of optimized penalty parameters poses a very important task.While many issues, such as image quality with respect to clinical significance or the speed of the algorithm are yet to be addressed, compressed sensing inspired reconstruction for phase contrast CT may open the door for future advanced applications such as 4D-PCCT.

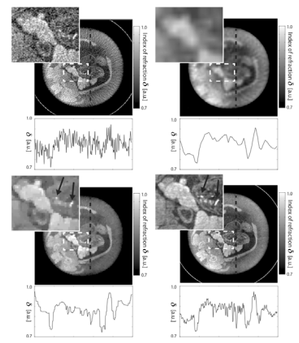

Figure 2: Reconstructions of a transverse slice of a fixated, de-calcified mouse. (a) NUFFT reconstruction of few-view undersampling (np=50, n=318); (b) few-view Nyquist sampling (np=50, n=32) interpolated to 318; (c) iterative reconstruction of few-view undersampling regaining image smoothness and resolving power comparable to the original; (d) fully sampled according to Nyquist (np=701, n=318).

5 ACKNOWLEDGEMENTS

I'd like to thank Guillaume Potdevin, Martin Bech, Peter Noël, Marian Willner, Arne Tapfer for the support in realizing this work.

6 REFERENCES

[1] Donoho, David L. „Compressed sensing." IEEE Trans Inf Theory, 2006.

[2] O'sullivan, J. D. „A fast sinc function gridding algorithm for Fourier inversion in computer tomography." IEEE Trans Medic Imag ,1985.

[3] Fessler, Jeffrey A. „On NUFFT-based gridding for non-Cartesian MRI." JMR 2007.

FREEHAND AND ROBOTIC ASSISTED SPECT ACQUISITION AND RECONSTRUCTION

J. Gardiazabal (GSISH Member)
Technische Universität München

N. Navab* (Advisor), S. Ziegler** (Co-Advisor)

* Technische Universität München, Department of Informatics, Boltzmannstr. 11, 85748 Garching, Germany.
** Technische Universität München, Klinikum rechts der Isar, Ismaninger Str. 22, 81675 München.

Functional imaging systems for intraoperative guidance have shown remarkable results. These results, even tough very positive in some cases, tend to suffer from high variability, highly correlated with the experience of the operator. A highly trained user produces datasets that, once reconstructed, can rival a gantry-based SPECT machine, while a novice user usually cannot get similar results.

At the same time, new hand-held detectors have been developed, and it is now possible to use a 2D gamma camera with hundreds of pixels instead of a single detector device. This new detector opens the door for faster acquisitions and better quality reconstructions, but presents big challenges for the calibration, acquisition pipeline and the reconstruction schemes. The proper solution to those challenges is critical to exploit the advantages of this new detectors.

This work presents the first steps towards solving those problems.

1 INTRODUCTION

During the last decade, the technological advances have enabled the use of more intra-operative imaging. This is a big step forward, since the pre-operative images have limited use inside the operating room. The main reason is the different position of the patient, leading to a non-linear displacement of the regions of interest. Many intra-operative imaging modalities are now part of the OR, like ultrasound devices or X-ray C-Arms.
Another newer example is freehand SPECT, where the objective is to provide accurate SPECT reconstructions inside the operation room for surgeon‘s guidance. This is currently used identify tumors and sentinel lymph nodes for resection. The system consists in a single pixel gamma detector with a tracking target rigidly attached. With this configuration, the gamma counts in the detector are then located in space. The surgeon with then move the probe covering the region of interest and that will generate pose/activity pairs that are then used to reconstruct the radioactive distribution. The major differences between a conventional SPECT and the freehand version is the number of events collected and the geometry of the acquisition.
The fixed geometry of the conventional SPECT provides a statistical significance and good coverage by design, but in the case of freehand SPECT this depend on the trajectory done by the user. An inexperienced user will probably perform a biased scan, for instance by leaving out important probe poses, not covering the whole area sufficiently by aiming only to the hot-spots.
In order to solve this problem, one solution is to replace the gamma detector with a gamma camera [1], thus increasing the readings and therefore improving the statistics. To provide consistent and repeatable results, a robotic arm was used to drive the camera [2].

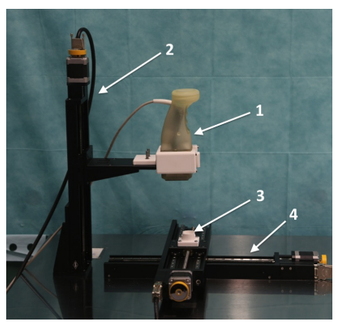

Figure 1: Gamma camera calibration.

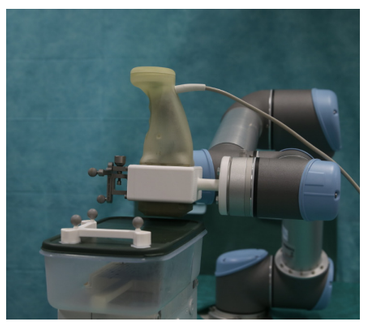

Figure 2: Experiment setup.

2 MATERIALS AND METHODS

The setup consists in a mini gamma camera (CrystalCam, Crystal Photonics, Germany), mounted in a robotic arm (UR5, Universal Robots, Denmark), using a custom designed holder that was then 3D printed. An optical tracking system (Polaris Spectra, Northern Digital Inc., Canada) was used.
The detector of the gamma camera is a 4x4[cm^2] CdZnTe crystal with 256 square pixels. The collimator can be swapped, and for the experiments a tungsten one of 12[mm] length was used.
To calibrate the gamma camera a positioning table was used, where the gamma camera was mounted and a radioactive 57Co point source was moved with respect to the camera, to obtain the spatial response of each pixel of the camera (Figure 1).
The experients were done using a phantom with 3 hollow speheres filled with 0.5-1 [Mbq] of 99mTc. The phantom was scanned from 6 different postions, for 10 seconds each.
The reconstruction was then computed using MLEM with 20 iterations and a voxel size of 2.5x2.5x2.5mm3.

3 RESULTS

Five gamma scans were performed and compared with a CT scan of the phantom. A point based registration between the CT scan and the optical tracking target was used to align the coordinate systems.
The generated reconstruction of the spheres had a mean error below 6[mm] in all the spheres. In all five scans it was possible to reconstruct all three spheres.
Compared to the standard freehand SPECT, the errors are much lower, but also the total number of events captured by the gamma camera is almost 10 times higher.

4 DISCUSSION AND CONCLUSIONS

The results of this very first attempt of reconstructing freehand SPECT acquisitions with a gamma camera are very promising.
The improvement in the position localization even tough the very low activity in the spheres show that using a gamma camera is a huge improvement over the traditional single pixel detector. This could be seen not only as an image quality improvement, but also as a scanning time reduction or a reduction in the radioactive dose injected to the patient.
The trade off, is of course the weight of the camera (about 1[kg]). This can be solved using a robotic arm, or a mechanical construction to support it.
The use of a robotic arm enables the possibility of using optimized trajectories[3] or feedback loops that update the trajectory scans depending on the already acquired counts.
The robot used for the experiments is not a medical certified unit, and it does not fulfill the medical safety standards, so to perform experiments with humans, a medically certified unit will be needed.
Future applications could include intraoperative thyroid imaging and liver radioambolization using 99mTc MAA.

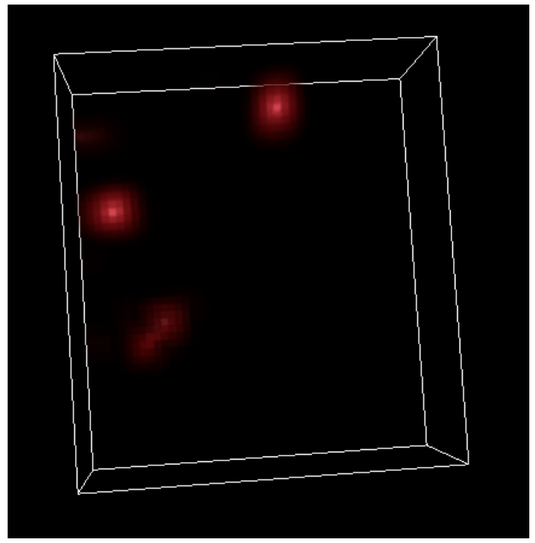

Figure 3: Reconstruction results.

5 ACKNOWLEDGEMENTS

This work was partially funded by DFG SFB 824 and DFG cluster of excellence MAP.

6 REFERENCES

[1] P. Matthies, K. Sharma, A. Okur, J. Gardiazabal, J. Vogel, T. Lasser, N. Navab: First use of mini gamma cameras for intra-operative robotic SPECT reconstruction. Proceedings of the 16th International Conference on Medical Image Computing and Computer Assisted Interventions (MICCAI), Nagoya, Japan, September 2013.
[2] J. Gardiazabal, T. Reichl, A. Okur, T. Lasser, N. Navab
First flexible robotic intra-operative nuclear imaging for image-guided surgery: Information Processing in Computer Assisted Interventions (IPCAI), Heidelberg, Germany, June 26, 2013.
[3] J. Vogel, T. Lasser, J. Gardiazabal, N. Navab. Trajectory optimization for intra-operative nuclear tomographic imaging. Medical Image Analysis 17(7):723-731, 2013.

CORRECTED JOINT SENSE RECONSTRUCTION, LOW-RANK CONSTRAINTS, AND COMPRESSED-SENSING-ACCELERATED DIFFUSION SPECTRUM IMAGING IN DENOISING AND KURTOSIS TENSOR ESTIMATION

V. Golkov (GSISH Member)
GE Global Research / Technische Universität München

Prof. Dr. Axel Haase * (Advisor), Prof. Dr. Daniel Cremers ** (Advisor), Dr. Marion I. Menzel *** (Advisor)

* Technische Universität München, IMETUM, Boltzmannstr. 11, 85748 Garching.
** Technische Universität München, Department of Computer Science, Boltzmannstr. 3, 85748 Garching.
*** GE Global Research, Freisinger Landstr. 50, 85748 Garching.

For the purpose of diffusion MRI denoising, the effects of low-rank contraints, line process denoising, and q-space compressed sensing on resulting diffusion weighted images and estimated kurtosis maps were demonstrated.

Each of the three methods showed both advantages and disadvantages in terms of image error, tensor stability and/or resolution.

Besides demonstrating specific effects of the methods, these results also led to the conclusion that the choice of the denoising method needs to be based on the final goals of the study.

1 INTRODUCTION

Signal-to-noise ratio (SNR) is a major challenge in diffusion MRI. For the purpose of SNR improvement, prior knowledge is incorporated into the reconstruction/postprocessing of diffusion-weighted images (DWIs). State-of-the-art prior knowledge formulations include low-rank constraints on the image series[1,2], finite-difference constraints based on common sparse edges for all DWIs (line process values)[2-5], and transform-domain sparsity of q-space data[6]. In the present work, we investigate the effects of these regularizations on resulting DWIs and on estimated diffusion and kurtosis tensors[7].

2 MATERIALS AND METHODS

As a low-rank constraint, truncated singular value decomposition (TSVD) of the M×Q matrix of reconstructed image magnitude values (M=#voxels, Q=#DWIs) was performed, keeping only L components whose linear combinations best represent the images, and discarding trailing (mostly noisy) components.

For comparison, SNR-enhancing joint SENSE reconstruction[3-5] (JSR) with corrections for intensity inhomogeneity and noise non-stationarity[5] was performed. Compressed sensing (CS) in q-space[6] was applied to the results of standard SENSE reconstruction (SR), of TSVD and of JSR.

The results of these methods were used for diffusion and kurtosis tensor[7] estimation using weighted linear least squares[8] up to bfit=5500mm/s2. A healthy volunteer scan was performed using a 3T GE MR750 clinical MR scanner (GE Healthcare, Milwaukee, WI, USA) equipped with a 32-channel head coil (single spin echo, TE=124.3ms, TR=1600ms, 96×96, slice=2.5mm, voxel size 2.5×2.5×2.5mm, ASSET factor 2, four repetitions) using diffusion spectrum imaging[9] 11×11×11 q-space cube, bmax=8000mm/s2 (convenient for estimation of orientation distribution function). Data of one scan repetition was undersampled in q-space with factor R=4 (Q=129) using a Gaussian pattern[6] before applying the compared methods. Ground truth was obtained by averaging three other standard SENSE-reconstructed repetitions (magnitude) and using fully sampled (R=1) q space data for tensor estimation.

3 RESULTS

TSVD visually outperformed SR (in terms of noise level) and JSR (in terms of feature preservation) – see Fig. 1. TSVD, followed by JS, outperformed SR also in terms of root-mean-squared error (RMSE) – see Fig. 3. TSVD fractional anisotropy (FA) maps are closest to ground truth.

However, TSVD yielded more kurtosis outliers than SR. JSR yielded the most stable tensor estimates, however at the expense of resolution. CS improved RMSE, and kurtosis stability. The most stable estimates were obtained by JSR+CS – see Fig. 2.

4 DISCUSSION

Diffusion model fitting has an intrinsic denoising effect by reducing Q=129 data points to a 22-parameter model in each voxel. Therefore, improving RMSE of the DWIs does not necessarily improve tensor stability, especially in the case of low-rank approximation, since model fitting operates similarly to low-rank approximation (reducing the degrees of freedom). The advantages and disadvantages of the compared methods are summarized in the following table:

method	advantage	disadvantage
TSVD	strongly improved RMSE	slightly reduced tensor stability
JSR	improved RMSE and tensor stability	reduced resolution
CS	improved RMSE and tensor stability	slightly modified kurtosis scale

Since the compared denoising methods have shown advantages and disadvantages, the choice of the method is an important decision and depends on the used quality assessment, which in turn depends on the final goals.

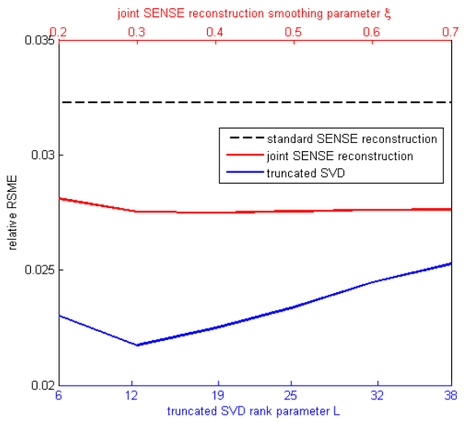

Figure 3: Root-mean-squared error (RMSE) in all DWIs of standard SENSE reconstruction, joint SENSE reconstruction (with different smoothing parameters ξ) and truncated singular value decomposition (with different rank parameters L), compared to ground truth (i.e. average of three other standard-reconstructed scan repetitions).

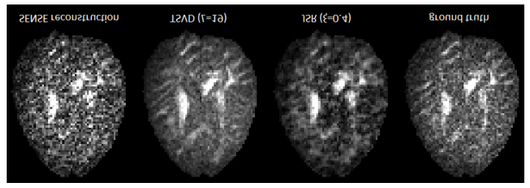

Figure 1: One of Q=129 DWIs after standard SENSE reconstruction, truncated singular value decomposition, and joint SENSE reconstruction, compared to ground truth (i.e. to average of three other standard-reconstructed repetitions).

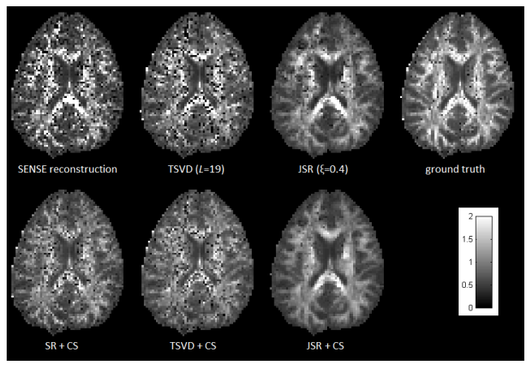

Figure 2: Radial kurtosis maps for standard SENSE reconstruction, truncated singular value decomposition, joint SENSE reconstruction, without q-space compressed sensing (top row) and in combination with q-space compressed sensing (bottom row), and for ground truth (top right).

5 ACKNOWLEDGEMENTS

Dr. Jonathan I. Sperl, Tim Sprenger, Anne Menini
Grant support: Deutsche Telekom Stiftung

6 REFERENCES

[1] H. Gao et al., 2013, Proc. ISMRM, 0610.

[2] F. Lam et al., 2013, MRM, in press.

[3] J.P. Haldar et al., 2013, MRM, 69:277-289.

[4] J.I. Sperl et al., 2012, Proc. ESMRMB, 265.

[5] V. Golkov et al., 2013, Proc. ESMRMB, in press.

[6] M.I. Menzel et al., 2011, MRM, 66:1226-1233.

[7] J.H. Jensen & J.A. Helpern, 2010, NMR-Biomed, 23(7):698-710.

[8] J. Veraart et al., 2011, MRM, 65(1):138-145.

[9] V.J. Wedeen et al., 2005, MRM, 54:1377-1386.

STEERING MECHANISM FOR ENDOVASCULAR TOOLS

E. C. Graf (GSISH Member)
Technische Universität München

T. C. Lüth* (Advisor), A. Knoll (Co-Advisor)**, V. Samper (Co-Advisor)***

* Technische Universität München, MiMed, Boltzmannstr. 15, 85748 Garching.
** Technische Universität München, Department of Informatics, Boltzmannstr. 3,85748 Garching.
*** GE Global Research, Freisinger Landstr. 50, 85748 Garching.

Several disorders of the cardiovascular system can be diagnosed and treated in a minimally invasive way with the use of cardiac catheters. Therefore, catheters must be inserted into the endovascular system and advanced to the target site.

Conventionally the operator manually pushes and rotates the catheters which allow uni- or bidirectional deflection of their tips.

However, these catheters have limited range and flexibility and the outcomes of the procedure depend on the operator's skills.

To overcome these limitations a mechanism for the remote steering of cardiac catheters with more degrees of freedom than conventional tip steering should be developed. To avoid damage of the heart and the vessels the mechanism should have an adaptive compliance.

As a first step a cardiac phantom for the evaluation of the steering mechanisms for cardiac catheters was built. The model representing the human anatomy was produced by molding of silicone.

1 INTRODUCTION

Minimally invasive medical technologies became increasingly popular because they offer advantages over conventional procedures such as less trauma, decreased pain for the patient and lower blood loss [1]. Several diagnostic and therapeutic procedures of the cardiovascular system can be performed by inserting a catheter through small incisions and advancing it to the target site inside the blood vessels. Those include imaging procedures that are based on intravascular ultrasound transducers as well as diagnosis and treatment of cardiac arrhythmias by electrophysiological mapping and ablation catheters [2]. Furthermore, tissue sampling and therapeutic cell delivery can be performed by catheters [3].

Cardiovascular catheters are introduced in the endovascular system at major vessels in the arm or the thighs and then advanced to the target site under x-ray fluoroscopy. Conventionally, the cardiologist stands next to the patient and rotates and pushes the catheter to reach the target. The operator can employ deflectable catheters that enable uni- or bidirectional bending of the catheter tip. Usually they have a fixed bending region and a limited bending radius. The tip is actuated by an integrated pull wire mechanism. The steering of the catheter tip can increase the success rates of the procedures [4] but the range and flexibility of the catheters is still limited and the outcomes rely on the operator's skill to manoeuver the tip and maintain stability at the target site [5].

2 NEW CONCEPT FOR REMOTELY STEERABLE CATHETER

To overcome these limitations the goal is to enable steering of the catheters with more degrees of freedom than conventional tip steering. In order to facilitate steering and positioning of the catheter in areas that are difficult to reach, either the position of the bending region should be selectable or two independently controlled bending regions should be available.

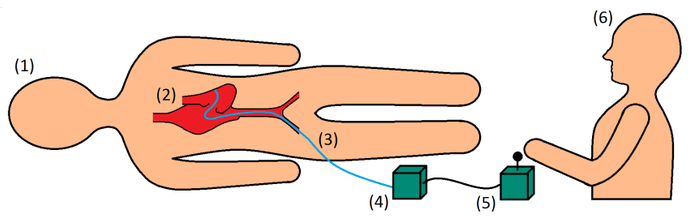

Figure 1: Scheme of the insertion of a remotely steered catheter into the right cardiac chamber (2) of the patient (1). The operator (6) inserts the catheter (3) via femoral access. He can control the catheter through a master console (5) and the actuation is transferred to the catheter by an actuation unit (4) that is located outside the patient.

The actuation mechanism should be integrated into a disposable catheter. Therefore, the mechanism must allow sufficient miniaturization. Furthermore, the mechanisms should be able to achieve a sufficiently small bending radius to enhance the mobility inside the spatially restricted cavity of the heart. To avoid damage of the heart and vessel walls the mechanisms may require an adaptive compliance to enable safe insertion of the catheter in a compliant state. On the other hand high stiffness and sufficient out-of-plane stability should be available when forces against the myocardial wall need to be maintained.

As a first step a cardiac phantom mimicking the human anatomy of a heart was built to facilitate the evaluation of catheters and steering mechanisms.

3 MATERIALS AND METHODS

The phantom was molded in silicone on the basis of a STL-file of a hollow heart. Tubes to resemble the vessels leading to and from the heart were attached to the model. The closed outer contour of the heart was used as a master form and models of the cavities of the heart chambers served as lost cores in the casting process.

The models were realized on a 3D printer (Spectrum Z510, 3D Systems, Rock Hill, USA) with a powder on gypsum basis (ZP131, 3D Systems, Rock Hill, USA). A silicone mold of the master form was built. The cores were then inserted into this mold and the cardiac model was produced with silicone VTX 950 (SLM Solutions, Lübeck, Germany), a transparent material with a shore hardness of 40. After the curing of the cardiac model the cores could be shattered and removed.

4 RESULTS

The silicone phantom of the heart including two completely separated cavities has the same dimensions as a human heart. Each of the chambers has three openings. Due to the surface roughness the phantom is not completely transparent but still allows visual tracing of devices inserted into the phantom. As the model is flexible and watertight it is suited for the simulation of heart motion and blood flow.

5 CONCLUSION

The goal of the project is to develop a steering mechanism for cardiac catheters. As a first step a hollow cardiac phantom for the evaluation of cardiac catheters was produced. The phantom is an anatomical representation of the heart with both chambers. Instruments can be inserted into the phantom through several openings.

Figure 2: Cardiac phantom made of silicone with a shore hardness of 40. The silicone heart consists of two completely separated cavities that represent the heart chambers. An instrument was inserted into the right heart chamber through one of its three openings.

6 ACKNOWLEDGEMENT

I would like to thank Arne Menz for the virtual model and Daniel Roppenecker for his support with the printing and molding of the phantom.

7 REFERENCES

[1] J. G. Webster, Minimally Invasive Medical Technology. London: Institute of Physics Publishing, 2001.

[2] M. J. Kern, The Cardiac Catheterization Handbook. Philadelphia: Saunders Elsevier, 2011.

[3] W. Sherman, T. P. Martens, J. F. Viles-gonzalez, and T. Siminiak, "Catheter-based delivery of cells to the heart," Nature, vol. 3, no. March, pp. 57–64, 2006.

[4] C. Piorkowski, H. Kottkamp, J.-H. Gerds-Li, A. Arya, P. Sommer, N. Dagres, M. Esato, S. Riahi, S. Weiss, S. Kircher, and G. Hindricks, "Steerable sheath catheter navigation for ablation of atrial fibrillation: a case-control study.," Pacing and clinical electrophysiology : PACE, vol. 31, no. 7, pp. 863–873, Jul. 2008.

[5] Y. Fu, H. Liu, W. Huang, S. Wang, and Z. Liang, "Steerable catheters in minimally invasive vascular surgery," The International Journal of Medical Robotics and Computer Assisted Surgery, vol. 5, no. 4, pp. 381–391, Dec. 2009.

3-D OPERATION SITUS RECONSTRUCTION WITH TIME-OF-FLIGHT SATELLITE CAMERAS

S. Haase (GSISH Member)
Friedrich-Alexander-Universität Erlangen-Nürnberg / Technische Universität München

J. Hornegger* (Advisor), H. Feußner** (Co-Advisor)

* Pattern Recognition Lab, Friedrich-Alexander-Universität Erlangen-Nürnberg, Martensstrasse 3, 91058 Erlangen.
** Technische Universität München, Klinikum rechts der Isar, Ismaninger Str. 22, 81675 München.

Minimally invasive procedures are of growing importance in modern surgery. Orientation is a major issue during these interventions as conventional endoscopes only cover a limited field of view.

We propose the application of a Time-of-Flight (ToF) satellite camera at the zenith of the pneumoperitoneum to survey the operation situs. Due to its limited field of view we propose a data fusion of different 3-D views to reconstruct the situs using photometric and geometric information. We are able to reconstruct the entire abdomen with a mesh-to-mesh mean error of less than 5mm compared to CT ground truth data, at a frame rate of 3Hz.

The framework was evaluated on real data from a miniature ToF camera in an open surgery pig study and for quantitative evaluation with a realistic human phantom. With the proposed approach to operation situs reconstruction we improve the surgeons' orientation and navigation within the human body and therefore speed up surgical interventions and increase safety.

1 INTRODUCTION

Navigation and orientation are of particular relevance for the surgeons in minimally invasive surgery due to the limited field of view with conventional endoscopes. To improve both, different concepts to insert additional cameras have been introduced [1,2] . For instance, Cadeddu et al. describe a video camera that is positioned on the posterior abdominal wall and guided by an anterior magnetic device. Instead, we propose the concept of 3-D Time-of-Flight (ToF) satellite cameras as illustrated in Fig.1. Nevertheless, due to size limitations in endoscopic procedures those satellite cameras still have shortcomings related to the hardware and optical systems. One of these is a very narrow field of view. To expand the limited field of view the camera will reconstruct the entire situs initially and then focus on the operation site. We use a truncated signed distance function (TSDF) [3] to reconstruct the interior abdominal space. For improved robustness we enhance the TSDF with confidence weights and integrate both the 3-D range data and photometric information measured by the ToF camera.

2 MATERIALS AND METHODS

ToF devices exhibit a low signal-to-noise ratio. Therefore, preprocessing range data is an essential step. We apply a real-time capable data enhancement pipeline for image denoising and defect pixel interpolation. To use the photometric information of the ToF sensor the data is normalized as their intensities depend on the distance.
The preprocessed data deliver photogeometric information of the situs from different points of view. For estimating the rotation and the translation between two successive frames, we apply an approximate iterative closest point (ICP) implementation on the GPU based on the random ball cover for efficient nearest neighbor search.

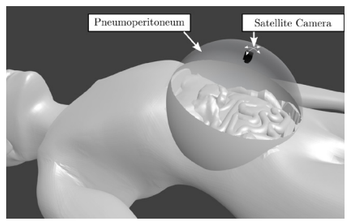

Figure 1: Illustration of the 3-D Time-of-Flight satellite camera hovering above the situs at the zenith of the pneumoperitoneum.

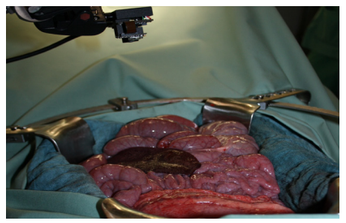

Figure 2: Experimental setup for acquiring in-vivo data in a pig study. Note the physical dimension of the miniature ToF camera.

The estimated transformations are used for data fusion to transform each 3-D point into a common coordinate system. The entire reconstruction is based on a volumetric model defined by a TSDF as described in [3] to fuse data in a frame-to-model manner, i.e. the current frame is not registered to the previous frame directly but to a raycasted image of the fused model seen from the camera of the previous frame. The TSDF is based on an implicit surface representation given by the zero level set of an approximated signed distance function of the acquired surface. In addition to the distance value, our approach stores and fuses photometric information. This enables photogeometric data fusion in a frame-to-model manner. For robust data fusion we assign a confidence weight to each TSDF value to describe the reliability of the new measurement. Here, we exploit three characteristics of ToF cameras. With higher distances to the center or lower photometric values the confidence decreases. To benefit from different views of the same observed area we merge successive TSDF values to provide temporal denoising.
The experiments are split into two major parts. On the one hand we acquired real in-vivo data in a pig study to evaluate the preprocessing of the sensor combined with the proposed 4-D fusion framework, see Fig.2. On the other hand for quantitative evaluation we acquired real data of a human phantom and compared it to CT ground truth data. For our experiments we used a CamBoard Nano miniature ToF camera from PMD Technologies GmbH, Siegen, Germany. It acquires ToF data with 60Hz with a resolution of 160×120px. As the current PMD CamBoard Nano device exceeds the physical dimension needed for minimally invasive surgery we performed our experiments in an open surgery scenario.

3 RESULTS

To illustrate the performance on real in-vivo data we reconstructed the abdomen of a pig, see Fig.3. The scene was reconstructed from 25 frames acquired from different camera positions.
In our experiments with CT ground truth data we achieved a mesh-to-mesh mean distance error of 4.73mm. Note that higher distance errors are located at the boundary of the reconstruction that was observed from one perspective only.

4 CONCLUSIONS

With experiments on real ToF data we have illustrated that our framework is capable to provide reliable reconstructions even in the presence of severe noise. Nevertheless, systematic errors in the measured ToF data and insufficient data at the boundary lead to locally imperfect reconstructions with higher mesh-to-mesh distance.
Future work will investigate the upcoming generation of miniaturized ToF cameras that are expected to have the geometry to fit through a trocar.

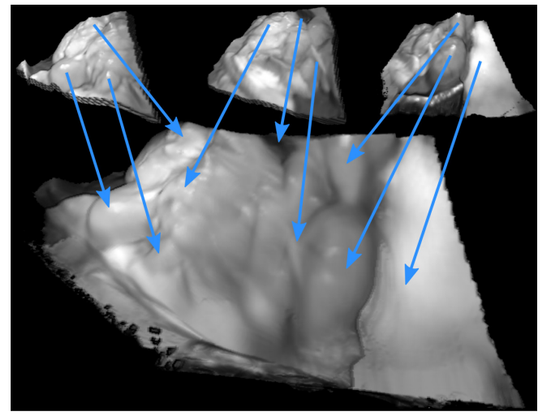

Figure 2: The first row depicts three single frames of a 25-frames ToF sequence, acquired in an experimental in-vivo pig study. Below, the reconstructed operation situs is illustrated. Note that recognizable shapes of individual frames are explicitly reconstructed.

5 ACKNOWLEDGEMENTS

We gratefully acknowledge the support by the Deutsche Forschungsgemeinschaft (DFG) under Grant No. HO 1791/7-1. This research was funded/supported by the Graduate School of Information Science in Health (GSISH) and the TUM Graduate School. The authors gratefully acknowledge funding of the Erlangen Graduate School in Advanced Optical Technologies (SAOT) by the DFG in the framework of the German excellence initiative. We thank the Dr. Pfleger Stiftung for their partial support.

6 REFERENCES

[1] Oleynikov, D. et al.: Miniature robots can assist in laparoscopic cholecystectomy. Surgical Endoscopy 19(4) (April 2005) 473-476.

[2] Cadeddu, J. et al.: Novel magnetically guided intra-abdominal camera to facilitate laparoendoscopic single-site surgery: initial human experience. Surgical Endoscopy 23 (2009) 1894-1899.

[3] Newcombe, R.A. et al.: KinectFusion: Real-time dense surface mapping and tracking. In: 10th IEEE International Symposium on Mixed and Augmented Reality. (October 2011) 127-136.

MODELING OF DETECTION PHYSICS IN FREEHAND SPECT RECONSTRUCTIONS

A. Hartl (GSISH Member)
Technische Universität München

N. Navab* (Advisor), S. Ziegler** (Advisor)

* Technische Universität München, Department of Informatics, Boltzmannstr. 3, 85748 Garching.
** Technische Universität München, Klinikum rechts der Isar, Ismaninger Str. 22, 81675 München.

Nuclear imaging is an important tool in todays cancer diagnostics, however in intra operative settings they suffer from drawbacks. Tomographic imaging like SPECT (Single Photon Emission Computed Tomography) and PET (Positron Emission Tomography) or too bulky for the intra operative setting and have too high acquisition times. On the other hand hand held probes and cameras only offer 1D and 2D imaging.

To offer 3D nuclear imaging during an intervention Freehand SPECT was developed. It combines a hand held gamma probe with an optical tracking system to receive the measurements of the probes synchronized with the position and orientation of the probe. This combined information is used to compute a tomographic reconstruction.

However in contrast to conventional tomographic systems the acquisition geometry is not fixed, which makes it necessary to compute the system matrix on the fly. For that accurate and computationally fast models of the detection physics are needed.

1 INTRODUCTION

Freehand SPECT is a new imaging modality which was developed to bring nuclear tomographic imaging into surgery [1]. Like SPECT it provides 3D functional imaging and employs gamma-ray emitting radiotracers. Freehand SPECT uses a hand held gamma-ray detecting probe with an optical tracking target attached to it. An optical tracking system provides the position and orientation of the probe which is synchronized with its readings. The combined data can then be used to compute a tomographic reconstruction of the radiotracer.
However in contrast to conventional tomographic systems Freehand SPECT has no gantry to provide a predefined acquisition geometry. Instead the probe is moved by hand and measurements are acquired at arbitrary positions. This makes it necessary that the system matrix is computed on the fly for each particular set of measurements. Hence the conventional methods to generate the system matrix are not directly applicable or have to be adapted to this situation. Furthermore the system was designed to be used during an intervention, which makes the computation time of the system matrix a limiting factor. In order to achieve this, computationally fast models of the detection process of the probe are required to generate the system matrix.
In addition the freehand acquisitions are incomplete and the quality of the reconstruction is highly dependent on the acquisition geometry. However the latter is extremely operator dependent and acquisition geometries are not reproducible.

2 MATERIALS AND METHODS

For this work two models of the detection physics for a low energy gamma probe with a scintillating crystal as detector were used. For the first model (M1) the assumption is made that the shielding around the detector is perfect, so only rays that pass through the unshielded front of the probe can be detected. The amount of radiation that reaches the detector from a single point source is then determined by the solid angle subtended by the point source and the front of the detector. The solid angle is computed with the distance (d) between source and probe and the radius (r) of the circle shaped front of the probe. Further the sensitivity of the probe towards the point source is influenced by the angle between the source and the probe. On the one hand the solid angle will decrease with increasing inclination angle between the source and the probe, which is approximated with the cosine factor of the angle. On the other hand the sensitivity of the detector towards the probe is affected as the mean length that rays pass through the detector and thus the probability for a detection changes. This effect is computed with the length of the cylindrical detector. In the second model (M2) the assumption of the perfect shielding is dropped. To compute the effects in the shielding and to model the detection process more accurately the mean lengths that rays take through the shielding and the detector are computed.
These lengths depend on the position of the source with respect to the probe. To get an approximation of these lengths some exemplary rays are considered which divide the detector/shielding into partitions in which these lengths change smoothly. The third model (M3) is a simple look up table of measurements acquired from a point source. During the reconstruction process the relative position of the probe to a voxel is computed and the respective measurement of the look up table is taken for the reconstruction.
Reconstructions are performed with Maximum Likelihood Expectation Maximization algorithm [2].

3 RESULTS

To evaluate the impact of the acquisition geometry and the detection models on Freehand SPECT reconstructions six sets of three measurements each from a phantom were acquired. The phantom consists of a box in which hollow spheres filled with a radioactive solution can be fixed on screws. Two hollow spheres (volume 250µl, diameter 9.86mm) were filled with of a solution of Tc99m with an activity of 0.5 MBq each. The spheres were then fixed in the middle of the box with 1.4cm distance between the centers of the spheres For the first set only measurements from one side of the box were acquired, for the second set measurements from two sides and for the following sets measurements from further sides were acquired without changing the total duration of three minutes (~3000 measurements each). With the acquired measurements both models were then used to perform a reconstruction of the activity distribution.

For the reconstruction a MLEM algorithm with 20 iterations was used to solve the system of linear equations. For the evaluation a CT scan of the phantom was made and registered with the reconstruction volume to serve as ground truth for the position of the sources. With the model M1 it was not possible to get correct reconstructions with the first two data sets where measurements were only acquired from one and two sides of the phantom, while model M2 was able to give roughly the correct location of the activity even with the first data set (Figure 1).

The data sets were three or more sides of the phantom were scanned with the probe produced useful reconstructions with both models, however the quality of the reconstructions did only increase slightly by scanning more than three sides. In the reconstructions with M1 it was mostly not possible to separate the spheres in the reconstruction while with M2 and M3 it was possible for most acquisitions where measurements were taken from at least three sides of the phantom, however the reconstructions with M1 and M2 produced less artifacts and were more smooth.
By computing the center of mass of the reconstructed activity and the sources the error in the position was determined. Model M2 and M3 reconstructed the position of the spheres better with a mean error of 4.8mm versus a mean error 6.5mm in the reconstructions with M1.

4 DISCUSSION

The results of the experiments show that model M1 is much more sensitive to the acquisition geometry of a scan than model M2 and M3. With measurements from three different sides all models provide good results but model M2 and M3 can separate the spheres better in the reconstructions. However in terms of computational time the model M1 and M3 are superior to model M2 which was about three times slower. With a precomputed look up table of M2 the computational time can be reduced to match that of the other models. For model M3 additional hardware for the acquisition of the look up table is required and an accurate acquisition will take several days.

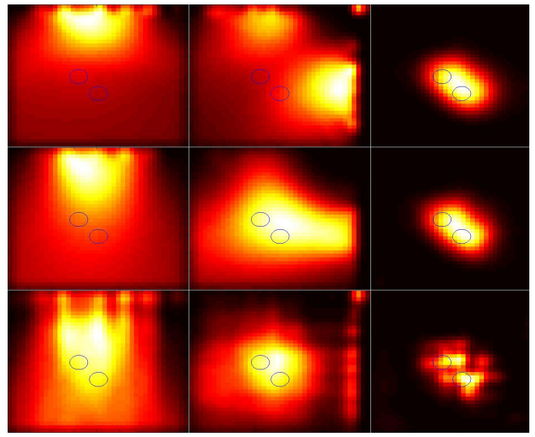

Figure 1: Slices of reconstructions with the models. From left to right one, two and three sides were scanned. From top to bottom models M1, M2 and M3 were used. The circles indicate the real positions of the spheres.

Model	M1	M2	M3
1 side	21.7 mm	15.3 mm	17.8 mm
2 sides	16.4 mm	13.2 mm	14.2 mm
3 sides	6.5 mm	4.8 mm	4.8 mm

Table 1: Error in the position of the spheres for all models with 1-3 sides scanned.

6 REFERENCES

[1] T. Wendler et. al. Proceedings of MICCAI 2007.

[2] L. A. Shepp Y V 1982 IEEE Transactions on Medical Imaging 1, 113122.

BOLD-BASED MAGNETIC RESONANCE IMAGING OF HYPOXIA IN THE HUMAN BRAIN

N. Hirsch (GSISH Stipend Holder)
Technische Universität München

A. Haase* (Advisor), C. Zimmer** (Co-Advisor)

* Technische Universität München, IMETUM, Boltzmannstr. 11, 85748 Garching.
** Technische Universität München, Klinikum rechts der Isar, Ismaninger Str. 22, 81675 München.

Hypoxia is a tissue state that is characterized by a pathological shortage of oxygen. It can occur for example in brain tumors or stroke and is useful for the prognosis of the course of disease.

In this project, existing, preclinical methods for hypoxia imaging have been assessed, adapted and optimized for application in the clinic, with the focus on robustness and short acquisition times.

Identification of hypoxic tumor niches as well as the detection of areas with decreased oxygen supply in stroke could be achieved.

With the investment of a few minutes of extra measurement time, additional valuable diagnostic information could thus be extracted from MR patient examinations.

1 INTRODUCTION

Hypoxia is a pathological state where a shortage of oxygen in the tissue prevents normal metabolic function. Hypoxic niches in brain tumors that emerge either spontaneously or are caused by anti-angiogenic treatment promote the proliferation of tumor cells [1]. Knowledge about the existence and the location of hypoxic spots is useful for tumor surgery planning in order to remove preferably the most aggressive tumor parts [2]. Hypoxia is also of use in stroke for the differentiation between affected but viable and irreparably damaged tissue where such information could be very helpful for further treatment decisions [3].

Methods in clinical use for the detection of hypoxia rely on immunohistochemical methods [4] or positron emission tomography [5], where the former includes resection of biopsy samples during surgery and the latter requires injection of a radioactive tracer. Magnetic resonance imaging offers a more patient-friendly option: The tissue tries to compensate the shortage of oxygen by locally increasing the oxygen extraction from blood into tissue. Since deoxyhemoglobin is paramagnetic, the magnetic susceptibility of venous blood is altered by this process. The resulting changes in the local magnetic field can be detected.

2 MATERIALS AND METHODS

An imaging protocol has been developed in phantom, volunteer and patient studies where all required parameters – the transverse relaxation times T2 and T2* as well as the cerebral blood volume CBV – are measured independently. Fast multi-slice imaging for T2 and T2* quantification and a routine DSC scan for CBV quantification were used for this purpose.

The measurements can be appended to a routine clinical patient examination with an additional acquisition time of a few minutes, thus minimizing the extra strain on patients [6].

Major confounding factors like magnetic field inhomogeneities due to local susceptibility differences [7], patient motion and effects arising from the pathological state of tissue have been addressed in the protocol as well as in the post-processing of the acquired data [6].

3 RESULTS

Whole-brain maps of diagnostic quality showing relative differences in the oxygen extraction were obtained for brain tumor and stroke patients [6, 8]. Identification of hypoxic spots in tumorous tissue was possible with the combined information from the maps and from structural images (Fig. 1). Preliminary validation using immunohistochemical methods showed promising results [6, 8].
Application in stroke and stenosis patients revealed extensive tissue areas around the focal ischemic core that are inadequately supplied with oxygen (Fig. 2) [6].

4 CONCLUSION

A clinically applicable protocol to map the oxygen extraction fraction in the brain with magnetic resonance imaging based on magnetic susceptibility differences of oxygenated and deoxygenated blood has been explored.
Although this approach currently does not enable absolute quantification, mainly due to partial volume effects and strong local background gradients and because of model simplifications and assumptions that might not be satisfied everywhere in the brain, relative oxygen extraction fraction maps obtained with the developed protocol add valuable diagnostic information to routine patient examinations.

5 REFERENCES

[1] Heddleston JM, Li Z, McLendon RE, et al. The hypoxic microenvironment maintains glioblastoma stem cells and promotes reprogramming towards a cancer stem cell phenotype. Cell Cycle, 8:3274 – 82, 2009, DOI: 10.4161/cc.8.20.9701
[2] Jensen RL. Brain tumor hypoxia: tumorigenesis, angiogenesis, imaging, pseudoprogression, and as a therapeutic target. J Neurooncol, 92:317 – 35, 2009, DOI:10.1007/s11060-009-9827-2
[3] Markus R, Reutens DC, Kazui S, et al. Hypoxic tissue in ischaemic stroke: persistence and clinical consequences of spontaneous survival. Brain, 127:1427 – 36, 2004, DOI: 10.1093/brain/awh162
[4] Bar EE, Lin A, Mahairaki V, et al. Hypoxia increases the expression of stem-cell markers and promotes clonogenicity in glioblastoma neurospheres. Am J Pathol, 177:1491 – 1502, 2010, DOI: 10.2353/ajpath.2010.091021
[5] Raichle ME and Mintun MA. Brain work and brain imaging. Annu Rev Neurosci, 29:449 – 76, 2006. DOI: 10.1146/annurev.neuro.29.051605.112819
[6] Hirsch NM, BOLD-based Magnetic Resonance Imaging of Hypoxia in the Human Brain - Adaptation of Measurement and Data Analysis Strategies for Clinical Requirements. Dissertation, 2013
[7] Hirsch NM, Preibisch C. T2* mapping with background gradient correction using different excitation pulse shapes. AJNR, 2012, Epub ahead of print, DOI 10.3174/ajnr.A3021
[8] Tóth V, Förschler A, Hirsch NM, et al.. MR-based hypoxia measures in human glioma. J Neurooncol, 2013, Epub ahead of print, DOI 10.1007/s11060-013-1210-7

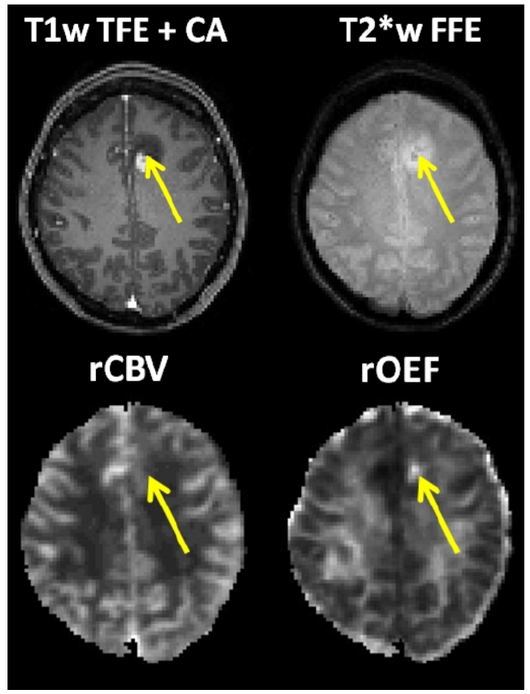

Figure 1: Single slice in a glioblastoma patient. The T1-weighted turbo field echo image after contrast agent application (T1w TFE+CA) shows partial CA enhancement in the tumor. A small hot spot marked by an arrow is visible in the relative oxygen extraction fraction (rOEF) map. Since it is located in a hyperintense region in the T2*-weighted fast field echo (T2*w FFE) image outside of edema and has moderate relative CBV (rCBV), it is a potentially hypoxic spot in non-enhancing tumor tissue. Figure from [6].

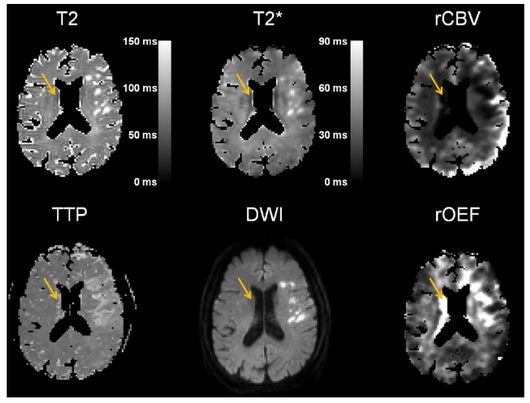

Figure 2: Single slice in a patient with subacute ischemic stroke. Input maps for rOEF calculation (T2, T2*, rCBV) are shown at the top. Time to peak (TTP) and diffusion weighted (DWI) images are shown for comparison of visible ischemic areas with potentially hypoxic areas. The arrow marks a potentially hypoxic area contralateral to the ischemic core. Figure from [6].

QUANTIFICATION METHODS FOR TIME-RESOLVED METABOLIC MAGNETIC RESONANCE IMAGING USING HYPERPOLARIZED [1-^{13}C]PYRUVATE

O. Khegai (GSISH Stipend Holder)
Technische Universität München

Prof. Dr. Steffen Glaser* (Advisor), Prof. Dr. Sibylle Ziegler** (Co-Advisor)

* Technische Universität München, Department of Chemistry, Lichtenbergstraße 4, 85748 Garching.
** Technische Universität München, Klinikum rechts der Isar, Ismaninger Str. 22, 81675 München.

Dissolution dynamic nuclear polarization enables real-time non-invasive measurement of metabolic fluxes using magnetic resonance spectroscopy. Quantitative kinetic information of in vivo metabolism is of great interest for medicine as a key characteristic of some diseases.

In this work, comprehensive methods for the data acquisition, quantification, interpretation and visualization of dynamic ^{13}C metabolite signals in vitro and in vivo were developed, with an emphasis on spatially resolved apparent rate constant mapping, using the example of hyperpolarized [1-^{13}C]pyruvate.

This novel type of quantitative contrast comprehensively visualizes metabolic activity of underlying tissues and organs. In comparison to individual metabolite images, apparent rate constant maps emphasize metabolically active tissues and suppress regions of high perfusion but low conversion (e.g. blood vessels).

Based on high metabolic activity of the tumor, its location can be clearly identified from the apparent rate constant maps.

1 INTRODUCTION

Dissolution dynamic nuclear polarization (DNP) enables MR signal enhancement of [1-^{13}C]pyruvate in liquid state by up to five orders of magnitude compared to thermal equilibrium [1]. High sensitivity of this technique allows in vivo measurement of metabolic fluxes in real time using magnetic resonance spectroscopy [2]. Biologically, after injection and perfusion, pyruvate is absorbed by tissues and enzymatically metabolized into downstream metabolites such as lactate, alanine, and bicarbonate. Quantitative kinetic information of pyruvate metabolism in tissue is of great interest as a key characteristic of some diseases. Therefore, the aim of this work is to develop comprehensive methods for the quantification, interpretation and visualization of dynamic hyperpolarized ^{13}C metabolite signals.

2 MATERIALS AND METHODS

Temporally resolved spectral-spatial data were acquired using IDEAL spiral chemical shift imaging (CSI) [3]. Applying a two-site exchange kinetic model [4], the temporal dimension is compressed into two characteristic rate constants:

i) the apparent build-up rate of downstream metabolites from pyruvate $k_{pyr\to m}$, and

ii) an effective decay rate $R_{eff,m}$ describing the cumulative effect of repetitive excitation, T_1-relaxation and backward conversion. In a time-discretized formulation this leads to following rate equation:

$$da_m(t)/dt = +k_{pyr\to m}a_{pyr}(t) - R_{eff,m}a_m(t)$$

(1) with a_{pyr} and a_m denoting signals of the pyruvate substrate and a certain downstream metabolite *m*, respectively. Transforming the Eq. (1) from time to frequency domain results into:

$$i\Omega\tilde{a}_m(\Omega) = +k_{pyr\to m}\tilde{a}_{pyr}(\Omega) - R_{eff,m}\tilde{a}_m(\Omega)$$

(2)

with $\tilde{a}_{pyr}(\Omega)$ and $\tilde{a}_m(\Omega)$ fourier transform of $a_{pyr}(t)$ and $a_m(t)$.

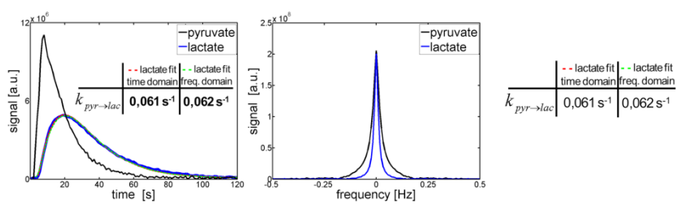

Figure 1: Typical in vivo metabolite signals in tumor area in time (left) and frequency (right) domains. The similar signal intensity of pyruvate and lactate at Ω = 0 in frequency domain can be explained by the estimated ratio $k_{pyr\to lac}/\bar{R}_{eff,lac} = \tilde{a}_{lac}(0)/\tilde{a}_{pyr}(0) \approx 1$

Both in time and frequency domain, Eq. (1) and (2) lead to over-determined systems of linear equations, which can be solved for $k_{pyr\to m}$ and $R_{eff,m}$ using the Moore-Penrose pseudo-inverse. Interestingly for Ω = 0, Eq. (2) provides a clear physical interpretation of the often used ratio of time-integrated metabolite signals

$$\int a_m(t)\,dt / \int a_{pyr}(t)\,dt = \tilde{a}_m(0)/\tilde{a}_{pyr}(0) = k_{pyr\to m}/R_{eff,m}$$

(3)

Conceptually, the proposed kinetic model accounts for variable inflow and outflow of pyruvate but assumes them to be the same (or negligible) for the downstream metabolite *m*. This formulation decouples the kinetics between pyruvate and its metabolic products into single differential equations. As a consequence, in this description no explicit arterial input function is required, as it is implicitly contained in the pyruvate signals.

3 RESULTS

Typical metabolite signals in time and frequency domain are illustrated in Fig. 1, demonstrating a sparse, DC-centered signal representation in the frequency domain. The main advantage of the frequency description is a natural compression of the signal dynamics into a few dominant Fourier coefficients and the avoidance of time differentiation, which generally results in noise amplification.

Figure 2 displays tumor slices in four rats in the form of time-integrated metabolite images of pyruvate (a) and lactate (b), ratios of time-integrated signals of lactate and pyruvate normalized by an average decay rate $\bar{R}_{eff,lac} = 0.1\,s^{-1}$ (c) and apparent build-up rate constant maps of lactate estimated in time (d) and frequency (e) domain. The data are displayed in form of image overlays using a high resolution gradient echo image of identical scan geometry as anatomical reference. The apparent build-up rate constant maps comprehensively visualize metabolic activity of underlying tissues and organs in a quantitative and spatially resolved manner. Eq. (3) shows the linear relationship between the apparent build-up rate constant and the ratio $R_{eff,m}$ of time-integrated metabolite signals with the apparent decay rate as a proportional coefficient. The later can be estimated from signal depletion due to repetitive excitation and assuming a constant T_1 relaxation time for lactate and negligible backward conversion as $\bar{R}_{eff,lac} \approx 0.1\,s^{-1}$.

The improved contrast provided by the apparent build-up rate maps (d,e) clearly identifies the tumor location as regions of enhanced metabolism with $k_{pyr\to lac} \approx 0.1\,s^{-1}$. Similar contrast behavior was obtained from the ratio of time-integrated metabolite signals normalized by the averaged decay rate (c).

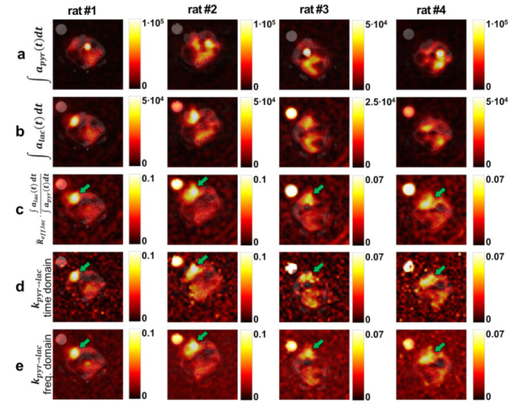

Figure 2: Time-integrated metabolite maps of pyruvate and lactate (a,b, in a.u.), normalized by $\bar{R}_{eff,lac} = 0.1\,s^{-1}$ ratio of time-integrated metabolite signals (c, in s-1), and time (d, in s-1) and frequency (e, in s^{-1}) domain derived apparent build-up rate constant maps of lactate in tumor slices of 4 different animals. A syringe containing [1-^{13}C]lactate (at the top-left corner of each image) was used as a reference for both 13C and proton images. High apparent build-up rate constants in the tumor (green arrows) indicate its high metabolic activity.

4 CONCLUSIONS

The proposed quantification methods were successfully applied to in vivo tumor rat experiments and demonstrates a new type of quantitative contrast displaying metabolic activity. Compared to the averaged metabolite maps, they allowed accurate visualization of quantitative metabolic information. Based on high metabolic activity of the tumor, its location was clearly identified from the metabolic rate constant maps. The obtained conversion rates in the tumor region depend on many factors, such as perfusion, tumor type and stage, and are specific for each animal. The utility of apparent build-up rate constant mapping for the non-invasive localization and characterization of tumors and their response to therapy needs to be further investigated in dedicated studies.

5 REFERENCES

[1] JH Ardenkjaer-Larsen et. al., PNAS 100:10158(2003).
[2] K Golman et al, PNAS, 100:10435(2003).
[3] F Wiesinger et. al. MRM 68(1):8-16(2012).
[4] SE Day et. al., Nat Med 13(11):1382-1387(2007).

DYNAMIC PET RECONSTRUCTION FOR COMBINED PET/MR DATA OF A [18F]-FET GLIOMA PATIENT

R. Kraus (GSISH Member)
Technische Universität München

Prof. S. I. Ziegler**(Advisor), Prof. N. Navab* (Co-Advisor)

* Technische Universität München, IMETUM, Boltzmannstr. 11, 85748 Garching.
** Technische Universität München, Klinikum rechts der Isar, Ismaninger Str. 22, 81675 München.

Dynamic (time-dependent) imaging is a prerequisite for extraction of biological kinetic parameters from PET, e.g., for improved diagnosis of brain glioma patients. However, conventional dynamic PET based on independent frame reconstruction suffers from noisy images especially when a high temporal resolution is needed. This work investigates fully 4D image reconstruction of [18F]FET data acquired with a hybrid Siemens Biograph mMR PET/MR scanner.

The work presented here is in progress. Future work will investigate use of MR-based anatomical regularization and non-linear models. Correlation of parametric FET images with tumor grading will be addressed.

1 INTRODUCTION

Dynamic positron emission tomography (PET) acquires a time series of 3D data for imaging the temporal evolution of radiotracer activity in tissue. Using pharmacokinetic modeling of tissue time activity curves (TACs), biologically relevant parameters can be extracted that describe the uptake kinetics of the injected radiotracer. Especially, reliable parametric images obtained from voxel-wise curve fitting are of high interest. But generation of such images is challenging due to the inherent noise in PET data, and thus post-reconstruction modeling often results in high variance and severe bias. Direct parametric reconstruction algorithms have been developed that reconstruct parametric images directly from sinograms [1]. This work investigates the application of linear spectral analysis models in a direct reconstruction algorithm [2] for clinical [18F]FET data acquired from the PET/MR scanner.

2 MATERIALS AND METHODS

Given a dynamic sequence *{yl}* of sinograms for each time frame *l*, a geometric system matrix *P = (pij)*, and a spatiotemporal linear model

$$\lambda_{X_{jl}} = \sum_k b_k \, a_{jk}$$

with a fixed set of temporal basis functions b^k, the coefficients of the k^{th} basis function for the j^{th} voxel are iteratively updated by

$$a_{jk}^{(n+1)} = \frac{a_k^{(n)}}{s_j \sum b_k} \sum_l b_k \sum_i p_j \frac{y_l}{n_l + \sum p_j \sum b_k \, a_{jk}^{(n)}}$$

A spectral analysis model is used with 50 exponentially decaying basis functions convolved with the input function $C_a(t)$ modeling the activity concentration in each voxel by

$$C_j(t) = \sum_{k=1}^{K} a_{jk} \int_0^t C_a(\tau) e^{-\beta_k (t-\tau)} d\tau,$$

where *ßk* are logarithmically-spaced between (*λ*s-1, 0.1 s-1] with decay constant *λ*. A blood volume term is added to the basis functions. Parametric images of tracer influx K_1 and volume of distribution (VD) are calculated from the estimated a_{jk} and compared with conventional post-reconstruction spectral analysis fitting (NNLS). An OS-EM algorithm with correction for random and scatter was used. A 40 min dynamic [18F]FET scan of a patient with a glioblastoma in the frontal lobe was acquired with the mMR. List mode data were binned to 21 frames (1×5 s, 9×10 s, 3×30 s, 1×2 min, 7×5 min). The dynamic algorithm was implemented in an in-house developed reconstruction framework tailored to mMR data. The 3D PET data were converted using Single Slice Rebinning to accelerate reconstruction.

3 RESULTS

An image derived input function was extracted from frame-wise OSEM reconstructed images by defining an internal arterial carotid region in the simultaneously acquired MR image.

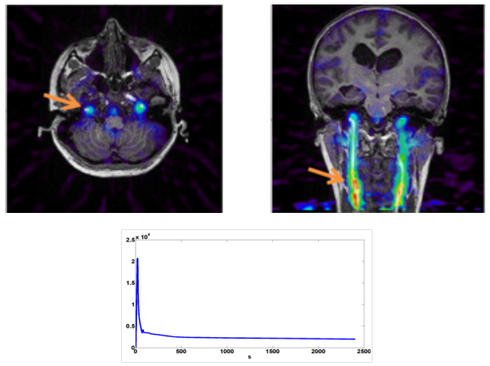

Figure 1: Image derived input function obtained from a manually drawn carotid region in the PET overlaid with the MR image (MPRAGE high contrast).

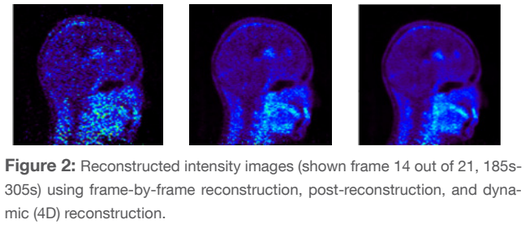

Figure 2: Reconstructed intensity images (shown frame 14 out of 21, 185s-305s) using frame-by-frame reconstruction, post-reconstruction, and dynamic (4D) reconstruction.

Dynamic PET reconstruction of intensity images shows significant improvement over both frame-by-frame and post-reconstruction modeling. Analysis of homogeneous ROIs (cerebellum, tumor) shows reduced standard deviation for the dynamic method (4X less noisy in longer frames and 8X in shorter frames) and good time activity curve fitting.

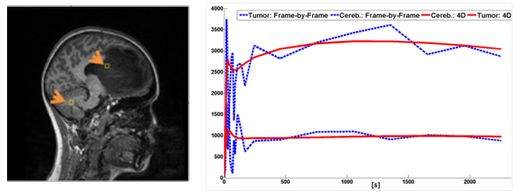

	Frame 11 (30s)		Frame 14 (120s)	
	Cerebellum	*Tumor*	*Cerebellum*	*Tumor*
Frame-by-frame recon.	84.8%	79.6%	41.0%	45.2%
Post recon. modeling	28.8%	27.2%	20.8%	19.0%
Dynamic recon.	10.5%	9.8%	10.3%	9.2%

Figure 3: MPRAGE image with ROI in cerebellum and tumor (3×3×3 voxels) used for evaluation (upper left), relative standard deviation of intensity images in ROIs (upper right), time activity curves for dynamic vs. frame-by-frame reconstruction in ROIs (bottom).

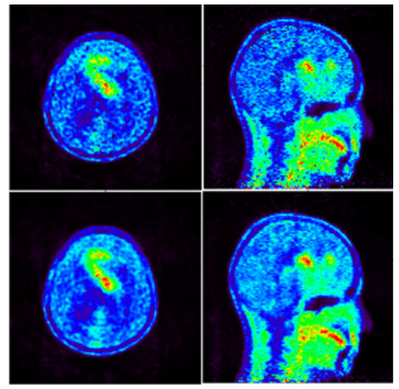

Figure 4: Parametric VD image in transversal and sagittal view. Post-reconstruction modeling is shown in upper row, direct modeling below.

Parametric images are smoother (rel. std. dev.) by approx. 40% for VD and 75% for K1, compared to post modeling.

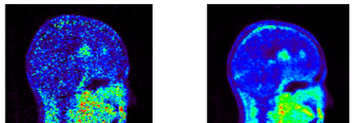

Figure 5: Parametric K1 image obtained from input response function (IRF) after 60s. Post-reconstruction modeling is shown on the left, direct modeling on the right.

4 CONCLUSION

The dynamic method is promising for FET kinetic analysis and improves image quality over conventional approaches for the hybrid mMR scanner. Especially parametric images show significantly reduced noise levels. Future work will investigate use of MR-based anatomical regularization, non-linear models, and correlation with tumor grading.

5 ACKNOWLEDGEMENT

I would like to thank Dr. Stefan Förster for providing the clinical PET/MR data used in this work.

6 REFERENCES

[1] J. Matthews et al., Phys. Med. Biol., 42(6):1155-1173, 1997.

[2] A.J. Reader et al., IEEE Nucl. Sci. Symp. Med. Imag. Conf., 1752–1756, 2006.

MOTION COMPENSATION IN MR/PET: DESIGN OF A MOTION PHANTOM

M. Kuschan (GSISH Member)
Technische Universität München

A. Haase* (Advisor), W. Kucharczyk** (Co-Advisor)

* Technische Universität München, IMETUM, Boltzmannstr. 11, 85748 Garching.
** University of Toronto, Fitzgerald Building, 150 College Street, Toronto ON M5S 3E2, Canada.

The combination of Magnetic Resonance/ Positron Emission Tomography hybrid imaging (MR/PET), which unites the advantages of the excellent soft tissue contrast yielded by MR imaging as well as its high-resolved anatomical information with the metabolic data gained by PET has a high potential in clinical diagnosis. To reduce the occurrence of image artifacts due to differences in acquisition times it is mandatory to develop motion compensation methods for this imaging technique.

Motions appear in involuntary movements of the patient during the clinical performance as well as due to physiological reasons like breathing or pulsing of the heart. To facilitate quantification of volumes with tracer uptakes and their allocation with the anatomical structure in clinical diagnose routines we investigated in motion compensation methods for MR/PET by constructing a micro controlled MR-compatible motion stage which moves along a one-dimensional trajectory.

1 INTRODUCTION

Magnetic Resonance Imaging (MRI), which delivers with its excellent soft-tissue contrast a detailed, multi-parametric knowledge of the anatomy, evolved into one of the most important imaging tools in clinical diagnosis. The combination of MR with Positron Emission Tomography (PET), which provides insights in biological function and metabolism, to a simultaneous MR/PET hybrid imaging system produces high-resolution images. However, long acquisition times lead in MRI as well in MR/PET to strong motion sensitivity. During the imaging process two types of motion occur, namely periodic motions, mostly organic induced, and movements caused by the subject. Plenty of reasons can cause patient motion, i.e. pathologic reasons are strokes, Parkinson or dementia like Alzheimer disease. In pediatric and geriatric imaging motions occur due to the patients lack of compliance. Motion results in less image quality with undesirable image artifacts which often render a complicated diagnosis. Within the scope of this project we will gain in a motion compensation method, which can be used in MR/PET.

2 MATERIALS AND METHODS

Motion compensation in MR/PET is invaluable since both imaging techniques are still suffering from motion artifacts. For instance, quiet breathing moves the thoracic wall and abdominal contents by 1-2 cm, approximately twice every 10 seconds[1].

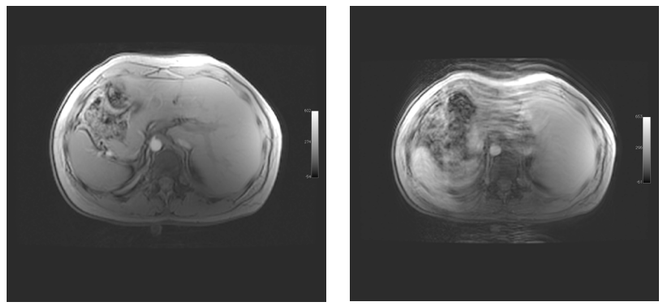

Figure 1: The differences in MR imaging of an abdomen with and without breathing are illustrated. Both MR images were acquired with a FAST GRE on a 3.0 T MR-System (Discovery* 750 w 3.0T, GE Healthcare) [TR: 200; TE: 3,104 ; FlipAngle: 45°; Image Size: 256x256 ; View Size: 573x409].
The left image contains a slice of the upper abdomen with an easy motion triggering: the patient was asked to stop breathing while the scan was performed. Only slight motion artifacts can be registered in the area of the abdominal wall (upper part). The right image shows representative motion artifacts in the same position. Image artifacts appear as bright noise, repeating densities, blurring and ghosting. Here, due to movement of the subject due to breathing and thus organic induced motion during the scanning time. There is ghosting in the phase encoding direction, aliasing artifacts as well as blurring easily recognizable in different parts of this image.

Contrarily, it takes several minutes to acquire a PET image, which then includes the information of several breathing as well as heart cycles.

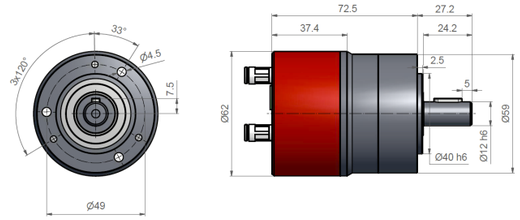

Figure 2: The pneumatic stepping motor rotates by means of an excitation of three internal pistons which are controlled by a external microcontrolling device. A precise rotation by 3° can be performed. This small stepping motor has been constructed to work in strong magnetic fields. It provides a torque of up to 1.7Nm [details in mm, BPS-1620-TL, Bibus AG, Austria].

To study and correct for motion-related issues it is useful to perform proper motion-induced experiments. Therefore in a first step a micro-controlled motion stage was designed and constructed. A primary mechanical requirement is the magnetic compatibility of the running computer-controlled moving stage and the compatibility of the driving mechanism, the motor itself, in a MR system. The motion stage will be used in a small animal system with limited dimensions as well as in a full-body MR-scanning system. The stage is configured to move a phantom of up to 1kg at velocities up to 10mm/0.1sec along a one-dimensional trajectory.

3 RESULTS

We have constructed a motion stage which will run motion induced MR-experiments with high accuracy, precision and reproducibility to compensate for linear motions in a first step. The existing stage constitutes the foundation of a bigger stage moving along a three-dimensional trajectory. The pneumatic stepping motor (Bibus AG) rotates now by means of an excitation of three internal pistons. A precise rotation by 3° can be performed depending on the air pressure and on the switching sequence of the control valves which are controlled by external micro controlling units (Arduino). The electronical realization including the controlling units (Arduino) is established. The first motion-induced MR-measurements will be performed when all calibration measurements and performances are fulfilled.

4 CONCLUSIONS

To proceed with the study of motion compensation methods for MRI and MR/PET we will complete the primary calibrations and measurements. The extension to a motion phantom which reproduces movements along three dimensions will then be performed and used for motion correction in a full-body MR/PET scanning system (Biograph mMR, Siemens AG).

Meanwhile, it is necessary to investigate in PET reconstruction with special regards to MR/PET. The compensation of image artifacts due to different acquisition times in MR and PET could be performed through MR motion registration, which will be used as additional input information in the PET reconstruction.

The progress in the scope of this project is coming along with the observation of motion artifacts in clinical routines with the simultaneous MR/PET scanning system. Our goal is to combine both operating experiences to gain in a motion compensation method which is useful in hybrid systems.

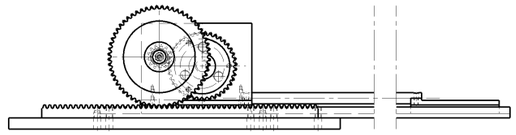

Table 1: Construction draft of the realized motion stage is shown which features limitations for width and height (height: 7,2 cm ; width: 8,3 cm) regarding the use in a small animal MR System (M2, Aspect Imaging, Shoham, Israel). The illustrated motion stage was build of PEEK. Contrarily to other constructions for motion experiments [2,3] we use a pneumatic motor instead of an electric stepping motor, thus electrical shielding is not necessary. Validation and calibration experiments have to compare with peak linear translation rates of 175mm/sec[2] or linear velocities up to 150mm/sec[3].

5 REFERENCES

[1] Wood ML, Henkelman RM. MR image artifacts from periodic motion. Med Phys 1985; 12:143–151.

[2] Drangova M, Bowman B, Pelc NJ. Physiologic motion phantom for MRI applications. J Magn Reson Imaging 1996; 6:513–518.

[3] Zhou Y, Carroll TJ, Grist TM, Frayne R. Design and validation of a motion stage for in vitro MR experiments. J Magn Reson Imaging 1999; 6:972-977.

VISUAL QUALITY ENHANCEMENT IN MULTISPECTRAL OPTOACOUSTIC IMAGING

S. Mandal (GSISH Member)
Helmholtz Zentrum München / Technische Universität München

Daniel Razansky * (Advisor), Vasilis Ntziachristos** (Co-Advisor)
* Helmholtz Zentrum München, Institut für Biologische und Medizinische Bildgebung, Ingolstädter Landstr. 1, 85764 Neuherberg.
** Technische Universität München, Klinikum rechts der Isar, Ismaninger Str. 22, 81675 München.

Recent advances in multispectral optoacoustic tomography (MSOT) have opened up new avenues in medical imaging. The current research aims to overcome some critical challenges and make the modality more useful for pre-clinical and clinical investigations.

Automation of image reconstruction in MSOT is vital for real-time imaging and visualization. Speed of sound (SoS) calibration is an intrinsic problem associated with the reconstruction process. We aim to introduce autofocusing measures to automatically calibrate the SoS. Further, it is observed that the temperature of the coupling medium (water) often drift during the signal acquisition, severely straining the image quality. The measures address these problems by iteratively determining the speeds with the changing boundary conditions with time.

In our study we also explore the capabilities of the newly developed volumetric MSOT (v-MSOT) in four dimensional (4D) optoacoustic imaging of perfusion in preclinical breast tumor model *in vivo*.

1 INTRODUCTION

Optoacoustics is an emerging new hybrid bioimaging modality which combines acoustical detection and EM absorption contrast. Optoacoustic imaging not only provides structural but also functional information of biological tissues [1]. Multi-Spectral Optoacoustic Tomography (MSOT) is capable of high resolution three dimensional (3D) visualizations of molecular probes located deep in scattering living tissues, with resolution and speed representative of ultrasound. This method can simultaneously deliver anatomical, functional and molecular information with both high resolution and penetration capabilities [1, 2]. The present generation of the system can scan 3D volumes at video rate and provide real time visualization of the imaged tissue [2]. The primary objectives of the doctoral dissertation are as follows:

1) Improve the reconstruction image quality through development of new quantification methodologies and reduction of artifacts, including speed of sound (SoS) corrections.

2) Employing multi-resolution signal processing techniques to enhance resolution and improve the signal to noise ratio (SNR) in optoacoustic images.

3) Defining quality benchmarks for image quality and algorithms (in terms of computational complexity and operation time. The dissertation envisages better visualization at real time and aims to develop a strategy of representing the multi-dimensional multi-spectral data in a clinically valuable way for the new generation of optoacoustic imaging systems.

2 MATERIALS AND METHODS

The current developments are focused on SoS calibration, real time 3D visualization, and functional imaging based on multispectral data. Both phantom studies and animal imaging are being conducted to evaluate the algorithms. More experiments in close collaboration of biologist and clinical partners are scheduled to enable better understanding and validation of methods. In the first project we develop a method for automated SoS calibration by factoring for the reconstruction image quality – using autofocussing algorithms.

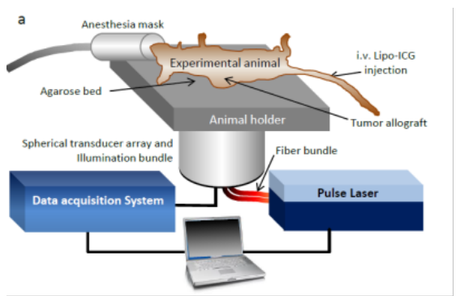

Figure 1: The experimental setup with spherically focused Optoacoustic detector array (256 elements), the specimen is illuminated with a pulsed laser connected by a fiber bundle. Sample is placed on agarose base to ensure proper ultrasonic coupling. The pulse laser and data acquisition system were managed by PC workstation.

In the proposed method we test multiple focus measures to find the image in sharp focus and having high signal to noise rations (SNR), thus allowing us to automatically determine the desired value of SoS. We also employed the same set of algorithms to calibrate the SoS under changing temperature conditions, by varying the temperature of the coupling medium over a given range. A correlation study was conducted between the changes in temperature and drifts in SoS [3, 4].

In the second project, we are conducting intravital imaging within heterogenic solid tumors, using real time volumetric MSOT (v-MSOT) [5]. The study is important for understanding blood perfusion profile, which defines hypoxia and nutrition gradients as well as cell viability, proliferation and drug response potentials. Herein, v-MSOT is used for imaging and analysis of perfusion and blood oxygenation profiles in and around solid breast tumor. Nude mice bearing breast tumor allografts were analyzed using internal contrast, which included visualization of blood oxygenation profiles. Blood perfusion kinetics in the breast tumors model was studied using nanoparticle-based fluorescent contrast agent.

3 RESULTS

The test results for the autofocussing approach for SoS calibration shows that a pre-processing approach greatly enhances the performance of focusing. Thus anisotrophic diffusion, an edge enhancement algorithm was incorporated in the workflow. Thereafter we used the consistent gradient mask [5X5] for determination of the focus measure. Other methods viz. Brenner's and Tennenbaum's gradients, wavelet based autofocussing methods were also tested. Further, it was also observed that with the change in temperature of the coupling medium results in varying SOS which impacts the reconstruction algorithms (filtered back-projection) and the quality of the reconstructed image. A comprehensive experiment was conducted with drop of 20°C and it was observed that even a change of 0.8°C caused a significant alteration of SOS thus affecting the quality of the reconstructed image.

In the 4-D perfusion studies, the v-MSOT setup proved not only to provide superior imaging speed and suitability for the 3D visualization of tumors, but also yielded detailed *in-vivo* volumetric images on a mesoscopic level. The standard cross-sectional MSOT system did not show the capacity for the detailed tumor resolution in all 3 imaging dimensions.

4 CONCLUSIONS

The SoS calibration method that is being developed is effective in reducing the need of human intervention in MSOT image reconstruction, thus enabling automatic processing of large datasets. This calibration method couples as a method for detection of parameter (Speed of Sound), and temperature based baseline correction in SoS during the image reconstruction process.

The later project proves that v-MSOT may develop into one of the primary mesoscopy imaging techniques with versatile contrast detection, real time 3D imaging capacity and detailed acquisition in all 3 imaging dimensions.. The superior imaging 3D capacity of the V-MSOT also opens the way for the clinical applications in skin or breast tumor detection and development of theranostic applications.

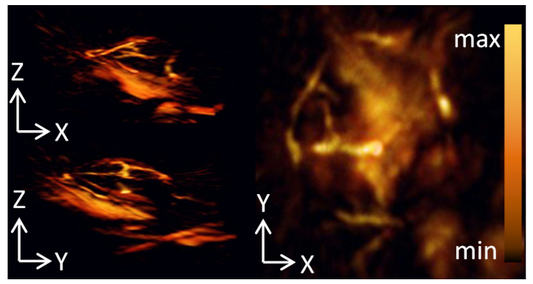

Figure 2: 2D reconstruction upon v-MSOT imaging in different imaging planes. Lipo – ICG was used as a contrast agent for real-time tracking and express the blood vessels better, enabling us to study perfusion kinetics in subcutaneous breast tumor.

5 ACKNOWLEDGEMENTS

SM acknowledges support (PhD Scholarship Award: A/11/75907) from the German Academic Exchange Service (DAAD).

6 REFERENCES

[1] D Razansky, M Distel, C Vinegoni, R Ma, N Perrimon, R W Köster, and V Ntziachristos. Multispectral opto-acoustic tomography of deep-seated fluorescent proteins in vivo. Nature Photonics, 3(7):412–417, 2009.

[2] A. Buehler, X. L. Den-Ben, J. Claussen, V. Ntziachristos and D. Razansky. Three-dimensional optoacoustic tomography at video rate. Optics Express (20):20, 2012.

[3] Subhamoy Mandal, Xose Luis Dean Ben, Daniel Razansky, „Automated calibration of temporal changes in the speed of sound in optoacoustic tomography", Proceedings of SPIE Vol. 8800, 88000K (2013).

[4] Van de Sompel, D., Sasportas, L. S., Dragulescu-Andrasi, A., Bohndiek, S., and Gambhir, S. S., "Improving image quality by accounting for changes in water temperature during a photoacoustic tomography scan," PLoS ONE 7, e45337 (10 2012).

[5] Dean-Ben, X.L.; Ozbek, A.; Razansky, D., „Volumetric Real-Time Tracking of Peripheral Human Vasculature With GPU-Accelerated Three-Dimensional Optoacoustic Tomography," Medical Imaging, IEEE Transactions on , vol.32, no.11, pp.2050,2055, Nov. 2013.

HYBRID PARALLEL-SERIAL MICROMANIPULATOR FOR ASSISTING OPHTHALMIC SURGERY

M. Ali Nasseri (GSISH Stipend Holder), **M. Eder** (GSISH Member)
Technische Universität München

Prof. Dr.-Ing. Alois Knoll*, Prof. Dr. Dr. Chris P. Lohmann**

* Technische Universität München, Department of Informatics, Boltzmannstr. 3, 85748 Garching.
** Technische Universität München, Klinikum rechts der Isar, Ismaninger Str. 22, 81675 München.

This project is about the design and development of a new robotic solution for assisting surgeons performing ophthalmic surgeries. The main task of this miniature robot, which is as small as an average surgeon's hand, is intra ocular micro manipulation in order to overcome the existing challenges in treatment of diseases like Retinal Vein Occlusion (RVO).

The novel hybrid mechanism designed for this robot enables micro scale motions with high stiffness against surgical site disturbances. This robot is easily integrated into standard operation rooms and does not require modification of conventional surgical tools. The device is an ergonomically optimized and compact microsurgical slave robot suitable for head mounting which addresses a key clinical requirement. The compatibility of the introduced robot with the current surgical setup were evaluated and confirmed in this work.

1 INTRODUCTION

Our main goal was to perform ophthalmic operations with fewer tremors and more precision, therefore not only improving many current clinical procedures but also getting the future possibility of new treatment options. This work investigates the design and development of a surgical assistance robot which overcomes the current limitations and moreover provides surgical abilities for treatment of diseases such as Retinal Vein Occlusion (RVO). The robot had to intuitively fit into the operation theater and guarantee the maximum patients safety.

2 MATERIALS AND METHODS

Based on 23G pars-plana vitrectomy equipment, a robotic additional interface tool was designed to dock to the patient's eye and stabilize the instrument during manipulation. The final precision of the device is ~5µm and the angular precision of the robot is 0.003 degrees which is largely sufficient for all ophthalmic applications. The working volume of the robot resembles a box of 50X50X50 mm with 360 degree free tool rotation while the maximum linear velocity of the tool motion is 40mm/s. The robot was designed with an adjustable remote center of motion point that allows it to be configured to manipulate the tool pivoting around the insertion point.

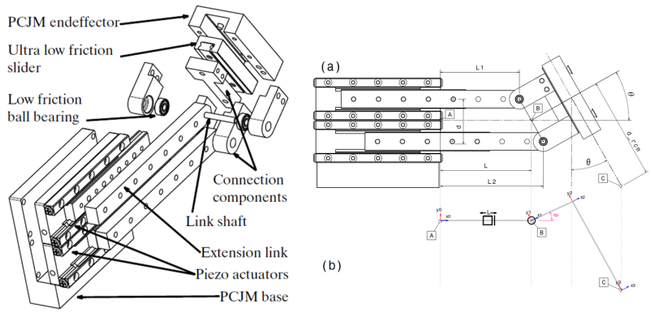

Figure 1: The Mechanical Design and Kinematics of the Robot.

The precision of the tool tip motion, based on the measured precision of each element and global vision based precision measurement (using OR microscope), is estimated to be less than 5 micron in x and y direction and 1 micron in z direction. The achieved precision is substantially better than the one needed for vein Cannulation, which is 20 micron in all directions as well as than the best human surgeon's precision recorded which is, as already mentioned, 108 micron.

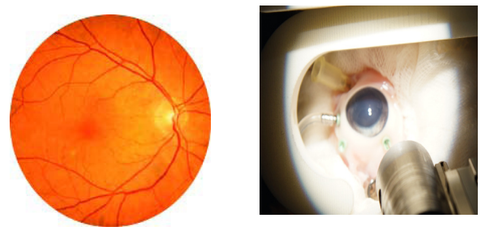

Figure 2: The retinal surface (Left) and the inserted tool for retinal manipulation using robot (Right).

Also the output forces of the robot's end effector that was measured as 4.97N in x and y and 2.84N in z directions are promising for the ophthalmic procedures. Based on the clinical motion data of the ophthalmic surgery during vitrectomy derived from [15], robot's motion in terms of positions and velocities was compared to the surgeon's motion during the operation. According to the observed data the robot with 28mm travel range actuators is suitable for vein occlusion.

3 RESULTS

A compact 6DOF robot smaller than human hand and with the weight of 312gr was developed. This robot is mounted on patient's head during the operation and holds conventional surgical tools. The surgeon controls the robot using a master console which is located close to the patient's head. Beside maximum safety consideration this approach enables scaling of surgeon's motion. The compatibility of the robot in the ophthalmic operation environment was evaluated. This evaluation approved that the robot won't conflict other surgical devices such as microscope and assured that the surgical area remains available for the surgeon. The entire setup was already tested successfully in the laboratory on cadaver eyes.

4 DISCUSSION

The design and development of a robotic solution for ophthalmic surgery was the outcome of this project. Joint elements of the robot consisting of parallel piezo actuator pairs have been introduced which enables stable and precise motion with high output force. A serial configuration of these joints as an ophthalmic robot together with its simplified models has been shown. Furthermore an intuitive and practical way of mounting the robot on the patient's head for conducting the procedure has been presented. Finally, a brief report of the compatibility evaluation of the robot with operation room has been given.

Summing up the mentioned points of the current robotic setup for ophthalmic surgery, the following advantages are concluded: Compatibility to OR, Patient's head fixtures, stiffness, variable RCM, intuitive tool holder and improved safety.

5 ACKNOWLEDGEMENTS

This work was supported by TUM – GSISH (Graduate School of Information Science in Health).

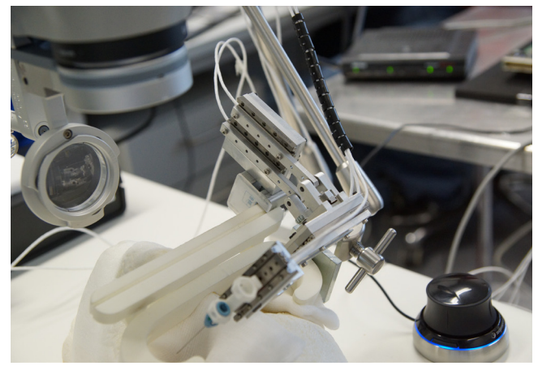

Figure 3: The developed robot with mounting mechanism and input device, the verification ex-vivo experiments were performed on porcine eye to confirm the adoptability of the setup with conventional ophthalmic operation theaters.

6 REFERENCES

[1] "Load-velocity Characteristics of a Stick-slip Piezo Actuator" M. Pak, A. Nasseri, Proceedings der Actuator 2012. International Conference on New Actuators (ACTUATOR-12), P. 755, Bremen, Germany, June 2012.
[2] "Clinical motion tracking and motion analysis during ophthalmic surgery using electromagnetic tracking system" M. Ali Nasseri, Emmanuel Dean-Leon, S. Nair, M. Eder, M. Maier, C. P. Lohmann, and Alois Knoll Proceedings of the 5th International IEEE Conference on BioMedical Engineering and Informatics (BMEI'12),pp. 1058 – 1062, Chongqing, China, October 2012.
[3] "The 3d eyeball FTA model with needle rotation" Jing Wu, M. Ali Nasseri, M. Eder, M. Azqueta Gavaldon, C. P. Lohmann and Alois Knoll APCBEE Procedia 3rd International Conference on Biomedical Engineering and Technology - ICBET 2012. Elsevier, May 2013.
[4] "Robot-assisted vitreoretinal surgery" M. Maier, M. Ali Nasseri, D. Zapp, M. Eder, K. Kobuch, C. P. Lohmann, and Alois Knoll The Association for Research in Vision and Ophthalmology (ARVO 2013), Seattle, USA, May 2013.
[5] "The introduction of a new robot for assistance in ophthalmic surgery" M. Ali Nasseri, M. Eder, E. Dean-Leon, S. Nair, D. Zapp, M. Maier, C. P. Lohmann, and Alois Knoll, 35th Annual International Conference of the IEEE Engineering in Medicine and Biology Society (EMBC'13). pp.5682--5685, Japan, July 2013.
[6] "Kinematics and dynamics analysis of a hybrid parallel-serial micromanipulator designed for biomedical applications" M. Ali Nasseri, M. Eder, D. Eberts, S. Nair, M. Maier, D. Zapp, C. P. Lohmann, and Alois Knoll, Proceedings of the International Conference on Advanced Intelligent Mechatronics (AIM2013). Pp.293--299, Wollongong, Australia, July 2013.
[7] "Embedded middleware and hard real-time based architecture for robot assisted ophthalmic surgery" S. Nair, M. Ali. Nasseri, M. Eder, Chris P. Lohmann, and Alois Knoll, The Hamlyn Symposium on Medical Robotics, London, UK,pp. 83 – 84, June 2013.
[8] "Robot for assisting Ophthalmic Surgery" Nasseri M. Ali, Maier M, Zapp D, Nair S, Eder M, Kobuch K, Chris P. Lohmann, and Alois Knoll, International Society for Medical Innovation and Technology(iSMIT), September 2013.

OPTOACOUSTIC TOMOGRAPHY OF WHOLE TUMOR ANGIOGENESIS

A. Oancea (GSISH Member)
Helmholtz Zentrum München / Technische Universität München

V. Ntziachristos** (Advisor), F. Pfeiffer* (Co-Advisor)

* Technical University of Munich, IMETUM, Boltzmannstr. 11, 85748 Garching, Germany.
** Helmholtz Zentrum München, Institut für Biologische und Medizinische Bildgebung, Ingolstädter Landstr. 1, 85764 Neuherberg.

This work targets the accurate imaging of vasculature, in particular microvasculature of mice. High-resolution and high-contrast images of mouse head and tumor vasculature are obtained non-invasively by optoacoustic tomography.

An optoacoustic imaging system has been developed, and its performance has been evaluated by imaging samples having tissue-mimicking light absorption properties. Subsequent to the characterization, the head vasculature of the mouse has been imaged non-invasively.

Finally, a HT29 mouse tumor was investigated in vivo. The obtained optoacoustic images reveal major tumor supply vessels as well as fine tumor microvessels, which are randomly oriented. Vessels with a diameter smaller than 20 micrometers have been discriminated.

1 INTRODUCTION

Pre-clinical studies on pharmaceuticals against tumor growth have shown the need to be able to visualize vasculature with resolutions down to 30µm. Optoacoustic imaging has shown its potential to cope with those requirements. Among its advantages are the facts that it is non-invasive, non-radiative, cheap to implement, useable in-vivo and that it can show molecular specificity. The underlying principle is called the photoacoustic effect. High-energy light pulses of a nanosecond pulsed laser are absorbed by the sample, causing it to emit a pressure wave. In general, the amplitude of the pressure wave relates to the absorbed energy. Assuming an isotropic light flux, the reconstructed image then shows the distribution of the absorption coefficient. Here is showcased how optoacoustic tomography can be applied to the imaging of whole tumor angiogenesis.

2 MATERIALS AND METHODS

The samples are excited by nanosecond light pulses from an optical parametric oscillator (OPO) laser (OPOTEK, Carlsbad, CA, USA) at a repetition rate of 20Hz, and apart from the pump beam at 532nm the OPO can tune in the 700-900 nm range, making it attractive for molecular imaging by multispectral optoacoustic tomography (MSOT). In an exemplary configuration, the beam size is firstly adjusted to the region of interest by lenses aligned as a Galilean telescope. All lenses are anti-reflection coated and the light paths in water are kept as short as possible to reduce losses in pulse energy.
The ultrasonic detection is provided by the high-frequency cylindrically focused transducer Panametrics NDT V319 with the following characteristics: resonance frequency (BW) and focal length: 15.28MHz (47.85%) and 0.757in.
--> in-plane resolution for tomography: 32µm.

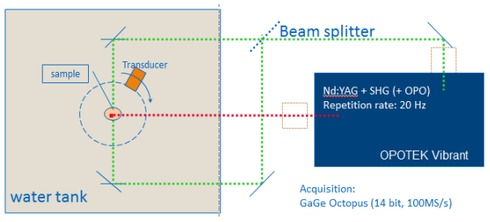

Figure 1: Schematic of an exemplary optoacoustic imaging setup configuration (free beam illumination). Red interrupted line illustrating the laser beam path of NIR illumination. Green beam path illustrating the laser beam path of 532nm illumination. The ultrasonic transducer rotates 360 degrees about the sample. The sample is placed in a water tank for ideal acoustic coupling between the sample and the ultrasonic transducer.

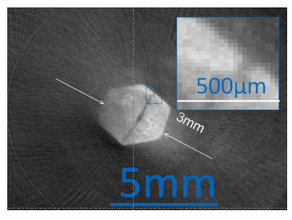

Figure 2: Optoacoustic imaging result of the agar phantom with tissue-mimicking optical properties.

Acoustic signals are recorded by a digital acquisition card (GaGe Octopus) at a sampling frequency of 100MHz via Labview. The optoacoustic images are reconstructed with a back-projection algorithm, after band pass filtering the acoustic signals in the 2-30 MHz range.

To evaluate the performance of the system, multiple phantom measurements with tissue-like absorption and scattering are conducted. An agar phantom with a hexagonal insertion is prepared containing Intralipid and black india ink leading to a reduced scattering coefficient of $\mu_{s'}$=10/cm and absorption coefficient values of μ_a=0.2/cm for the background and μ_a=1/cm for the insertion.

As to biological investigations, head and tumor vasculature of mice is imaged at 532nm and in with NIR illumination. The mouse is a CD1 nude mouse. In the imaging system, the brain axis is oriented horizontally. The head is illuminated from the top for both wavelengths (700nm and 532nm).
The tumor of interest is a HT29 tumor. Initially 105 cells are implanted centrally on the back of the nude mouse. After a growth time of 10 days, the mouse tumor is imaged in vivo at 532 nm excitation to exploit the high intrinsic contrast of hemoglobin in the blood vessels. Acoustic signals are acquired at 900 angular projections and for multiple slices at a transversal step size of 150 µm.

3 RESULTS

Tissue mimicking agar phantom
The acquired optoacoustic image of the agar phantom is shown in Fig. 2. Therein, it is illustrated that the light absorption of the insertion is significantly superior to the light absorption in the background. In particular, the hexagonal shape of the insertion is revealed.

Mouse head vasculature
Fig. 3 shows the head vasculature of the mouse down to the level of the skull as unweighted overlay of an optoacoustic image acquired at 532nm illumination wavelength with an optoacoustic image acquired at 700nm illumination wavelength.

Mouse tumor vasculature
Fig. 4 shows the tumor vasculature of the mouse as a maximum projection image based on an image stack of 10 images. The top 2mm of the tumor are illustrated. Large tumor supply blood vessels as well as fine randomly oriented tumor microvessels are revealed.

4 DISCUSSION

Tissue mimicking agar phantom
Other than expected from visual inspection of the sample, the insertion shows to be inhomogeneous, i.e., it has a fine structure. This is further illustrated by the insertion in Fig. 2.

Mouse head vasculature
532nm illumination provides high blood vessel contrast, revealing fine superficial microvasculature. On the other hand, light with a wavelength of 700nm penetrates deeply into the tissue and reveals the profound mid-cranial artery of the mouse. By overlaying the two images, a detailed impression on the fine microvessels and large major vessels of the head of the mouse is obtained.

Mouse head vasculature
The high blood vessel contrast at an illumination wavelength of 532nm in combination with the high imaging resolution of the system allow to discriminate blood vessels down to a vessel diameter below 20µm.

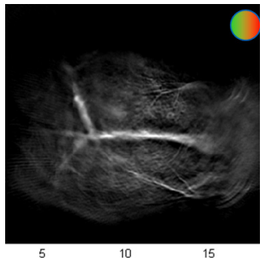

Figure 3: Mouse head vasculature acquired non-invasively with 532nm and 700nm illumination (overlay image).

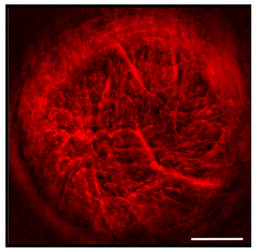

Figure 4: Mouse tumor vasculature acquired non-invasively with 532nm illumination (MIP of top 2mm, scale-bar 2mm).

5 ACKNOWLEDGEMENTS

The authors thank the technical assistants for their aid with tumor preparation and animal handling throughout the experiments. A.O. acknowledges support from the TUM Graduate School of Information Science in Health.

6 REFERENCES

[1] Maslov et al., „Optical-resolution photoacoustic microscopy for in vivo imaging of single capillaries“, Opt. Lett. 33, 9 (2008).
[2] Bühler et al., „Video-rate optoacoustic tomography of mouse kidney perfusion“, Opt. Lett. 35, 14 (2010).
[3] Taruttis et al., „Real-time imaging of cardiovasc. dynamics and circulating gold nanorods with MSOT“, Opt. Exp. 18, 19 (2010).
[4] Wang et al., „Noninvasive laser-induced photoacoustic tomography for structural and functional in vivo imaging of the brain“, Nat. Biotech. 21, 7 (2003).
[5] Ma et al., „Multispectral optoacoustic tomography (MSOT) scanner for whole-body small animal imaging“, Opt. Exp. 17, 24 (2009).

ADVANCED IMAGE RECONSTRUCTION IN 3D OPTOACOUSTIC TOMOGRAPHY

D. Queirós (GSISH Stipend Holder)
Helmholtz Zentrum München / Technische Universität München

Prof. Vasilis Ntziachristos*, ** (Advisor), Prof. Markus Schwaiger** (Co-Advisor)

* Helmholtz Zentrum München, Ingolstädter Landstraße 1, 85764 Neuherberg, Germany.
** Technische Universität München, Klinikum rechts der Isar, Ismaninger Str. 22, 81675 München.

Optoacoustic tomography is a noninvasive, hybrid imaging technique that takes advantage of both the benefits of optical and ultrasonic imaging. In principle a nanosecond laser pulse, typically in the near infrared regime of the electromagnetic spectrum, excites tissue. There the light energy gets absorbed and, following thermoelastic expansion generates a pressure wave that can be detected by ultrasonic transducers positioned around the region of interest.

In this way images reconstructed from optoacoustically generated signals benefit from high optical contrast and ultrasonic resolution. Optoacoustic reconstruction algorithms generally assume point-like detectors. In practice ultrasonic transducers with a finite size and focusing are often used to measure optoacoustic pressure waves from selective regions with sufficiently high signal to noise ratio. This discrepancy blurs the different structures reconstructed and reduces the resolution and overall image accuracy.

We developed a three-dimensional reconstruction algorithm that incorporates all geometric detector properties thus improving image resolution in all spatial dimensions.

1 INTRODUCTION

Mathematically, optoacoustic signal generation can be modeled by the wave equation Cauchy-problem. An explicit expression for the solution is given by the Poisson type integral

$$P(\vec{x},t) = \frac{\partial}{\partial t}\left\{\frac{a_s^2}{4\pi c\, t_p}\frac{1}{s}\iint_{|\vec{x}-\vec{x}'|=c_s t} f(\vec{x}')\,dS(\vec{x}')\right\},$$

which forms the basis of a recently presented model-based reconstruction algorithm, termed interpolated model-matrix inversion (IMMI) [1]. Here $\vec{x}$ is the spatial and t the temporal variable. $P(\vec{x},t)$ is the optoacoustic pressure, β the isobaric volume expansion coefficient, c_s the speed of sound, C_p stands for specific heat. $f(\vec{x})$ describes the spatially varying absorption coefficient defining the image.

The algorithm reconstructs images in two steps. First it builds a model matrix which represents a discretized formulation of the solution of the wave equation above. Thereby this matrix incorporates all parameters as the speed of sound or geometric positions of the detectors. Then, signals predicted by the model can be obtained by a simple matrix-vector multiplication, $P = M \cdot f$. In a second step the actual image f_{rec} is reconstructed by numerically minimizing the error between predicted signals P and measured signals P_{sig} with a least squares minimization procedure, $f_{rec} = \arg\min_f \left\| P_{sig} - M \cdot f \right\|$.

The above theory, as well as all commonly used reconstruction algorithms, assumes the detectors to be restricted to points. This deviates severely from cylindrically focused transducers in widely-used cross-sectional imaging setups resulting in a loss of resolution and image quality.

We introduced two methods to incorporate all geometric detector properties into the 3D model-based inversion algorithm improving resolution and making quantification accurate.

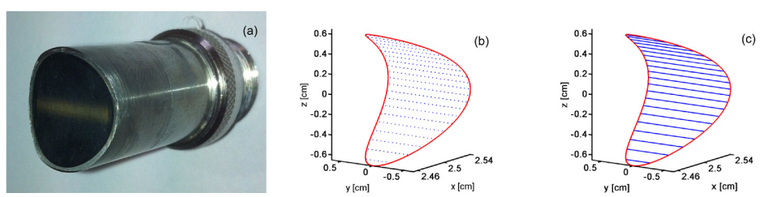

Figure 1: Cylindrically focused transducer (a) and the approximation of the surface by points (b) and lines (c).

2 MATERIALS AND METHODS

In order to incorporate the shape of a cylindrically focused transducer into the reconstruction algorithm, the detection surface has been approximated by either a set of points or a set of lines.

In case of the set of points, a new matrix for inversion M_{sum} is derived by summing up all matrices M representing point detectors covering the surface. This approach works for all detectors as any surface shape can be approximated by a set of points.

Then again, the spatial impulse response (SIR) of a line detector can be calculated analytically [2]. It can be introduced into the matrix M by temporal convolution of the SIR with the matrix. Thereby, by summing up the SIRs of a set of lines covering the detector surface one can approximate all geometric properties of a cylindrically focused transducer. By convolving this sum of SIRs with the matrix one incorporates all geometric properties into a new matrix M_{conv}. This approach is especially worthwhile for large detector surfaces as typically much less lines than points are needed for modeling the surface equally accurate. Therefore this approach needs much less calculation time.

In both scenarios a new system of linear equations, represented by the matrices M_{sum} and M_{conv} is obtained and can be subsequently inverted by means of a least squares minimization algorithm to reconstruct an image.

In order to corroborate the benefits of modeling cylindrically focused transducers, numerical studies and experiments have been performed. Experiments were conducted with agar phantoms containing as biological specimen an ex vivo spleen of a mouse. For that cylindrical phantoms with a diameter of 2 cm were prepared using a gel made from distilled water, containing Agar (Sigma-Aldrich, St. Louis, MO, USA) for jellification (1.3% w/w) and an Intralipid 20% emulsion (Sigma-Aldrich, St. Louis, MO, USA) for light diffusion and more uniform illumination (6% v/v). Optoacoustic measurements were conducted on a high throughput optoacoustic tomographic system described in detail in [4]. It consists of a cylindrically focused 64 transducer array covering 172° and scanning in the z-direction.

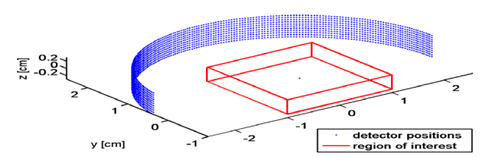

Figure 2: Detector positions and region of interest of the optoacoustic tomographic system used in the experiments. The 172° detector array is scanned in the z-direction.

3 RESULTS

A comparison of the results obtained with the model considering point transducers and the model incorporating the detector geometry is displayed in Fig. 3.

An improvement in the elevational resolution is obtained with the enhanced model as shown in the maximum intensity projection (MIP) along the y direction (Fig. 3b and Fig. 3d). The out-of-plane artifacts are especially significant for the background absorption, which generates mainly low frequency acoustic waves, and the focusing capacity of the transducer is lower in this case. The reduction of the out-of-plane artifacts corresponding to low spatial frequencies also improves the visual quality of the MIP along the z direction.

The overall background noise observed in the point detector reconstruction (Fig. 3a) was considerably reduced in the reconstruction incorporating the transducer shape (Fig. 3c).

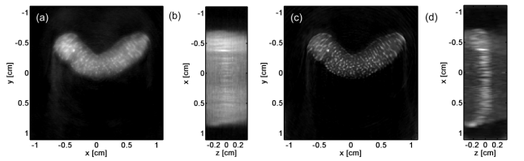

Figure 3: Reconstruction of a mouse spleen. (a) and (c) shows maximum intensity projections obtained via a point transducer model. (b) and (d) are the corresponding reconstructions from an enhanced model with the detector properties incorporated.

4 CONCLUSIONS

In this work we adapted a model-based reconstruction algorithm to account for the effects of cylindrically focused transducers in tomographic optoacoustic reconstructions. Typical artifacts in 3D optoacoustic tomography resulting from data collected by currently used ultrasonic transducers could be efficiently and thoroughly corrected.

5 REFERENCES

[1] A. Rosenthal, D. Razansky, and V. Ntziachristos, „Fast Semi-Analytical Model-Based Acoustic Inversion for Quantitative Optoacoustic Tomography,“ Ieee Transactions on Medical Imaging 29(6), 1275-1285 (2010).

[2] A. Rosenthal, V. Ntziachristos, and D. Razansky, „Model-based optoacoustic inversion with arbitrary-shape detectors,“ Medical Physics 38(7), 4285-4295 (2011).

[3] D. Queirós, X. L. Déan-Ben, A. Buehler, D. Razansky, A. Rosenthal, and V. Ntziachristos, „Modeling the shape of cylindrically focused transducers
in three-dimensional optoacoustic tomography,“ Journal of Biomedical Optics 18(7), 076014 (2013).

[4] A. Buehler, E. Herzog, D. Razansky, and V. Ntziachristos, „Video rate optoacoustic tomography of mouse kidney perfusion,“ Optics Letters 35(14), 2475-2477 (2010).

MAGNETIC RESONANCE WITH MAGNETIC NANOPARTICLES

C. Rümenapp (GSISH Member)
Technische Universität München

S. Glaser* (Advisor), B. Gleich** (Co-Advisor), A. Haase** (Co-Advisor)

* Technische Universität München, Chemistry Department, Lichtenbergstraße 4, 85747 Garching, Germany.
** Technische Universität München, IMETUM, Boltzmannstr. 11, 85748 Garching, Germany.

Magnetic nanoparticles were manufactured for the detection of specific molecular interactions. The particles were colloidal stable and showed a narrow size distribution. They were characterized according to their size, their core material, their magnetization and their surface chemistry.

For the detection of molecules or cells they were functionalized with antibodies, which bind specifically to the desired target. The binding of their antigen to the magnetic nanoparticles can be detected through the change in the NMR T2 relaxation time.

With this method avidin molecules and S. cerevisiae cells were detected. The later is of special interest to the quality control in the alcohol-free beverage industry.

1 INTRODUCTION

Magnetic nanoparticles have been used as ferrofluids in a variety of technical applications, but also in life sciences [1]. In the biomedical field they have been used as carriers for mag-netic drug targeting and for the magnetic transfection of cells, in the hyperthermia treat-ment of cancer, as contrast agents for magnetic resonance imaging and for magnetic separation and purification of samples [2]. For the separation and purification techniques the magnetic nanoparticles are functionalized with small molecules, proteins or genetic material to be able to bind specifically to their target. If magnetic nanoparticles bind spe-cifically to a target the nuclear magnetic resonance T2 relaxation time is changing [2]. This fact can be used for a detection system based on the binding of magnetic nanoparticles to their target and/or their clustering in fluids and on the change of the nuclear magnetic resonance T2 relaxation time. As a first target organism Saccharomyces cerevisiae was chosen, which is one of the main spoiling organisms in the production of alcohol free beverages.

2 MATERIALS AND METHODS

In this work small, monodisperse, colloidal stable, magnetic nanoparticles (MNPs) with a narrow size distribution were prepared in large volumes using a combination of a co-precipitation of iron salts and a polyol method. In a chemical synthesis reactor iron (III) and iron (II) salts were dissolved in diethylene glycol, mixed and heated. Magnetite was pre-cipitated with NaOH according to the stoichiometric equation

$$Fe2+ + 2\ Fe3+ + 8\ OH- \longrightarrow Fe3O4 + 4\ H2O.$$

After an incubation of two hours the particles were cooled to room temperature, magneti-cally separated and peptized with 1 M HNO_3. The obtained particles were coated with tetraethoxysilane (TEOS) and functionalized with (3-amino-propyl)triethoxysilane (APTES) for further functionalization with antibodies. The particles were characterized using transmission electron microscopy (TEM), dynamic light scattering (DLS), Mössbauer spectroscopy, electron diffraction pattern, Fourier-transformed infrared spectroscopy, Zeta potential measure-ments, M(H) measurements as well as magnetic particle spectroscopy.

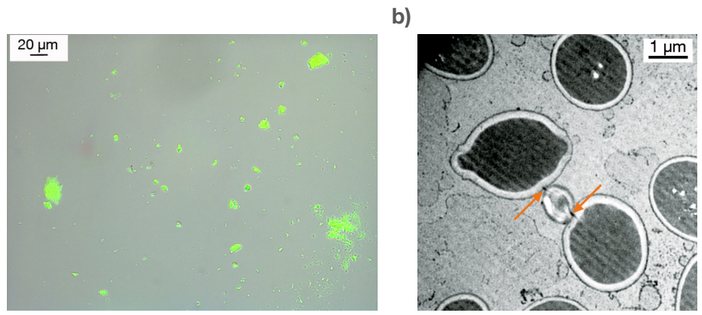

Figure 3: Visualization of the cluster formation. a) fluorescence microscopic image of anti-avidin magnetic nanoparticles clustered through the binding of FITC-avidin (green); b) transmission microscopic image of S. cerevisiae bound together through anti-S. cerevisiae magnetic nanoparticles (orange arrows).

3 RESULTS

Figure 1 shows a schematic drawing of the manufactured MNPs with indication of the diameters of each manufacturing step.

Figure 2 depicts M(H) measurements of all manufacturing states. To establish the measurement set-up consisting of a 21.7 MHz (≈ 0.5 T) nuclear magnetic resonance relaxometer and the manufactured magnetic nanoparticles, the particles were functionalized with an anti-avidin antibody for the detection of FITC-avidin. The lowest detectable concentration of FITC-avidin was 1.35 fM FITC-avidin with anti-avidin magnetic nanoparticles of 1 mM Fe and a change in the NMR T2 relaxation time of approximately 25% between start of the incubation and after 15 min of incubation. The clustering of the particles was visualized by fluorescence microscopy (Figure 3a). This system was developed further for the detection of food spoiling organisms in the food and beverage industry.

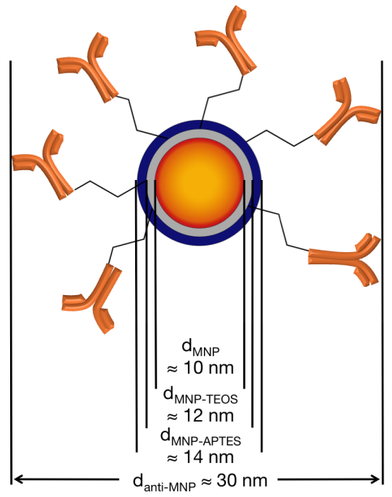

Figure 1: Schematic drawing of the manufactured magnetic nanoparticles with the indication of the hydrodynamic diameters of each manufacturing step.

S. cerevisiae was detected at a concentration of 4•108 cells/ml using anti-S. cerevisiae magnetic nanoparticles at an iron concentration of 1 mM. The binding of the anti-S. cerevisiae MNP to the yeast cells is shown in Figure 3b.

4 DISCUSSION OR CONCLUSIONS

The results show a very good detection limit for FITC-avidin, but an improvable detection limit for S. cerevisiae. The detection limit for FITC-avidin was half the detection limit of the literature, making the measurement set-up twice as sensitive[3]. The used antibodies for S. cerevisiae showed a very low binding affinity to S. cerevisiae, being a possible cause for the ob-served high detection limit.

5 ACKNOWLEDGEMENTS

TEM imaging was performed by Dr. M. Hanzlik of the Chemis-try Department and Mössbauer spectroscopy was performed by Prof. F. Wagner of the Physics Department, Technische Universität München. M(H) measurements were performed by Dr. M. Opel from the Walther-Meissner Institute, Garching.

6 REFERENCES

[1] R.E. Rosensweig. Ferrohydrodynamics. Dover Publications, Inc., Mineola, New York, Jul 1997.

[2] S. Laurent, D. Forge, M. Port, A. Roch, C. Robic, L. Vander Elst, and R. N. Muller. Magnetic iron oxide nanoparticles: synthesis, stabilization, vectorization, physicochemical characterizations, and biological applications. Chem Rev, 108 (6): 2064–2110, Jun 2008.

[3] D. Issadore, C. Min, M. Liong, J. Chung, R. Weissleder, and H. Lee. Minia-ture magnetic resonance system for point-of-care diagnostics. Lab Chip, 11:2282–2287, Jul 2011.

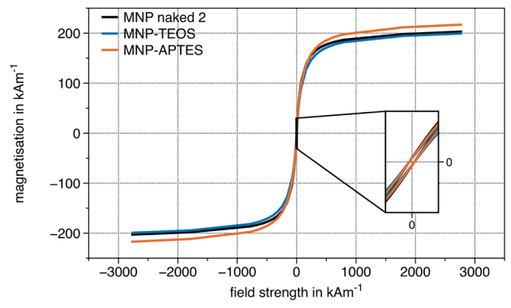

Figure 2: M(H) measurements of the manufactured particles at the different stages of preparation.

QUANTIFIED PH DETERMINATION WITH HYPERPOLARIZED MAGNETIC RESONANCE

D. J. Scholz (GSISH Stipend Holder)
Technische Universität München

A. Haase* (Advisor), M.I. Menzel** (Co-Advisor)

* Technical University of Munich, IMETUM, Boltzmannstr. 11, 85748 Garching.
** GE Global Research Center, Freisinger Landstr. 50, 85748 Garching.

pH is a key parameter in many biochemical processes. Several diseases like cancer, inflammation, hypoxia and many others come along with alterations in pH. To use the pH value as a disease marker, it would be desirable to detect pH in vivo spatially separated and even more favorable in a non-invasive way but so far no clinical tool is established to map pH *in vivo*. Using hyperpolarized 13C-Bicarbonate (13C-BiC) in magnetic resonance imaging (MRI) could close this gap.

This work deals with the quantification of the quality of pH detection and compares it with the current medical "gold-standard" of pH electrode measurements. Different sources of errors of pH were taken into account and its influence in time and spatial dimensions to pH phantoms and the translation to *in vivo* targets.

1 INTRODUCTION

As pH plays a crucial role in several diseases, such as cancer but also hypoxia, inflammation etc., it is desirable to detect pH in vivo. Ideally, the detection should noninvasive and spatially localized. Despite the medical impact, a clinical tool for pH mapping is not yet available. A promising candidate to achieve pH mapping in vivo is 13CMMR. Biochemical important molecules as Pyruvate, Lactate and others can be 13C labeled and detected in vivo in NMR with dissolution DNP. Specifically, using hyperpolarized 13C-Bicarbonate, Gallagher et al. showed in 2008 the proof of concept.[1]

To apply this promising method of pH detection to different diseases, it is important to quantify the method and compare it to already established methods of pH detection. With a known dissociation constant (pKs), pH can be directly estimated by the concentrations of Bicarbonate and CO2 via the Henderson-Hasselbalch equation due to their chemical equilibrium, depending on the pH of the environment as depicted in figure 1.

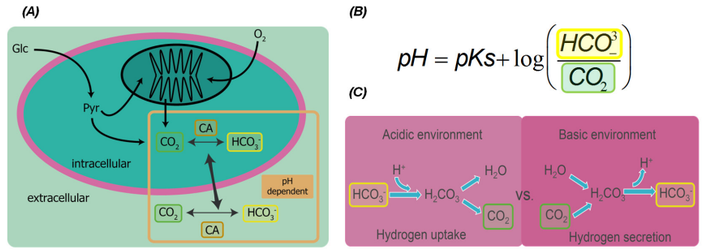

Figure 1: (A): Chemical equilibrium of Bicarbonate and CO2 catalyzed by carbonic anhydrases (CA). (B): Henderson-Hasselbalch equation. (C): Chemical reaction of Bicarbonate to CO2 and back conversion depending on environmental pH. Figures from [2].

2 MATERIALS AND METHODS

13C enriched Cs-bicarbonate was synthesized and chemically prepared with D2O, Glycerole, OXO63 radical and Gadolinium to achieve best parameters for DNP. Subsequently the13C-BiC was dissolved with pH and osmolality adjusted buffer and injected. Custom made pulses were designed for individual spatial and spectral (SPSP) excitation of BiC and CO2. For the comparison of MR vs. electrode measurements, highly concentrated (1Mol/l) phosphate buffers of different pH were used. Diverse organs (kidney, heart, bowel, liver) of healthy buffalo rats were pH mapped. MR measurements were carried out on a 3T (GE Signa HDx). For intra- and extracellular pH determination T1 of MCF-7 cell spheroids were measured on 3T and 11T bruker spectrometers.

3 RESULTS

Simulated pH, on the base of hyperpolarized Bicarbonate spectra, leads to a region of good detection sensitivity (pH error <0.2) as depicted in figure 2.

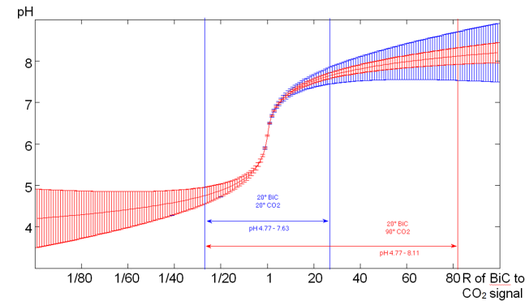

Figure 2: Region of reasonable pH estimation (pH error <0.2) with assumed pKs of 6.2. Smallest error at pH=pKs at ratio (R) of BiC signal/CO2 signal = 1. Blue lines show limits for equal flip angle (FA) excitation. FA_{BiC} = FA_{CO2}= 20°. Red limits show extended limits with FA_{CO2}=90°.

First in vitro test of the method using hyperpolarized Sodium-Bicarbonate and Phosphate buffers and pH-phantoms showed good correlation between the derived pH value and the reference pH (+/- 0,03), obtained by pH electrode. An analysis of the signal dynamics revealed that the correct Bicarbonate to CO2 signal ratio is established after 20 seconds, without the addition of carbonic anhydrases. After the equilibrium is created, pH stays stable. The pH-mapping error of Cesium- Bicarbonate pH measurements (pKs = 6.2) in an experiment with a SPSP excitation was determined. As a result a validity range of pH detection ranging from pH 6.6 to pH 7.6 could be established as depicted in figure 3; and applied to healthy rats as depicted in figure 4.

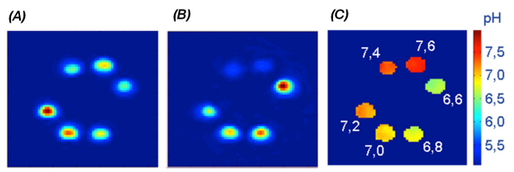

Figure 3: (A): Bicarbonate raw signal at 10° flip angle excitation. (B): CO2 raw signal at 30° flip angle excitation. (C): Calculated pH from flip angle corrected signals with assumed pKs=6.2. White numbers show the reference pH, measured by pH electrode.

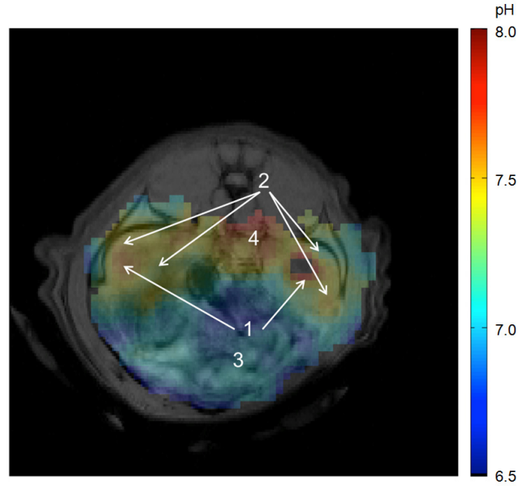

Figure 4: pH map of a healthy rat with a FOV of 8*8cm and slice thickness of 1cm. pH gradient from pH 7.6 at center of kidneys (1) to pH 7.2 at kidney cortex (2). Lowest pH values of 6.8 to 7.0 in bowel region (3). Vena cava (4) shows increased blood pH around up to pH 7.7 due to high bicarbonate administration.

4 CONCLUSIONS

The quantification analysis shows good sensitivity of pH detection with hyperpolarized bicarbonate in the range of biological relevant pH from 6 to 8. In vitro experiments show that the measured pH is in good comparison with pH measured by electrode. The method was successfully applied on in vivo targets.

The successful implementation of the method opens a broad field of detecting and monitoring different diseases. First trials are planned for hypoxia, inflammation and tumor pH measurements.

5 ACKNOWLEDGEMENTS

The author wants to thank TUM and GSISH for supporting the thesis. This research was partly funded by BMBF grant #01EZ1114A.

6 REFERENCES

[1] F. A. Gallagher et al., "Magnetic resonance imaging of pH in vivo using hyperpolarized 13C-labelled bicarbonate" Nature 453, no. 7197 (2008): 940-943.

[2] D. J. Scholz et al., "Quantitative pH analysis with sodium 13C-Bicarbonate at small pH variations", Annual meeting 2012 ESMRMB, Present. Nr. 774

COMPUTER-ASSISTED IMAGING FRAMEWORK FOR INTRA-OPERATIVE RADIO-GUIDANCE WITH POSITRON-EMITTING RADIOTRACERS

D. I. Shakir (GSISH Stipend Holder)
Technische Universität München

N. Navab* (Advisor), S. Ziegler**, M. Schwaiger** (Co-Advisor)

* Technische Universität München, Department of Informatics, Boltzmannstr. 3, 85748 Garching, Germany.
** Technische Universität München, Klinikum rechts der Isar, Ismaninger Str. 22, 81675 München.

Peri-operative imaging in conjunction with positron-emitting radiotracers has become state-of-the-art in the diagnosis and staging of many types of cancer in the last few decades. Yet, the potential of this subset of radiotracers for intra-operative radio-guidance is not fully exploited.

Our project aims at developing two novel intra-operative imaging modalities that work in conjunction with positron-emitting radiotracers for real-time guidance in cancer surgery. The first one is called epiphanography and is based on a direct detection of positrons. The second one is called freehand PET and is based on volumetric imaging by the detection of annihilation photons. The application scenario for the former imaging modality is the detection of post-resection residual tumors, while the application scenario for the latter is the localization of radio-marked metastatic lymph nodes (LN) targeted for surgical resection.

We present our work for integrating i) epiphanography into the neurosurgical management of low-grade gliomas (LGG) of the central nervous system and ii) freehand PET into the surgical management of head and neck squamous cell carcinoma (HNSCC).

1 INTRODUCTION

The bulky devices associated with state-of-the-art nuclear imaging technologies PET and SPECT have hindered their intra-operative applicability to a great extent. Due to this reason, endeavor in the last two decades is towards the development of hand-held detectors that can be utilized intra-operatively. Examples are beta probes [1,2], capable of detecting positrons directly, and high-energy probes [3,4], capable of detecting annihilation (511 keV) photons. Although a great innovation, these devices still fall short of meeting intra-operative demands, primarily due to the fact that they do not provide images; but rather count-rates. Our research work is focused on combining hand-held beta and high-energy probes with 3D tracking systems [5] (see fig. 1), and enhancing this combination with ad-hoc models of detection physics that allow for iterative reconstruction of superficial (epiphanography) and quasi-tomographic (freehand PET) radiotracer distribution [6], in order to provide real-time imaging in challenging surgical treatment scenarios.

2 MATERIALS AND METHODS

An ad-hoc model of detection physics allows for mathematically describing a scan performed with a navigated nuclear probe as a linear system:

$$Ax = m$$

where the vector **x** represents an unknown 3D radiotracer distribution of a pre-defined surface/volume of interest (SOI/VOI); the vector **m** is the set of obtained nuclear probe measurements; and finally the matrix **A** consists of coefficients assigned by the ad-hoc model as the contribution of each element $\mathbf{x}_j$ of the SOI/VOI to each probe measurement $\mathbf{m}_i$ [7,8].

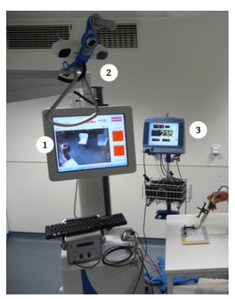

Figure 1: System setup: (1) augmented reality display, (2) tracking system, (3) nuclear probe control unit (probe hand-held on the right).

Figure 2: Neurosurgery phantom: a compact disc (CD) box with 18F-FET glued inside a mixing bowl; a 96 well microplate attached rigidly on the CD box, and filled with 18F-FET in predefined T/B activity ratios, simulating residual tumor among healthy brain tissue.

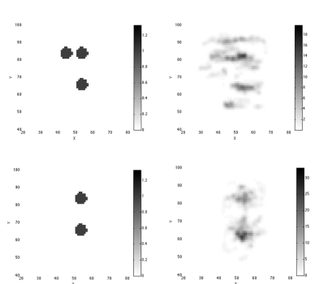

Figure 3: Epiphanography images (right) of the neurosurgery phantom in fig. 2. Left: ground truth images. Right: Images reconstructed from datasets with 2:1 (upper) and 8:1 (lower) T/B ratio.

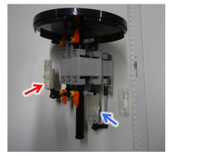

Figure 4: Upper: neck phantom construction. Lower: phantom being scanned by an operator.

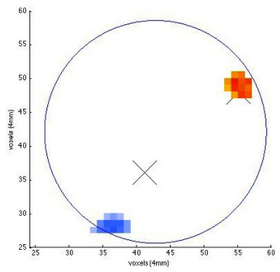

Figure 5: Upper: neck phantom construction. Lower: phantom being scanned by an operator.

Such a linear system can be inverted using e.g. maximum likelihood expectation maximization (MLEM) to obtain the radiotracer distribution within the SOI/VOI (i.e. reconstruction).

We have designed realistic open-neurosurgery mimicking brain phantoms for a proof-of-concept of epiphanography in terms of detecting post-resection residual tumor (T) masses in LGG neurosurgery. See one such phantom in fig. 2. We have configured and scanned this phantom with 18F-FET in realistic tumor-to-background (T/B) ratios.In terms of freehand PET, we have designed a realistic neck phantom simulating a metastatic LN and a tumor mass (see fig. 4), after retrospectively evaluating ^{18}F-FDG-PET/CT datasets of 7 patients with proven HNSCC. Two operators scanned this phantom using freehand PET. In addition we have used freehand PET to obtain the first intra-operative datasets of a patient with 4 metastatic LNs of thyroid carcinoma.

3 RESULTS

The epiphanography images from two of our scans with our brain phantoms can be seen in fig. 3. We could identify the simulated residual tumors in 67 % of scans with a realistic T/B ratio of 2:1. The success rate in higher T/B ratios was much higher (see fig. 6).

In our neck phantom study we were able to identify the simulated LN in all 17 scans. On the other hand, we were able to identify the simulated tumor in only 6 of these scans [6]. The intra-operative freehand PET images (see fig. 7) of the patient revealed the 4 metastatic LNs we were after. We do not have any quantitative evaluation for these datasets, as we had no registered pre-operative ^{18}F-FDG-PET/CT of the patient. However the surgery team gave us very positive qualitative feedback about the images during the surgery.

4 DISCUSSION

Validation of both imaging modalities must be performed on phantoms before moving to pre–clinical and later to clinical studies. We have laid down the foundations for this and performed the first studies with realistic phantoms [7,8]. The nature of positron radiation makes it very challenging to configure reproducible phantoms for epiphanography. Further research should go in this direction. In terms of freehand PET, the high unspecific uptake of 18F-FDG and the neck anatomy make viable images very difficult to obtain. Further research should focus on enhancing the reconstruction using prior information (e.g. registering pre-operative data) and developing a better scan protocol [6].

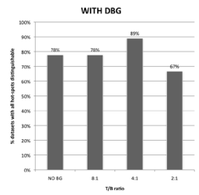

Figure 6: The detectability of the simulated tumor residuals in the neurosurgery phantom study, each column representing a different T/B ratio.

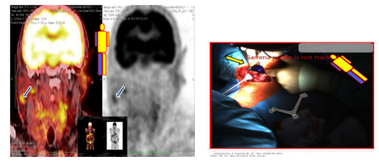

Figure 7: Left: pre-operative 18F-FDG-PET/CT image of the patient with the arrows indicating the metastatic LNs. Right: intra-operative freehand PET image showing the reconstructed LNs (the blue blob indicated by the yellow arrow).

5 ACKNOWLEDGEMENTS

TUM Graduate School of Information Science in Health (GSISH), TUM Graduate School (TUM GS), DFG SFB 824, DAAD PROCOPE.

6 REFERENCES

[1] F. Daghighian et al. “Intraoperative beta probe: a device for detecting tissue labeled with positron or electron emitting isotopes during surgery”. Medical physics, Vol. 21, No. 1, pp. 153–157, Jan. 1994.
[2] F. Bogalhas et al. “Development of a positron probe for localization and excision of brain tumours during surgery”. Physics in Medicine and Biology, Vol. 54, No. 14, p. 4439+, July 2009.
[3] S. A. Gulec et al. “PET-Probe: Evaluation of Technical Performance and Clinical Utility of a Handheld High- Energy Gamma Probe in Oncologic Surgery”. Annals of surgical oncology, July 2006.
[4] B. Meller et al. “High energy probe for detecting lymph node metastases with 18F-FDG in patients with head and neck cancer”. Nuklearmedizin, Vol. 45, No. 4, pp. 153–159, 2006.
[5] T. Wendler et al. “Navigated three dimensional beta probe for optimal cancer resection”. Medical image computing and computer-assisted intervention, Vol. 9, No. Pt 1, pp. 561–569, 2006.
[6] D. I. Shakir et al. “Towards intra-operative PET for head and neck cancer: lymph node localization using high-energy probes”. Medical image computing and computer-assisted intervention, Vol. 15, No. Pt 1, pp. 430–437, 2012.
[7] D. I. Shakir et al. “Acquisition Model for Iterative Reconstruction of Navigated Beta-Probe Surface Images”. In: Proceedings of the IEEE Nuclear Science Symposium and Medical Imaging Conference (NSS-MIC), Nov. 2010.
[8] D. I. Shakir et al. “Evaluation of Navigated Beta-Probe Surface Imaging on a Realistic 3D Phantom”. In: Proceedings of the IEEE Nuclear Science Symposium and Medical Imaging Conference (NSS-MIC), Oct. 2011.

ADVANCED DIFFUSION MR METHODS TO STUDY HUMAN BRAIN

T. Sprenger (GSISH Member)
Technische Universität München / GE Global Research

Prof. Dr. Axel Haase * (Advisor), Dr. Philipp Sämann ** (Advisor), Dr. Marion I. Menzel *** (Advisor)

* Technische Universität München, IMETUM, Boltzmannstr. 11, 85748 Garching.
** Max Planck Institute of Psychiatry, Kraepelinstraße 2-10 80804, München.
*** GE Global Research, Freisinger Landstr. 50, 85748 Garching.

A new approach to find a more disease specific parameter in diffusion MRI is the so called kurtosis tensor model (1). The kurtosis tensor extends the conventional MR-diffusion model which assumes a Gaussian distribution of the defusing molecules by a quadratic term.

This allows a better characterization of the underlying micro structure within a voxel which causes the deviation from the Gaussian distribution. However, to calculate the kurtosis tensor, the acquisition of the full diffusion spectrum (q-space) is necessary which needs much more time.

This drawback can be partially compensated by an undersampled Diffusion Spectrum Imaging (DSI) acquisition and a compressed sensing reconstruction (2).

1 INTRODUCTION

The study of diffusion properties of white matter by MRI methods gained significant importance to characterize MS [1]. Previous MS diffusion studies reported significant increase of mean diffusivity (MD) as well as a significant decrease of fractional anisotropy (FA) for diseased tissue compared to healthy [2,3], with considerable potential for disease monitoring and prediction [4]. While conventional diffusion metrics are based on a Gaussian diffusion model, Jensen et al. introduced diffusional kurtosis as non-Gaussian measure to quantify diffusion in angular and radial direction [5]. Non-Gaussian diffusion components in biological tissue are caused by barriers (e.g. membranes) and compartments (e.g. intracellular and extracellular spaces). Due to demyelination and axonal pathology induced by MS, the diffusion barriers are reduced which alters the overall diffusion amount and directionality. Beside decreased FA and increased MD, a reduced diffusional kurtosis as a measure for the non-Gaussian diffusion components should be observable. In this abstract, we present results from a single MS patient, employing diffusion spectrum imaging (DSI) [6] based estimation of FA, MD and kurtosis.

2 MATERIALS AND METHODS

Echo-planar DSI of 4 healthy volunteers and one MS patient was performed using a 3T GE MR750 MR scanner (GE Healthcare, Waukesha, WI, USA), equipped with a 32 channel head coil (TE=96.2 ms, TR=3.8 s, 96×96, 18 axial slices, FOV=24×24×4.5 cm^3, slice thickness 2.5 mm, ASSET factor 2, bmax=4,000 s/mm^2, scan duration 20 min) reading out an 11×11×11 q-space cube where 515 points were sampled within a sphere. In addition, corresponding axial FLAIR images were acquired.
An in-house tool has been used to fit the DTI and kurtosis tensors (22 unknowns) to the DSI data. Afterwards, conventional DTI metrics (MD, FA) as well as kurtosis metrics (mean kurtosis and radial kurtosis) were calculated. Segmentation of the data in 3 tissue compartments (grey matter, white matter [WM], cerebrospinal fluid) was performed by applying a FA threshold (0.25) and an individualized MD-threshold to restrict the analysis to WM.

3 RESULTS

Figure 1a shows an exemplary axial slice of a patient MS with typical hyperintense WM lesions in pericallosal areas.Figures 1b,c and d show the diffusion metrics FA, mean kurtosis and radial kurtosis. Figures 2, 3 and 4 show normalised histograms (total area set to 1, Number of bins is 30) of FA, MD and mean kurtosis of the WM compartment that included the normal appearing and pathological WM. Both, the patient's FA and mean kurtosis histogram was left-shifted as compared with 4 healthy subjects.

Furthermore there is a clear increase of MD for the MS Patient which agrees with previous publications [3,4]. In addition, MD and mean kurtosis of the patient exhibited a broadening of the distribution.

3 CONCLUSIONS

Qualitative FA, MD and mean kurtosis analysis as gained from demonstrated histogram differences of the WM compartment of an individual, moderately affected MS patient compared with 4 healthy subjects. With histogram analysis of MD and FA being an established technique, coming studies will focus on the question, whether kurtosis measures provide higher sensitivity to MS-related pathology or higher specificity of the underlying histopathology. For future work we will apply a new technique called Compressed Sensing DSI (CS-DSI), which was recently developed at our site. Thereby we can use an acceleration factor up to 4, without losing significant information which allows full volume coverage in a clinical applicable timeframe of 15 to 20 minutes [7].

5 ACKNOWLEDGEMENTS

Dr. Jonathan I. Sperl, Vladimir Golkov.

6 REFERENCES

[1] Geet. al Applications of diffusion tensor MR imaging in multiple sclerosis. Ann N Y Acad Sci. 2005;1064:202-19.

[2] Heide et al. Diffusion imaging of experimental allergic encephalomyelitis. Magn Reson Med 1993; 29: 478–484.

[3] Filippi et al. Diffusion tensor magnetic resonance imaging in multiple sclerosis. Neurology. 2001; 56(3):304-11.

[4] Sämann et al. Brain volume and diffusion markers as predictors of disability and short-term disease evolution in multiple sclerosis. AJNR Am J Neuroradiol. 2012; 33(7):1356-62.

[5] Jensen et al. MRI Quantification of Non-Gaussian Water Diffusion by Kurtosis Analysis. 2010; 23(7): 698–710.

[6] Wedeen et al. Diffusion spectrum magnetic resonance imaging (DSI) tractography ofcrossing fibers Neuroimage. 2008; 41(4):1267-77.

[7] Menzel et al. Accelerated diffusion spectrum imaging in the human brain using compressed sensing. MagnReson Med. 2011;66(5):1226-33.

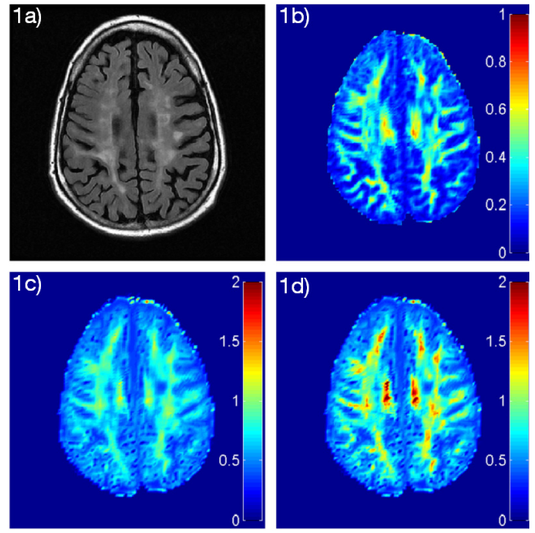

2)

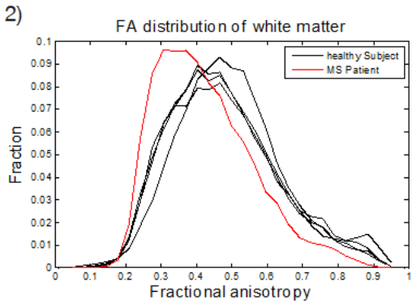

3)

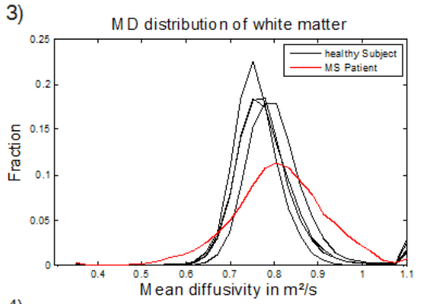

4)

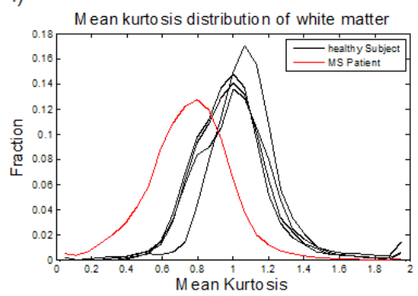

AUTOMATION OF HEMODYNAMIC REGULATION IN POST-OPERATIVE PATIENTS IN THE INTENSIVE CARE UNIT

N. Sprunk (GSISH Stipend Holder)
Technische Universität München / Deutsches Herzzentrum München

A. Knoll* (Advisor), R. Bauernschmitt** (Co-Advisor)

* Technische Universität München, Department of Informatics, Boltzmannstr. 3, 85748 Garching.
** Isar Heart Center, Department of Cardiology and Intensive Care Medicine, Sonnenstr. 24-26, 80331 München.

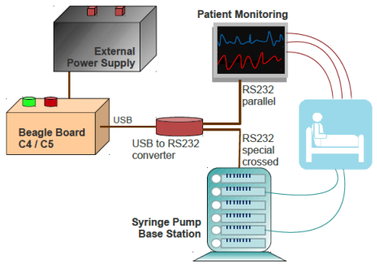

Figure 1: Data acquisition device.

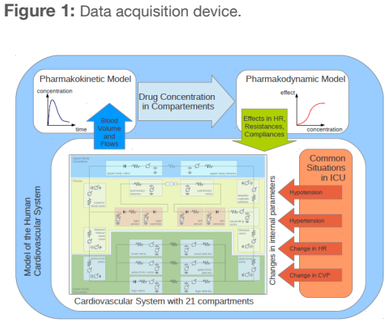

Figure 2: Cardiovascular Simulation.

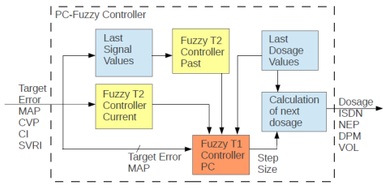

Figure 3: Adaptive controller with internally three fuzzy controllers.

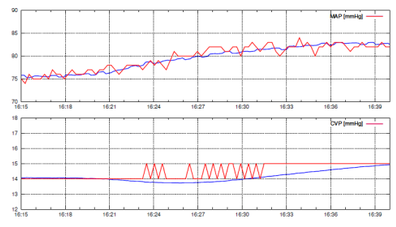

Figure 4: Comparison of patient data with simulated data in increment of vasoconstrictor dosage.

1 INTRODUCTION

Patients in the intensive care, especially after cardiac surgery, need to be monitored all the time. Hemodynamic instability or some degree of congestive heart failure is very common in these cases. To keep the patients in a stable state nonetheless, a physician is taking the current physiological signals into account to regulate certain variables. For patients with imminent danger of congestive heart failure the most important variables, to be monitored, are the mean arterial pressure (MAP) and the cardiac output (CO). Those variables are regulated by infusing adequate drugs intravenously. Programmable pumps are available for this purpose, which can run at different speeds and intervals to achieve the desired concentration of the drug. But as those pumps do not evaluate any feedback from the patient, a physician still needs to monitor the patient‘s signals to adapt the settings of the pumps every now and then. If the monitoring and regulating of these ‚standard‘ patients can be automated, the physicians will be able to spend more time diagnosing and attending the critically ill. It is desirable to develop an automated system, which incorporates the knowledge and expertise of the clinical personal, to monitor hemodynamic variables and keep them in a stable state. Such a system will decrease the workload on the clinical personal immensely and also improve the quality of the patient care. As such a controller cannot not be tested on real patients in the beginning, another part of this research project is the development of a cardiovascular simulation, which helps to evaluate the automatic controller.

2 MATERIALS AND METHODS

In a first step different data acquisition methods have been pursued to use in the development of both the automatic controller and the simulation environment. The cardiovascular simulation has been set up and verified using real patient data. Thus it was possible to test and verify the automated controller in the simulated environment.

2.A DATA ACQUISITION

On the one hand a hardware device has been setup to collect data from real patients and the treatment they receive (figure 1). This work has been published in [4]. The data collected was used to identify common critical situations, which happen in the intensive care unit (ICU) after cardiac surgery. Furthermore the reactions to certain drugs in the simulation were fine-tuned using the data from the ICU. In the other hand a questionnaire was used to gather knowledge about the treatment approaches within the medical personal. The fuzzy controller was setup with this information

2.B SIMULATION OF CARDIOVASCULAR SYSTEM

A cardiovascular model was used to simulate a patient in the cardiac intensive care unit. This model is based on a 21 compartment model with electrical equivalents for the different elements in the cardiovascular system. The model comprises of a cardiovascular model, a pharmacokinetic and a dynamic model (figure 2). It has been published in [1]. Test cases were set up using the patient data gathered in the ICU. The seven most common critical situations were implemented as test cases and used to evaluate the different automatic controllers.

2.C Fuzzy Controller

The first fuzzy controller implemented, was set up with the knowledge of one single physician. The fuzzy type-1 controller showed promising results in both the simulation and animal experiments and proved that automation of hemodynamic regulation using drugs is a feasible task as published in [2]. In a second step the data from the survey in the medical personal was incorporated into a fuzzy type-2 controller. This adds even more uncertainty to the system, but also makes use of collective knowledge of several experts in this area. The fuzzy sets were calculated using the enhanced interval approach (EIA). This controller was also tested and evaluated with the simulation. An offline learning method was developed based on Münsteraner Fuzzy Optimisation System (MFOS). The method showed promising results in an international completion and the work has been published in [3]. Unfortunately there is not enough suitable data available to train the hemodynamic controller with this offline learning method. Finally the controller has been extended with an adaptive algorithm [5]. The controller consists internally of two type-2 fuzzy controllers and another type-1 controller (figure 3). Additional inputs are the last dosages given and the changes in the input signals. With those the controller decides upon a stepwise change in dosage. This way the controller can adapt to a current situation in each patient.

3 RESULTS

The simulation has been tested and verified with real patient data for both critical situations and drug reactions. The different controller types have been tested with the simulated test cases and the results showed that the adaptive algorithm shows the best results overall.

Figure 4 shows the comparison of increment in dosage for vasoconstrictor norepinephrine with a dosage of 0.0038 ug/min/kg, with patient data in red, simulated data in blue. It shows that the patient data can be simulated sufficiently well.

The different controllers have been evaluated with the test cases in the simulation. Figure 5 shows the different performances in the test case ‘Decrase of Central Venous Pressure’. Only the adaptive algorithm is able to control the blood pressure without frequent oscillations.

4 CONCLUSIONS

The proposed controllers have shown that automated blood pressure regulation can be achieved by a fuzzy controller, both of type-1 and type-2. However the results of the simulated test cases showed how important an adaptive of self-tuning algorithm is. In spite of the already promising results in the simulation, it will still take years for a device to be commercially available. Before ’endangering’ patients with a device under research, extensive tests have to be performed, analysed and possible errors eliminated.

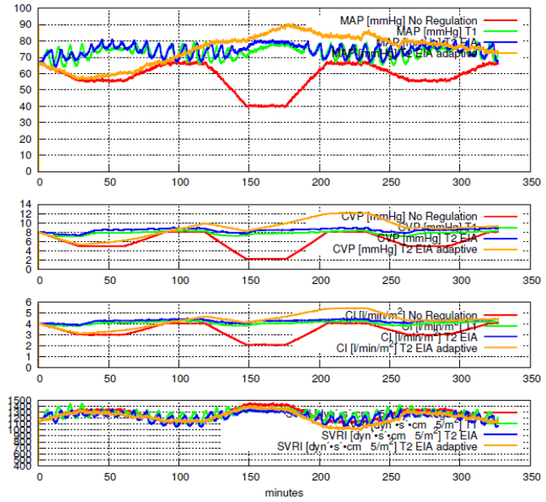

Figure 5: Comparison of performance of different controller types in test case ‘Decrase of Central Venous Pressure”.

5 ACKNOWLEDGEMENTS

Supported by the TUM Graduate School of Information Science in Health.

6 REFERENCES

[1] Cardiovascular model for development and test of automated hemodynamic regulation with medication; Sprunk, N.; Garcia, A.M.; Schreiber, U.; Bauernschmitt, R.; Knoll, A.; Computing in Cardiology, 2011, Publication Year: 2011 , Page(s): 153 - 156.

[2] Hemodynamic regulation using fuzzy logic Sprunk, N.; Mendoza G, A.; Knoll, A.; Schreiber, U.; Eichhorn, S.; Horer, J.; Bauernschmitt, R., Fuzzy Systems and Knowledge Discovery (FSKD), 2011 Eighth International Conference on, Volume: 1, Publication Year: 2011 , Page(s): 515 - 519.

[3] Learning a fuzzy system from training data using the Münsteraner Optimisation System, Sprunk, N.; Garcia, A.M.; Knoll, A., Fuzzy Systems (FUZZ-IEEE), 2012 IEEE International Conference on, Publication Year: 2012 , Page(s): 1 - 7.

[4] System design for simultaneous data acquisition from patient monitor and syringe pumps in intensive care unit, Sprunk, N.; Kaur, M.; Bauernschmitt, R.; Mendoza G, A.; Knoll, A., Biomedical Engineering and Sciences (IECBES), 2012 IEEE EMBS Conference on , vol., no., pp.878,882, 17-19 Dec. 2012.

[5] to be published : Evaluation of an adaptive algorithm for fuzzy type-2 control in blood pressure regulation, Sprunk, N.; Mendoza G, A.; Bauernschmitt, R; Knoll, A , Fuzzy Systems (FUZZ-IEEE), 2013.

QUANTITATIVE X-RAY PHASE-CONTRAST COMPUTED TOMOGRAPHY AT 82 KEV

M. Willner (GSISH Member)
Technische Universität München

F. Pfeiffer* (Advisor), J. Herzen** (Co-Advisor Physics), A. Fingerle*** (Co-Advisor Radiology)

* Technische Universität München, Department of Physics, James-Franck-Str. 1, 85748 Garching.
** Institute of Materials Research, Helmholtz-Zentrum Geesthacht, Max-Planck-Straße 1, 21502 Geesthacht.
*** Technische Universität München, Klinikum rechts der Isar, Department of Radiology, Ismaninger Str. 22, 81675 München.

Potential applications of grating-based X-ray phase-contrast imaging are investigated in various fields due to its compatibility with laboratory X-ray sources. So far the method was mainly restricted to X-ray energies below 40 keV, which is attributed to the high demands on the gratings utilized in the interferometer. However, progress in the manufacturing process increasingly allows to perform at high energies.

We report on the results of a phase contrast computed tomography of a phantom at 82 keV. The phantom consists of well-defined solid materials covering a wide range of densities as well as electron densitites surrounded by water and has been scanned with high-resolution at a synchrotron radiation source.

The reconstructed slices in attenuation and phase contrast have been analyzed in terms of quantitative material properties and signal-to-noise ratios.

The results show very good agreement to theoretical values and improved image quality in phase contrast.

1 INTRODUCTION

In the past few years grating-based X-ray phase-contrast imaging has increasingly arisen interest as the method had been successfully adapted to work with laboratory X-ray sources [1]. The high potential to improve the soft tissue contrast compared to standard attenuation-based tomography has been multiply demonstrated at synchrotrons as well as lab-based setups [2,3]. Due to certain requirements on the gratings, the examinations have been mainly limited to X-ray energies below 40 keV. However, advances in the grating manufacturing process allow to continuously move to higher energies and open up new possibilities to apply the technique in industrial testing and medical imaging [4].

2 MATERIALS AND METHODS

A grating interferometer enables to measure a small local refraction signal of X-rays that is correlated to the phase shift caused by an object. A phase grating creates an interference pattern with periodic intensity modulations at certain distances downstream. An object in the beam causes variations of these intensity modulations that can be resolved with a conventional X-ray detector by using an analyser grating (Figure 1).
The conventional attenuation signal is recorded at the same time and using a filtered backprojection based reconstruction algorithm, quantitative information on the linear attenuation coefficient μ and the refractive index decrement δ distribution within the object can be obtained [5,6].

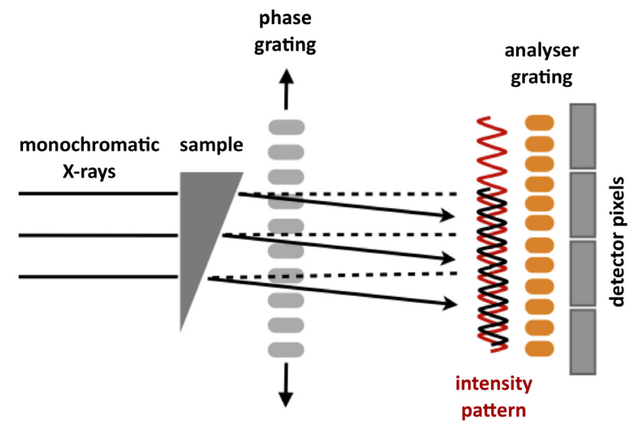

Figure 1: Principle of a grating-based X-ray interferometer. The phase grating creates a periodic intensity pattern that can be resolved by placing an analyser grating in front of the detector. A sample in the incident beam causes slight refraction, which results in a local shift of the analysed pattern. (Adapted from Willner et al., Optics Express, 2013 [7].)

The performance of the grating interferometer regarding the phase information and the resulting image quality strongly depends on the ability of the analyser grating to absorb the X-rays. The grating structures are made of gold, but grating periods of only a few micrometers still demand very high aspect ratios when moving to higher X-ray energies. Recently, the manufacturing of gratings with heights of more than 100 μm became feasible and guarantees a high absorption above the absorption edge of gold (80.72 keV).
To explore the image formation process and to demonstrate the quantitativeness of the method at high energies, a phantom consisting of well-defined solid materials (PMMA, PTFE, glass, PVC, titanium, aluminum) covering a wide range of densities as well as electron densities has been scanned with high-resolution (pixel size: 8 μm) at an X-ray energy of 82 keV at the Synchrotron beamline ID19 at the European Synchrotron Radiation Facility (ESRF, Grenoble, France) [7].

3 RESULTS

Exemplary reconstructed slices of the phantom in attenuation and phase contrast are shown in Figure 2.
The good quality of the phase-contrast images clearly demonstrates the feasibility of grating-based X-ray phase-contrast imaging at high X-ray energies by now. The signal-to-noise ratios of PMMA and PTFE are around seven to eight times higher than those in the attenuation-contrast images (Table 2).
The experimental δ- and μ-values of the materials in the phantom are in very good agreement to tabulated data which proves the quantitativeness of the method in this energy range.

Material	Signal-to-noise ratio Attenuation contrast	Signal-to-noise ratio Phase contrast
PMMA	3,1	25,2
PTFE	20,6	146,4
Glass	29,3	159,6
PVC	17,8	46,7
Titanium	192	442,7
Aluminum	42,9	214

Table 1: Signal-to-noise ratios obtained for the different materials with respect to water. An enhanced image quality in phase contrast compared to conventional attenuation contrast can be observed especially for low absorbing materials like PMMA or PTFE.

4 CONCLUSIONS

Grating-based X-ray phase-contrast computed tomography at 82 keV is practicable and offers the known advantages over the conventional attenuation-based X-ray imaging like better image quality and the quantitative determination of the refractive index decrements δ in addition to the attenuation coefficients μ. These results consolidate the high expectations on the method for various applications in the future. For more detailed information on this study please refer to Willner et al., Optics Express (2013) [7].

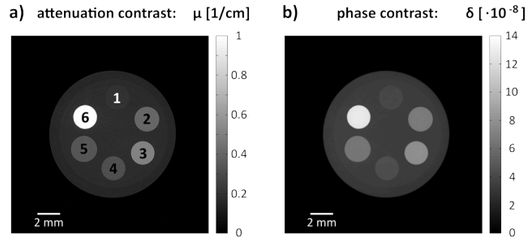

Figure 2: Imaging results. Attenuation contrast (a) and phase contrast (b) of a phantom consisting of PMMA (1), glass (2), aluminum (3), PVC (4), PTFE (5) and titanium (6). (Adapted from Willner et al., Optics Express, 2013 [7].)

5 ACKNOWLEDGEMENTS

I want to thank the coauthors of our correspondent publication [7] and all collaborators within the various other projects. We acknowledge financial support through the DFG Cluster of Excellence Munich-Centre for Advanced Photonics (MAP), the DFG Gottfried Wilhelm Leibniz program and the European Research Council (ERC, FP7, StG 240142). The work is carried out with the support of the Karlsruhe Nano Micro Facility (KNMF, www.kit.edu/knmf), a Helmholtz Research Infrastructure at Karlsruhe Institute of Technology (KIT).

6 REFERENCES

[1] Pfeiffer et al. (2006), Nature Physics 2(4), 258-261.

[2] Bech et al. (2009, Physics in Medicine and Biology 54(9), 2747-2753.

[3] Donath et al. (2010), Investigative Radiology 45(7), 445-452.

[4] Kenntner et al. (2010), Proceedings of SPIE 7804, 780408.

[5] Pfeiffer et al. (2007), Physical Review Letters 98, 108105.

[6] Herzen et al. (2009), Optics Express 17(12), 10010-10018.

[7] Willner et al. (2013), Optics Express 21(4), 4155-4166.

X-RAY PHASE-CONSTRAST AND DARK-FIELD IMAGING SIMULATION

J. Wolf (GSISH Member)
Technische Universität München

F. Pfeiffer* (Advisor), A. Knoll** (Co-Advisor)

* Technische Universität München, Department of Physics, James-Franck-Str. 1, 85748 Garching.
** Technische Universität München, Department of Informatics, Boltzmannstr. 3, 85748 Garching.

X-ray phase-contrast and dark-field imaging have great potential for various applications in the fields of medicine and materials science. Phase contrast provides enhanced contrast in soft tissue as compared to conventional absorption-based X-ray imaging and can improve e.g. mammography systems. Dark-field contrast yields information about the inner structure of an object on a scale smaller than a detector pixel.

In this project, we have developed a numerical wave-optical simulation framework, which is able to quantitatively reproduce the propagation of X-ray waves and the outcome of imaging experiments. The tool can be used for the planning and optimization of new setups as well as to further examine the image formation and gain new knowledge about the two new imaging modalities.

1 INTRODUCTION

X-ray imaging has been applied successfully in various fields such as medicine, materials science or security screening. For more than a hundred years the way medical X-ray images were created relied on the same principle: X-rays that pass through matter get attenuated leading to decreased intensity at the detector behind the object.

Recently, two new modalities have been developed that exploit different characteristics of X-rays: the first, phase-contrast imaging, is based on the phase shift that a wave front experiences on its way through a sample enhancing contrast in soft-tissue [1,2]. The second, X-ray dark-field imaging, evaluates the scattering of rays by small structures within an object, and thus delivers additional information on a scale that cannot be resolved by commonly used detectors [3].

All three signals – absorption, phase-contrast and dark-field – can be obtained in a single measurement by introducing a Talbot-Lau interferometer into a conventional X-ray setup. The interferometer consists of three gratings with periods of few micrometers (fig. 1): The source grating provides the necessary coherence of the X-ray beam, the phase grating imposes a defined phase shift on the wave front, and the analyzer grating enables the analysis of the interference pattern. The measured intensity at the detector is affected by the absorption, phase shift and scattering inside the sample, which allows the extraction of the three different signals.

For gratings, sources and detectors are expensive devices, numerical simulations play an important role in the development, investigation and optimization of the new modalities. As Monte-Carlo methods are not able to mimic the wave nature of X-rays, we developed a wave-optical simulation tool, which shows good results in emulation of the physical effects [4].

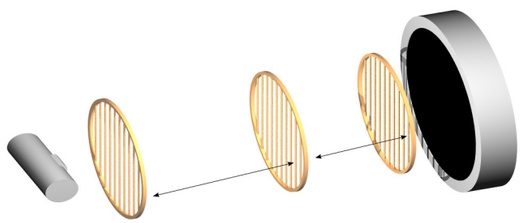

Figure 1: Talbot-Lau interferometry setup consisting of three gratings, an X-ray source (left) and a detector (right). The phase grating (middle) imposes a defined phase shift on the incoming wave front leading to an interference pattern at certain distances downstream (Talbot distances). Horizontal stepping of the analyzer grating (near the detector) converts the pattern into an intensity modulation as its period is too small to sample it with commonly used detectors. The source grating provides the necessary coherence of the X-ray beam.

2 MATERIALS AND METHODS

The framework is an objected-oriented software package written in Python. All parts of a Talbot-Lau interferometry setup including source, gratings, detector, and analytically described or pixelated samples can be added and parameterized. Specific materials can be chosen by giving their chemical formula and density. Their refractive index is computed to define their interaction with X-rays of a certain wavelength. Gratings and samples are considered flat in projection approximation.

The X-rays are represented as a wave front in a two-dimensional array of complex values, which propagates through the virtual setup as described by Fresnel optics. The propagation is implemented through direct evaluation of the Fresnel propagation integral or angular-spectrum propagation to account for cone-beam geometry according to [5].

3 RESULTS

The simulation results prove to be in good accordance with the expected outcome. Fig. 2 shows the simulated interference pattern with a period of 5 µm as it would form at the first fractional Talbot distance. It can be clearly seen how a carbon sphere in the beam path distorts the pattern compared to the case without sample (so-called flat field).

By stepping the analyzer grating, an intensity curve is extracted both from the flat-field and the object scan. Further processing of the two curves allows the calculation of absorption, differential phase-contrast and dark-field images (fig. 3).

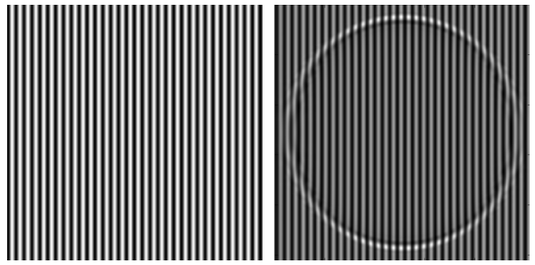

Figure 2: The interference pattern without any sample in the beam path at the first fractional Talbot distance. By comparing the flat field (left, period 5 µm) and a scan of an object (right, carbon sphere, diameter 150 µm) the absorption, phase-contrast and dark-field images can be calculated.

4 DISCUSSION

The described wave-optical simulation framework is a valuable tool to predict the outcome of experiments and support the planning of new setups for special purposes such as materials science or medical applications. Furthermore, the possibility to easily change parameters facilitates detailed examinations of the system behavior and the image formation.

The further development of the framework will include a noise model to make results more realistic and enhance comparability to real measurements; moreover, a mode to reduce the hardware footprint of the simulations will be added as the necessity to oversample the interference pattern leads to very large wave-front arrays already for small sample sizes.

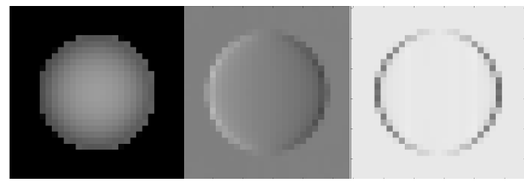

Figure 3: Absorption (left), differential phase-contrast (middle, DPC) and dark-field (right, DCI) images of an aluminum oxide sphere (diameter 1 mm) simulated with a detector pixel size of 50 µm. As the interferometer is only sensitive to phase shift and scatter in horizontal direction the signal at top and bottom of the sphere is weaker than on the sides in the two images on the right. The change in the gray values in the DPC image indicates that the wave front is shifted to different sides at the opposite sides of the sphere. Scattering occurs at the projected edges as can be seen in the DCI image.

5 ACKNOWLEDGEMENTS

The author would like to thank Dr. Andreas Malecki for initiating the software framework and his valuable help and advice, and the GSISH for the financial support of my project.

6 REFERENCES

[1] Weitkamp, T., Diaz, A., David, C., et al. (2005) X-ray phase imaging with a grating interferometer. Opt Express 13: 6296.

[2] Pfeiffer, F., Weitkamp, T., Bunk, O., et al. (2006) Phase retrieval and differential phase-contrast imaging with low-brilliance x-ray sources. Nat Phys 2: 258–261.

[3] Pfeiffer F, Bech M, Bunk O, et al. (2008) “Hard x-ray dark-field imaging using a grating interferometer”, Nat Mater 7:134-137.

[4] Malecki, A., Potdevin, G., Pfeiffer, F. (2012) Quantitative wave-optical numerical analysis of the dark- field signal in grating-based x-ray interferometry. Europhys Lett 99: 48001.

[5] Schmidt J. D., Numerical Simulation of Optical Wave Propagation With Examples in MATLAB, 1st edition (SPIE Press, Bellingham, Wash., USA) 2010.

DEVELOPMENT AND PROCEDURAL EVALUATION OF IMMERSIVE MEDICAL SIMULATION ENVIRONMENTS

(Extracted from [1])

P. Wucherer (GSISH Member)
Technische Universität München

Prof. Dr. N. Navab* (Advisor), Prof. Dr. med. E. Euler** (Co-Advisor)

* Technische Universität München, CAMP, Boltzmannstr. 3, 85748 Garching.
**Ludwig-Maximilians-Universität München, Klinikum Innenstadt, Nußbaumstr. 20, 80333 München.

We present a method in designing a medical simulation environment based on task and crisis analysis of the surgical workflow. The environment consists of real surgical tools and instruments that are augmented with realistic haptic feedback and VR capabilities. Inherently, we also addressed a broad spectrum of human sensory channels such as tactile, auditory and visual in real-time. Lastly, the proposed approach provides a simulation environment facilitating deliberate exposure to adverse events enabling mediation of error recovery strategies.

To validate the face validity of our simulator design we chose a spinal procedure, the vertebroplasty, in which four expert surgeons were immersed in our medical simulation environment. Based on a Likert-scale questionnaire, the face validity of our simulation environment was assessed by investigating surgeon behavior and workflow response.

The result of the conducted user study corroborates our unique medical simulation concept of combining VR and human multisensory responses into surgical workflow.

(Extracted from [1])

1 INTRODUCTION

Medical education is still based on the Halstedian approach of see one, do one, teach one [2] or learning by doing [3]. This leads to the inevitable exposure of patients to inexperienced practitioners which does not correspond to one of the principal beliefs of the Hippocratic Oath: Primum non nocere – first, do no harm. Thus, novel approaches in medical education have to be formulated. One of them can undoubtedly be medical simulation-based learning. Medical simulation learning with computer controlled equipment provides an environment for acquiring knowledge, skills and attitudes without putting patients' health at risks [4]. It offers a highly standardized environment for objective performance assessment [5]. The possibility to repeatedly practice procedures enables mediation of error recovery strategies, skill amelioration and clinical outcome optimization [6]. Further, medical experience can be gained conducting difficult procedures or even inducing complications affecting the workflow of the procedure.

2 MATERIALS AND METHODS

Our setup consists of a haptic device for instrument interaction (Figure 1-1), a pad into which the instruments can be inserted (Figure 1-2), a CT scanner mock-up including a positioning laser (Figure 1-3), a foot switch triggering CT image acquisition (Figure 1-4) and a monitor showing acquired CT images (Figure 1-7). A computerized mannequin simulator is placed onto the operating room (OR) table (Figure 1-5), the pad is fixed on the mannequin using a tension belt and the haptic device is attached to the table using a standard clamp. The computerized mannequin simulator is connected to the diagnostic devices (Figure 1-8) and finally draped. Real surgical instruments (Figure 1-9) can be attached to and detached from the haptic device using a clipping mechanism (Figure 1-6). CT imaging data is used to generate haptic feedback delivered to the instrument and visualize the patient's anatomy in combination with the simulated instrument on the CT monitor. The pad, essentially a box covered with synthetic skin, acts as housing for the instruments to avoid damage to the mannequin.

Figure 1: VR surgical procedural simulator for vertebroplasty.

Surgical workflow steps and crisis simulation.
The procedural steps were extracted from live surgery video recordings and literature [7] in conjunction with the feedback from expert surgeons.

Through a skin incision (workflow step I), the surgeon introduces a trocar into the virtual patient's body and advances it further through the pedicle into the vertebral body using CT guidance (workflow step II). Feedback generated by the haptic device gives the surgeon tactile information on the anatomy in contact with the instrument. Bone structures are discernible and clearly distinguishable from soft-tissue.

When the desired position is obtained with the trocar inside the vertebral body, the surgeon injects bone cement using a syringe (workflow step III). A cement model is used to discern the amount injected and it is consequently augmented on the CT slice images.
Crisis simulation (workflow step IV): an "unexpected event" is induced in terms of a cement extravasation into a perivertebral vein causing a lung embolism. The aim here is to provoke communication between anesthesiologist and surgeon to relay proper response for this adverse event.

3 RESULTS

Four surgeons participated in a user-study involving the completion of the surgical workflow steps described in the previous section. The participants had varied experience: two senior experts (>150 executed vertebroplasties) and two junior experts (<150 executed vertebroplasties). Each participant was immersed individually in our VR surgical simulator in combination with a mannequin connected to the monitoring device. An independent person with knowledge of physiological responses and monitoring acted as the anesthesiologist. The surgeons were asked to give feedback using the Likert scale - a type of psychometric response and the most widely used scale in survey research. The subjects specified their level of agreement to a statement in our questionnaire. The 5-pt Likert scale format was: (1) Strongly disagree, (2) Disagree, (3) Neither agree nor disagree, (4) Agree, (5) Strongly agree. We assessed the face validity of the medical simulation environment, which is a subjective validation and usually used during the initial phase of test construction [5]. However the intent of the evaluation goes even beyond, trying to get answers related to obstacles hindering immersion into the simulation scenario and to disseminate these to the research community.

Survey results
There were consistently high levels of agreement for all the questions. The group of surgeons thought that the modeling of workflow step I is realistic. The majority found that the realism is high during workflow step II. They considered the simulation of workflow step III and IV realistic as well. The questions pertaining to the face validity of the simulation setup were answered with an overall Likert score of 4.5- signifying that the simulation is realistic.

4 CONCLUSIONS

This study has demonstrated the face validity or realism of our medical training environment. Our conclusions validate the importance of incorporating surgical workflow analysis together with VR, human multisensory responses, and the inclusion of real surgical instruments when considering the design of a simulation environment for medical education. The proposed training environment for individuals can be certainly extended to training medical teams.

5 ACKNOWLEDGEMENTS

Philipp Stefan, Pascal Fallavollita, Prof. Dr. N. Navab, Prof. Dr. med. Euler, Stefanie Passauer-Baierl, NARVIS Lab group.

6 REFERENCES

[1] P. Wucherer, P. Stefan, S. Weidert, P. Fallavollita, N. Navab.: Development and procedural evaluation of immersive medical simulation environments IPCAI, Heidelberg, Germany, June 26, 2013.

[2] J. M. Rodriguez-Paz, M. Kennedy, E. Salas, A. W. Wu, J. B. Sexton, E. A. Hunt, and P. J. Pronovost.: Beyond see one, do one, teach one: toward a different training paradigm. Quality Safety Health Care, Bd. 18, Nr. 1, pp. 63–68 (2009).

[3] R. Kneebone.: Simulation, safety and surgery. Quality and Safety in Health Care, vol. 19, no. 3, p. i47-i52 (2010).

[4] F. Lateef.: Simulation-based learning: Just like the real thing. J Emerg Trauma Shock, Bd. 3, Nr. 4, pp. 348–352 (2010).

[5] G. Gallagher, G. C. O'Sullivan.: Fundamentals of Surgical Simulation Principles and Practices. London ; New York : Springer (2012).

[6] T. P. Grantcharov, V. B. Kristiansen, J. Bendix, L. Bardram, J. Rosenberg, and P. Funch-Jensen.: Randomized clinical trial of virtual reality simulation for laparoscopic skills training. British Journal of Surgery, vol. 91, no. 2, pp. 146–150 (2004).

[7] J. Barr und D. Resnick.: Vertebroplasty and Kyphoplasty. Thieme Medical Publishers (2005).

OVERLAP INDEPENDENT IMAGE REGISTRATION USING STRUCTURE PROPAGATION*

M. Yigitsoy (GSISH Member)
Technische Universität München

N. Navab (Advisor)

Technische Universität München, Department of Informatics, Chair for Computer Aided Medical Procedures, Boltzmannstr. 3, 85748 Garching.

Mosaicing is a commonly used technique in many medical imaging applications where subimages are stitched together in order to obtain a larger field of view. However, stitching, is often challenging when the information shared by subimages is absent or small. While it is not possible to perform an alignment without overlap using existing techniques, imaging artifacts such as distortions towards image boundaries present further complications during registration by decreasing the reliability of available information. Without taking these into consideration, a registration approach might violate the continuity and the smoothness of structures across subimages. In this paper, we propose a novel registration approach for the stitching of subimages. By using a perceptual grouping approach, we extend subimages beyond their boundaries by propagating available structures in order to obtain structural maps which are then used to establish correspondences between subimages. Our approach is unique in that it also enables contactless stitching. We demonstrate the effectiveness of the proposed method by performing several experiments on synthetic and medical images.

*This work has been published in [5].

1 INTRODUCTION

Image mosaicing is the process of stitching two or more images together in order to obtain an extended field of view (FOV). It has many application areas ranging from computational photography, to computer vision, to medical imaging. The main step of mosaicing is the stitching of subimages by estimating transformations that will bring them into a spatial alignment which is usually done by using an image registration algorithm. Classical image registration techniques usually assume minor differences in the viewpoints of images to be registered. However, this is not the case in microscopic imaging [1,2,3]. Therefore, there are specific challenges of creating wide field of view images/volumes in these cases. Special registration techniques are needed which can handle 1) very small or distorted overlap between subimages or subvolumes (as in the confocal microscopy case), 2) adjacent images having no overlap at all (maybe just touching each other as in 3D histology case).

2 MATERIALS AND METHODS

In this work, we aim at proposing novel registration techniques addressing the above-mentioned challenging issues. We focus on developing strategies for the registration of subimages having limited or no overlap while ensuring the global continuity and the smoothness of structures crossing their boundaries. It should be noted that, for a successful registration, it is important that image structures have inherent continuity, which is a property of the most natural images. We propose a novel technique which uses tensor voting for the inference of structures beyond image boundaries in order to establish a region shared by the subimages to be stitched as demonstrated in Figure 1.

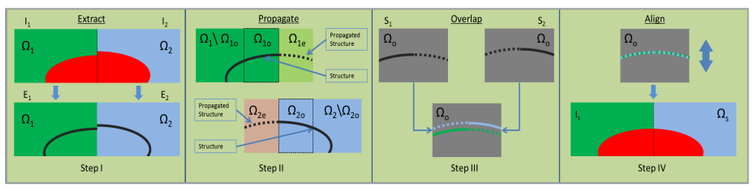

Figure 1: Overview of the proposed four-step stitching method using structure propagation. Here, we use a simple example where two pieces of a partial ellipse are to be stitched together. In Step I, the edge images, Ei are obtained by extracting structures, i.e. the edges, from the input images, Ii. This is followed by the propagation of structures into a predefined region Ωie for Ei in Step II. We create structure images denoted by Si in Ωo, which is constructed by combining the extended, Ωie, and the overlapped, Ωio, regions of the edge image Ei in Step III. Finally, these newly reated images are registered to each other followed by the application of resulting transformations to the original images, Ii in Step IV.

To this end, we create structure maps by propagating salient structures from image regions into non-image regions. Then, these structure maps are used for the subsequent stitching of subimages. Finally, resulting transformations are transferred to the original subimages for the optimal alignment with respect to the global smoothness and continuity of structures across subimage boundaries. So far, we are not aware of the use of a conceptual grouping technique for the mosaicing of medical images. Once structure maps are created, then, they can be registered to each other in order to find the necessary transformation. Transformations can be linear or non-linear depending on the needs of applications. Here, we will only consider linear cases for which we employ a registration method based on Markov Random Fields (MRF) as proposed in [4].

3 RESULTS

To evaluate the proposed technique, several experiments have been conducted on synthetic and real medical images. Synthetic images were used to demonstrate the capabilities of the proposed approach especially in cases, where not only there is no overlap but also there is a physical gap between the subimages to be stitched together as well as in cases where the images to be stitched are noisy.

The proposed method has also been applied to the stitching of real medical images. To do this, we have extracted 2D slices from a two-photon microscopic image data set acquired from a rat brain. Again, as in the synthetic experiment case, slices were cut into two and several transformations constructed in the same way were applied to one of the subimages. Furthermore, four microscopic image pairs with overlapping subimages to be stitched are used without applying any initial transformations. These experiments were important in that they showed the feasibility of the proposed method for being used for the stitching of real medical images.

For the evaluation of results, in addition to the visual assessment, we have compared the stitched images to the ground truth data using a correlation method. Furthermore, we evaluated the performance of the method in recovering the applied individual transformation parameters. Figure 1 shows stitched microscopic images using the proposed method.

4 DISCUSSION OR CONCLUSIONS

The proposed stitching method presented here is designed to overcome the limitations of classical techniques by enabling a “perceptually good“ alignment of images under difficult conditions by means of structure propagation. The method is addressing the state of art. However, there are still several limitations of the technique arising either from the employed method for the structure propagation or from the used image registration technique. Although promising results were observed during experiments, the obtained registration errors (see [5]), indicate that the proposed registration is still far from being compared to the classical registration techniques. However, it should be noted that these results are despite the absence of an overlap whereas no errors have been reported so far in such challenging cases.

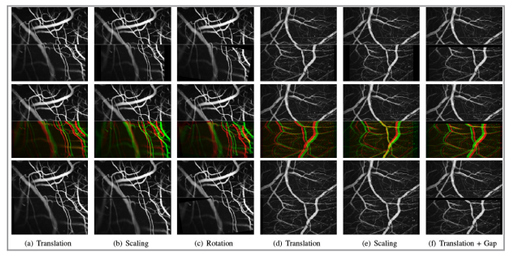

Figure 2: Stitching experiments on 2D microscopic images. There are two microscopic image pairs P1 [(a)-(c)] and P2 [(d)-(f)] used for the experiments. The first row shows the initial stitchings obtained by applying affine transformations. In the second row, the final stitchings after the alignment is overlayed onto the initial one where red and green colors are used for initial and final versions of the aligned subimage. The last row shows the final stitchings without overlay. In (a)-(b), similarly in (d)-(a), misalignments caused by the variations in the translation and scaling parameters, respectively, are restored. In (c), the correction of a misalignment due to rotation is demonstrated. Finally, a misalignment caused by a translational transform in the presence of a physical gap between the subimages is recovered in (f).

5 ACKNOWLEDGEMENTS

The authors thank Dr. Martin Groher and David Brucker for providing the microscopy data.

6 REFERENCES

[1] C.-L. Tsai et al, “Robust, globally consistent and fully automatic multi-image registration and montage synthesis for 3-d multi-channel images.” J Microsc, vol. 243, no. 2, pp. 154–171, 2011.
[2] M. Feuerstein et al, “Reconstruction of 3-d histology images by simultaneous deformable registration,” Medical Image Computing and Computer-Assisted Intervention–MICCAI 2011, pp. 582–589, 2011.
[3] U. Bagci et al, “Automatic best reference slice selection for smooth volume reconstruction of a mouse brain from histological images.” IEEE Trans Med Imaging, vol. 29, no. 9, pp. 1688–1696, Sep 2010.
[4] D. Zikic et al, “Linear intensity-based image registration by markov random fields and discrete optimization.” Med Image Anal, vol. 14, no. 4, pp. 550–562, Aug 2010.
[5] M. Yigitsoy et al. Structure Propagation for Image Registration IEEE Trans. Med. Imag., vol. 32, no. 9, pp. 1657-1670,2013.

DOCTORAL CANDIDATES´ PROJECTS

TELEMONITORING SYSTEM USING WIRELESS SENSOR NETWORKS FOR CHRONIC ILL PATIENTS

C. Chen (GSISH Member)
Technische Universität München

A. Horsch* (Advisor), A. Knoll** (Co-Advisor)

* Technische Universität München, Klinikum rechts der Isar, Ismaninger Str. 22, 81675 München.
** Technische Universität München, Department of Informatics, Boltzmannstr. 3, 85748 Garching.

Remote monitoring systems for elderly using modern ICT is quite popular nowadays attracting researchers' attention.

In this paper, we propose a wireless body sensor network (WBSN) platform prototype with three-layered framework which integrates wearable sensors, smartphone and PC for monitoring physical activities of elderly over distance.

We build the system based on Bluetooth and WLAN communication technologies and transmit captured data from sensors to application running on a smartphone and then further to a remote server for health assessment.

1 BACKGROUD

Remote monitoring systems for elderly using modern ICT is quite popular nowadays attracting researchers' attention. We propose a wireless body sensor network (WBSN) platform prototype with three-layered framework which integrates wearable sensors, smartphone and server for monitoring various physiological signs of elderly with chronic disease over distance. We build the system based on Bluetooth and WLAN communication technologies and transmit captured data from sensors to application running on a smartphone and then further to a remote server for health assessment

2 ARCHITECTURE

The presented system utilizes 3-layer infrastructure to construct wireless communication system in our project (Figure 1).

Body sensor layer

The system uses SHIMMER node [1] (Realtime Technologies Ltd., Dublin, Ireland) to capture physiological data from subjects. SHIMMER is a motion detection sensor with a 3-axial accelerometer that is commonly accepted for physical activity measurements, health monitoring, and gait analysis [2]. It stands out for its compatibility, openness and flexibility due to the use of the microprocessor MSP430F1611 and CC2420 radio, both of which make SHIMMER easy to program for different research purposes. Moreover, SHIIMMER is small enough so that its placement on the human body is quite flexible. One or more SHIMMER nodes may form a star network topology to collect data at the same time at a certain sampling frequency (normally 50 Hz). Besides, SHIMMER contains Bluetooth and 802.15.4 radio modules as potential means for realizing data streaming.

Personal network layer

An Android smartphone (HTC Hero) functions as base station for data analysis, storage and relay. Besides its extendibility of user-defined applications based on its Linux-kernel, Android is open source in line with SHIMMER approach compared to other mobile operating systems. The version running on the smartphone is Android 2.2. Given data from SHIMMER via Bluetooth connection, application on Android conducts low level information processing and displays either separated or combined axial accelorometry data graphically on the smartphone. Further, the mobile application forwards the data to a remote server through WLAN. Persistent data storage into a local SQLite database is also possible on the smartphone. The smartphone application is supposed to display feedback to subjects, for instance, by popping up a reminder for low battery level of a sensor.

Global network layer

A PC works as remote server on this layer. The functions are based on the HTTP service. As the top level of the communication framework, the server is normally in charge of storing processed data it got from the base station for health evaluation. If an emergency situation is detected, the server may utilize web applications and services through 3G or Wi-Fi connections to, e.g., call a nearby healthcare center for help. In our prototype, Apache Geronimo server, an open source framework implemented in Java EE, was used to support the backend PostgreSQL databases on the server. It is responsible for sending commands, mainly in SQL, to the Android smartphone for synchronization and parameter settings.

3 RESULTS

Currently the basis of the system is functional, but the project is still ongoing and all results are being released as open source during implementation, as a contribution to the free resources for SHIMMER, Android applications and Ubuntu Server.
Future work is needed for e.g. management GUI of monitoring, long-term validation of system performance. Promising wireless technologies will be investigated and taken into the project with the aim of improving the quality and flexibility of the system.

4 DISCUSSION

The advantage of using a smartphone as base station rather than a laptop or stationary PC is that it no longer limits the subjects' mobility. Regarding outdoor activities, robust roaming is required to ensure a continuous monitoring without disruption due to the switch of mobile networks.

Another crucial factor in the WBSN design is energy consumption. Bluetooth is preferred because of its common interface provided on most of the current mobile devices. However, Bluetooth is a quite power-hungry standard, consuming energy fast. Through our experience obtained from system tests, a fully-charged SHIMMER runs out of battery after 7-8 hours if sensing at 50Hz through Bluetooth streaming. Solutions come up with other technologies of low energy demand like ZigBee. Nevertheless, Bluetooth Special Interest Group (SIG) has issued a new version with low power consumption [3] recently, which is very likely to outperform other wireless transmission standards, considering the big market share of Bluetooth.

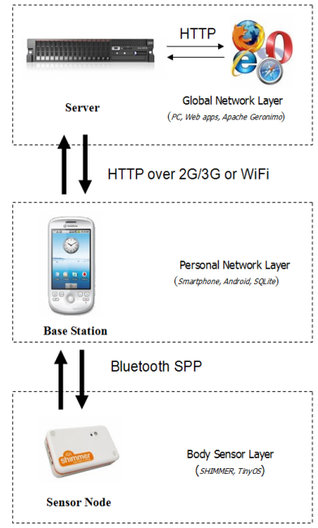

Figure 1: 3-layer architecture of WBSN

5 ACKNOWLEDGEMENTS

The authors thank the Graduate School of Information Science in Health (GSISH) at TUM for the project support and sponsorship, as well as all the students for their contributions to this project.

6 REFERENCES

[1] SHIMMER Research.
http://www.shimmer-research.com/

[2] KJ. O'Donovan, BR. Greene, and D. McGrath, et al., SHIMMER: A new tool for temporal gait analysis. Conf Proc IEEE Eng Med Biol Soc. 2009: 3826-9

[3] Bluetooth SIG, Bluetooth low energy V4.0.
Available from http://www.bluetooth.com/English/Technology/Building/Pages/Specification.aspx

CLASSIFICATION OF EXACERBATION EPISODES IN COPD PATIENTS

A. Dias (GSISH Member)
Technische Universität München / University of Tromsø

A. Horsch* (Co-Advisor), G. Hartvigsen** (Advisor)

* Technische Universität München, Klinikum rechts der Isar, Ismaninger Str. 22, 81675 München.
** Department of Computer Science and Department of Clinical Medicine, University of Tromsø, Norway.

Chronic obstructive pulmonary disease (COPD) is a progressive disease affecting the airways, which constitutes a major cause of chronic morbidity and a significant economic and social burden throughout the world. Despite the fact that in COPD patients exacerbations are common acute events causing significant and often fatal worsening of symptoms, an accurate prognostication continues to be difficult.

Build computational models capable of distinguish between normal life days from exacerbation days in COPD patients, based on physical activity measured by accelerometers.

Methods: We recruited 58 patients suffering from COPD and measured their physical activity with accelerometers for 10 days or more. During this period we recorded 6 exacerbation episodes in the patients, accounting for 37 days. None of the individual feature sets provided robust information for reasonable classification of PA recording days in the 52 COPD patients in exacerbation days and control days. A support vector machine classifier achieved an AUC of 90% ± 8.

1 INTRODUCTION

Chronic obstructive pulmonary disease (COPD) is a progressive disease affecting the airways. It constitutes a major cause of chronic morbidity and mortality and constitutes a significant economic and social burden throughout the world [1]. It is ranked the fifth leading cause of death worldwide, with forecasts indicating an increase of prevalence and mortality in the coming decades [2].

Despite exacerbations of COPD, which are defined as acute events with a significant worsening of lung function and symptoms, being both common and often fatal, accurate prognostication of patients hospitalized with an exacerbation is difficult. The median frequency of exacerbations is 2 per year [3].

The mechanisms of COPD exacerbation are complex, with respiratory viruses and bacteria playing a major role in the cause of these events [4]. Patients who rapidly receive treatment after onset of symptoms have better outcomes than those who wait several days to seek treatment.

2 MATERIALS AND METHODS

We recruited 58 patients with COPD (35 males, 23 females) undergoing LTOT who had been admitted for a 3-week in-patient Pulmonary Rehabilitation (PR) program. The diagnosed COPD in all cases was related to smoking at stage IV of the GOLD classification. We assessed the PA of wrist and ankle using the uniaxial piezoelectric GT1M accelerometer (Actigraph LLC, Pensacola FL, firmware version 4.2.0), attached by means of an elastic belt and labeled in order to avoid misplacement.

In this first approach to the overall prediction problem of exacerbations we focused on a simpler task of classifying exacerbation days from control days.

Figure 1: One of the study participants wearing the sensors, with arm and hip sensors visible.

Features	LOG	NN	SVM
Set 1	45.0 (13.6)	68.7 (3.0)	74.0 (20.3)
Set 2	65.7 (14.0)	67.0 (17.6)	82.0 (21.4)
Set 3	58.9 (12.1)	59.5 (7.1)	75.0 (16.5)
All	66.5 (15.3)	82.5 (16.2)	90.0 (8.7)

Table 1: Area under the curve values for all the combinations of features and classifiers. Values are average (standard deviation).

For each day of the study, n, we extracted features from the data set of day n-w, … n-1 and n. We extracted 3 sets of features from the accelerometer data for classification. The first set (Set 1) quantifies the characteristics of the PA data from each individual sensor separately. These are standard features used in machine learning, not dependent on the application domain, extracting basic information from the time series. The second set (Set 2) included frequency and time-scale features of each sensor. These are features commonly used in signal processing problems, and have been previously used in the classification of accelerometer data, namely in the scope of activity detection through accelerometers. They are based on the frequency domain analysis of the data, an important tool for signal processing. In the last set (Set 3) we explored the cross-information of data collected at different body parts, as it is known that the placement of the sensors influences the type of information recorded. For this we implemented features based on the cross information among sensor pairs, and thus body parts. We also explored a set of features composed of all the features together for which we selected the most important using a serial feature selection method (Set 4). After extracting all the features we implemented three different classification methods to apply to the datasets. They were logarithmic regression (LOG), support vector machines (SVM) and feed-forward neural network (NN) with 50 neurons in the hidden layer.

3 RESULTS

Overall SVM achieved the highest AUC while logarithmic regression showed the lowest performance. Overall the results indicate a fairly low classification capacity of the different algorithms. With the best classifier, SVM using all the features, if we find acceptable a specificity level of 85% then we can achieve 100% sensitivity. That is, to have all exacerbation episodes correctly classified we will have 17 out of 20 of the non-exacerbations classified as exacerbation episodes. Table 1 shows the results for the different features sets and algorithms.

4 CONCLUSION

Overall the classifiers achieved poor performance, preventing the application of the method to a medical setup, even if the alternative is having no classification method at all. Even if the SVM had a 90% AUC for the last set, the other classifiers never exceeded 82%.

Overall SVM showed to be the most robust classifier for this task. As for features, none of the basic feature sets, with distinct types of features, proved robust enough for this problem. Only the combination of all the extracted features, after a feature selection process, provided enough information for reasonable classification power.

The results indicate sensors can provide relevant information for the task of assessment of the patient state, but the extraction process was not optimized and produced results not good enough for clinical application. In our study we used a very simple approach for feature extraction. We didn't experiment with existing algorithms to identify activities from the accelerometer data, such as sitting and walking, and use that identification, together with their duration, to better estimate the activity pattern. This approach can potentially produce better features for the classification step. Because we decided to use off the shelf and validated sensors, with simple interface and usage requirements we were limited on the sampling rate of the accelerometers. We believe that higher sampling rates can strongly contribute to the improvement of the results. Current technological development will bring easy to use and validated accelerometers to the market in short term.

5 ACKNOWLEDGEMENTS

The Graduate School of Information Science in Health and the Technische Universität München Graduate School. André Dias is supported by the Portuguese Foundation for Science and Technology, scholarship SFRH/BD/39867/2007 and Research Council of Norway Grant 174934.

6 REFERENCES

[1] Global Initiative for Lung Diseases. Global strategy for the diagnosis, management, and prevention of chronic obstructive pulmonary disease [internet]. Jun 2009 [cited 12 July 2010]. Available from: www.goldcopd.com.

[2] Mathers CD, Loncar. D. Projections of global mortality and burden of disease from 2002 to 2030. PLoS Med. 2006;3:e442.

[3] Wilkinson T, Wedzicha J. Strategies for improving outcomes of COPD exacerbations. J Chron Obstruct Pulmon Dis. 2006;1:335--342.

RISK OF FALLS IN ELDERLY: THE ROLE OF GAIT, PHYSICAL ACTIVITY, AND ANEMIA

K. Thaler-Kall (GSISH Member)
Technische Universität München

C. Meisinger* (Advisor), A. Horsch** (Co-Advisor), A. Knoll*** (Co-Adivsor)
* Helmholtz Zentrum München, Institute for Epidemiology II, Ingolstädter Landstraße 1, 85764 Neuherberg.
** Technische Universität München, Klinikum rechts der Isar, Ismaninger Str. 22, 81675 München.
*** Technische Universität München, Department of Informatics, Boltzmannstr. 3, 85748 Garching.

Falls are known to be a major problem in elderly people which causes disability and even mortality. Anemia with a high prevalence in people aged 65 plus could be one cause for falls. Different gait patterns could also be predictors for falls. Gait parameters describing gait can be measured e.g. with an electronic walkway.

This project is investigating the association between anemia and falls on one hand and the association between different gait parameters measured with an electronic walkway and falls on the other hand.

After a literature review, data of over 1,000 people aged 65 plus will be analyzed, including blood samples, answers to fall questionnaires and gait parameters.

The first publication about the association between anemia and falls is currently under review. We are now working on the analysis of the gait parameters.

1 INTRODUCTION

Falls and fall-related fractures are a principal cause for disability, admission to hospital care, and mortality in older people. Thirty percent of seniors aged 65 plus experience a fall at least once per year, and 15% at least twice per year [1]. If this people are not able to get up again without help, they have to experience a “long lie”. Half of the people, who did lie longer after a fall, die within 6 months [2]. Furthermore falls are associated with high costs. Heinrich et al. estimated costs between 2.1 and 3.8 billion Euros per year in Germany [3]. Due to these serious health and economic consequences, the identification of treatable risk factors for falls of older people is important.

Anemia is a common problem in elderly people. The Third National Health and Nutrition Examination Survey (NHANES III) study found a prevalence of approximately 11% in persons aged 65 and older and a rate greater than 20% in those individuals aged 85 years or older [4]. Symptoms of anemia include low energy, fatigue, dizziness, and general weak-ness. Late life anemia is also associated with subsequent physical decline, as illustrated by increased disability, impaired performance, and muscle weakness. Through these con-sequences, anemia could result in an increased risk of subsequent falls, although research that confirms such a potential link is limited.

Regarding gait analysis several studies exist which have identified changes in spatial and temporal gait parameters as independent predictors of fall risk. Two publications observed e.g. that increased stride-to-stride variability in stride length, stride speed and double support time as well as increased stride width were predictors for falls [5, 6].

The first task of this doctoral thesis is to review the existing publications regarding anemia, overall physical activity and different changes in gait parameters as predictors for falls in elderly. Then data of over 1,000 people aged 65 plus will be analyzed to describe the association between anemia and falls risk as well as the correlation between different spa-tial and temporal gait parameters and fall risk in elderly.

2 MATERIALS AND METHODS

The data to be analyzed were collected in 2009 during the KORA (Cooperative Health Research in the Region of Augsburg)-Age study [7]. Participants were aged 65 years or older, taken from a population based random sample (n=5,991). In total, 4,127 people participated in a standardized telephone interview (response 67%). Out of this group a randomly drawn sample of 1,079 cohort members additionally underwent extensive physical examinations including amongst others the registration of drug intake, collection of blood samples, anthropometric exami-nation, grip force measurement, gait analysis, and an additional interview.

Blood samples and answers to fall questionnaires were available for 1,048 participants. After excluding further 76 participants due to missing data on any of the included variables or confounders, the final database for the anemia analysis consists in 972 participants, 478 women and 494 men.

The GAITRite® system (CIR systems, Haverton, PA, USA) is a validated electronic walkway [8], capturing spatial-temporal gait parameters by sensor pads encapsulated within the 488 x 61cm sized walkway mat. These sensor pads are activated as the participant walks across the walkway and the footprints are immediately transferred to the connected monitor. Participants were asked to walk with four walking speeds: normal, slow and fast velocity as well as dual task walking, i. e. one normal walk with the additional task of counting backwards in steps of 2 beginning with the number 50. The GAITRite® measurement was available for 945 participants [9].

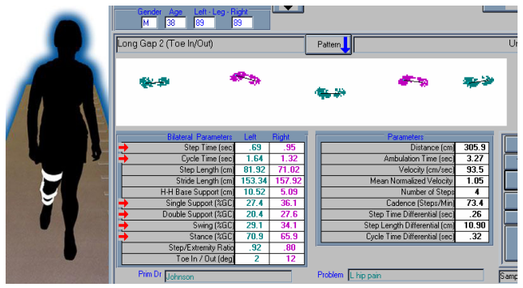

Figure 1: example for a GAITRite walk. Footsteps are marked as left (cyan) or right (magenta). Some gait parameters are visualized directlx in the tool.

After excluding further 32 participants due to missing walks, variables or confounders, the final database for the gait parameters analysis consists of 913 participants, 453 women and 463 men. For each participant 113 different gait parameters per walk are available, that makes 452 parameters per person. The study was approved by the ethics committee of the “Bayerische Landesärztekammer”; all subjects provided a written in-formed consent. Besides descriptive analyses, logistic regression models will be used to assess associations of anemia and gait parameters with falls. All analyses will be performed with SAS (Statistical Analysis System, version 9.2, SAS Institute Inc, Cary, NC).

3 ONGOING AND FUTURE WORK

The analysis of the anemia data set has already been finished with surprising results. The publication is currently under review at BMC Geriatrics. At the moment we work on the analy-sis of the correlation between gait parameters and falls which is more complicated than expected because of the high number of different gait parameters.

4 ACKNOWLEDGEMENTS

The authors would like to thank all study participants, the KORA Augsburg field staff and all members of the Institute of Epidemiology II from the Helmholtz Zentrum München who were involved in planning and/or conducting the study. This research was supported by the Graduate School of Information Science in Health (GSISH) and the TUM Graduate School.

6 REFERENCES

[1] Tromp, A.M., et al., Predictors for falls and fractures in the Longitudinal Aging Study Amsterdam. J Bone Miner Res, 1998. 13(12): p. 1932-9.

[2] Lord, S.R., C. Sherrington, and H.B. Menz, Falls in older people. Risk factors and strategies for prevention. , in Cambridge University Press. 2001: Cambridge.

[3] Heinrich, S., et al., Fall and fracture prevention based on the National Expert Standard. Implementation and costs in a real world setting in nursing homes. Z Gerontol Geriatr, 2012. 45(2): p. 128-37.

[4] Guralnik, J.M., et al., Prevalence of anemia in persons 65 years and older in the United States: evidence for a high rate of unexplained anemia. Blood, 2004. 104(8): p. 2263-8.

[5] Maki, B.E., Gait changes in older adults: predictors of falls or indicators of fear. J Am Geriatr Soc, 1997. 45(3): p. 313-20.

[6] Hausdorff, J.M., et al., Increased gait unsteadiness in community-dwelling elderly fallers. Arch Phys Med Rehabil, 1997. 78(3): p. 278-83.

[7] Peters, A., et al., Multimorbidity and successful aging: the population-based KORA-Age study. Z Gerontol Geriatr, 2011. 44 Suppl 2: p. 41-54.

[8] McDonough, A.L., et al., The validity and reliability of the GAITRite system‘s measurements: A preliminary evaluation. Arch Phys Med Rehabil, 2001. 82(3): p. 419-25.

[9] Autenrieth, C.S., et al., Decline in gait performance detected by an electronic walkway system in 907 older adults of the population-based KORA-Age study. Gerontology, 2013. 59(2): p. 165-73.

GSISH ALUMNI

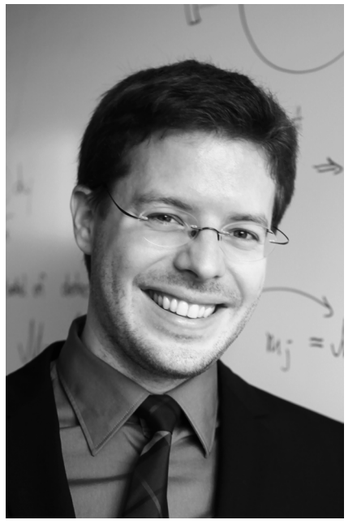

DR. RER. NAT. TOBIAS LASSER

"The GSISH provided a perfect framework to perform research. The structured dissertation program provided a solid background for me to lean on, while still allowing more than enough freedom in research. The requisite credit points to be earned during the curriculum are all based on activities natural to ‘doctoral life‘, and in my case didn’t require any additional efforts.

A particularly welcome addition to the regular scientific program were the transferable skills courses offered by GSISH, as this kind of courses was just not available otherwise. Examples include rhetoric and time-management seminars as well as career-planning and leadership workshops."

DR. RER. NAT. LUKAS GORZELNIAK

"The GSISH provided an ideal framework to conduct interdisciplinary research at the interface of informatics and medicine. During the course of my doctoral studies I became familiar collaborating with engineers, medical doctors, epidemiologists and statisticians at different research laboratories, clinics and institutes.

Beyond the work on my thesis, the GSISH provided many opportunities to broaden one‘s professional horizon by means of international workshops, summer schools and symposia. The curriculum of the GSISH also includes socalled soft skill training courses, designed to develop leadership, communications and organizational skills."

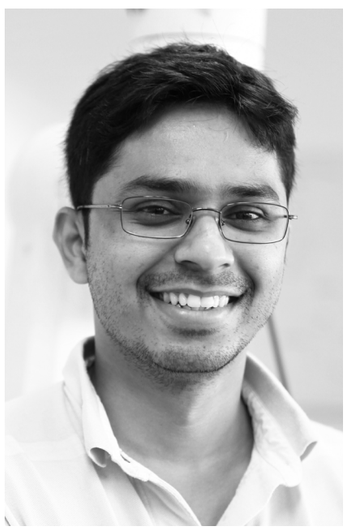

DR. RER. NAT. SURAJ NAIR

"I was enrolled in GSISH as an associate member and primarily involved in the project *Robot-assisted microscopic manipulation for vitreo-retinal ophthalmologic surgery*. My experience at GSISH over was very pleasant and professionally beneficial. I was involved in various colloquiums and seminars through which I interacted with many important people in the area of Biomedical Engineering and Imaging. These events were always very well organized and managed resulting in maximum throughput for the candidates. The doctoral program was very well structured and was realized in a systematic manner through regular milestones and professional guidance.
Overall, my experience with GSISH and its members was very helpful both personally and professionally, I would recommend GSISH to fellow students and professionals."

QUOTATIONS BY GSISH ALUMNI*

"GSISH managed to generate a milieu
where people coming from different worlds meet and exchange."
Dr. rer. nat. Thomas Wendler

"GSISH provided the great chance to practice this interdisciplinarity not only
in talks or meetings but also while having fun and party in a *Biergarten* or at an excursion."
Dr.-Ing. Kurt Höller

Dr. rer. nat.
Thomas Wendler

Dr. rer. nat.
Selen Atasoy

Dr. rer. nat.
Fabian Prasser

Dr.-Ing.
Kurt Höller

Dr. rer. nat.
Tobias Reichl

Dr. rer. nat.
Christian Schäfer

"GSISH puts a large emphasis on interdisciplinarity
and also on international collaboration."
Dr. rer. nat. Selen Atasoy

"In our interdisciplinary setting, it is not sensible to perform research
in the ivory tower, since whatever we design needs
to actually be applicable to the medical setting."
Dr. rer. nat. Tobias Reichl

"As interdisciplinarity was at the heart of my research project,
the interdisciplinary environment provided by GSISH
offered great opportunities."
Dr. rer. nat. Fabian Prasser

"I liked seeing my vision getting realized while having the freedom
to incorporate own ideas into my project."
Dr. rer. nat. Christian Schäfer

*This section only gives a rough overview of GSISH Alumni - by October 2013 already 11 GSISH members sucessfully finished their doctoral projects.

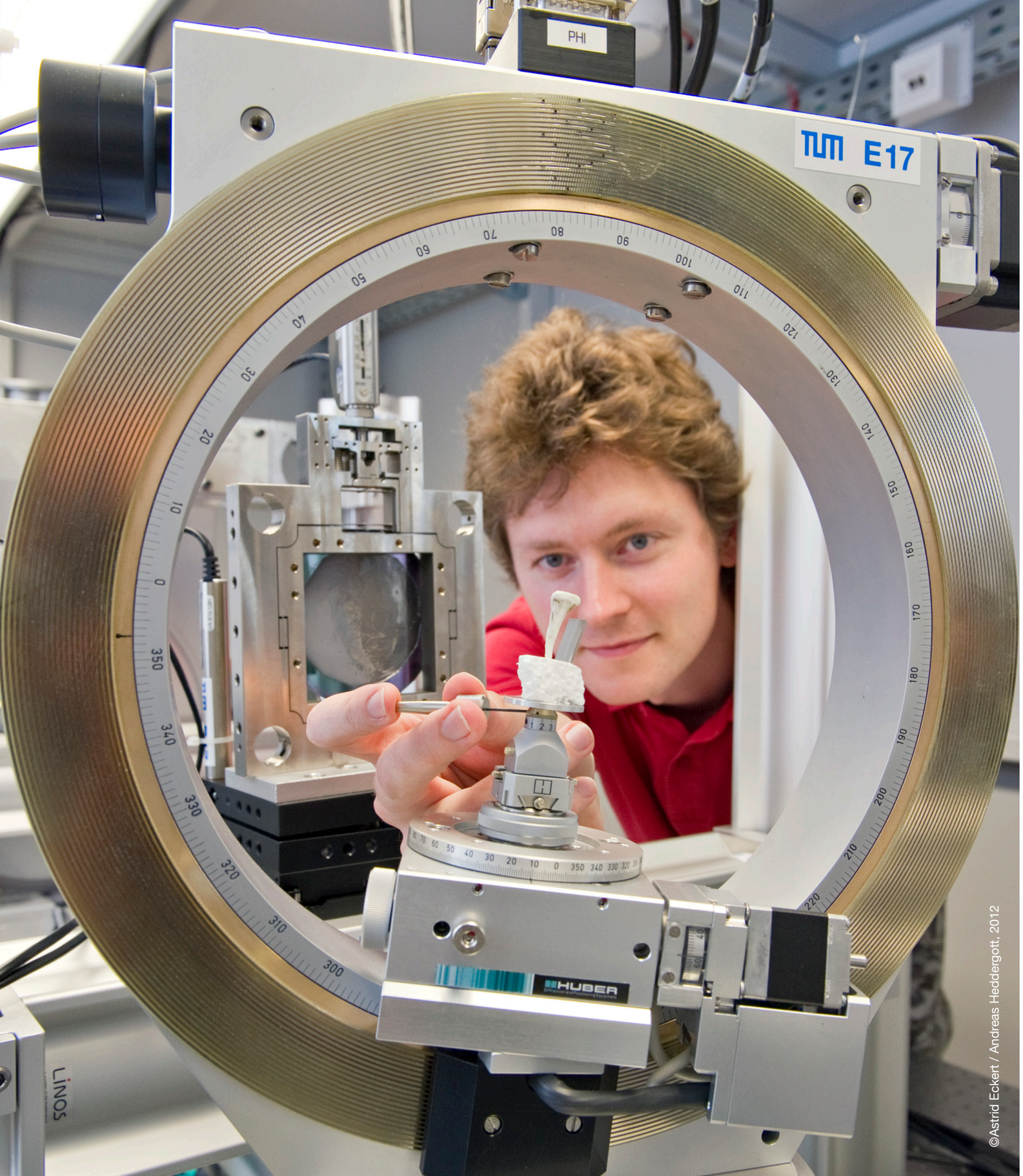

©Astrid Eckert / Andreas Heddergott, 2012

RESEARCH OUTCOMES

PUBLICATIONS
BY GSISH DOCTORAL CANDIDATES

October 2012 - October 2013
(62 in total)

R. Grimm, **S. Bauer**, J. Sukkau, J. Hornegger, G. Greiner
"Markerless Estimation of Patient Orientation, Posture and Pose Using Range and Pressure Imaging"
International journal of computer assisted radiology and surgery, 7(6), p. 921-9, 2012.

S. Bauer, B. Berkels, S. Ettl, O. Arold, J. Hornegger, M. Rumpf
"Marker-Less Reconstruction of Dense 4-D Surface Motion Fields Using Active Laser Triangulation for Respiratory Motion Management"
Proceedings of the Medical Image Computing and Computer-Assisted Intervention (MICCAI), Springer, p. 414-21, 2012.

J. Wasza, **S. Bauer**, J. Hornegger
"Real-Time Motion Compensated Patient Positioning and Non-Rigid Deformation Estimation Using 4-D Shape Priors"
Proceedings of the Medical Image Computing and Computer-Assisted Intervention (MICCAI), Springer, p. 576-83, 2012.

M. Koch, **S. Bauer**, J. Hornegger, N. Strobel
"Towards Deformable Shape Modeling of the Left Atrium Using Non-Rigid Coherent Point Drift Registration"
Bildverarbeitung Für Die Medizin 2013. Springer, p. 332-7, 2013.

B. Berkels, **S. Bauer**, S. Ettl, O. Arold, J. Hornegger, M. Rumpf
"Joint Surface Reconstruction and 4d Deformation Estimation from Sparse Data and Prior Knowledge for Marker-Less Respiratory Motion Tracking"
Medical Physics, 40(9), 2013.

S. Bauer, H. Hofmann, T. Blum, J. Wasza, M. Balda, H.-P. Meinzer, N. Navab, J. Hornegger, L. Maier-Hein
"A State-of-the-Art Survey on Time-of-Flight and Depth Imaging, Chap.
Real-Time Range Imaging in Health Care: A Survey"
To be published in: LNCS 8200, 2013.

T. Köhler, **S. Haase**, **S. Bauer**, J. Wasza, T. Kilgus, L. Maier-Hein, H. Feußner, J. Hornegger
"Tof Meets Rgb: Novel Multi-Sensor Super-Resolution for Hybrid 3-D Endoscopy"
Proceedings of the Medical Image Computing and Computer-Assisted Intervention (MICCAI), Springer, p. 139-46, 2013.

J. Wasza, **S. Bauer**, J. Hornegger
"Real-Time Respiratory Motion Analysis Using Manifold Ray Casting of Volumetrically Fused Multi-View Range Imaging"
Proceedings of the Medical Image Computing and Computer-Assisted Intervention (MICCAI), Springer, p. 116-23, 2013.

S. Haase, **S. Bauer**, J. Wasza, T. Kilgus, L. Maier-Hein, A. Schneider, M. Kranzfelder, H. Feußner, J. Hornegger
"3-D Operation Situs Reconstruction with Time-of-Flight Satellite Cameras Using Photogeometric Data Fusion"
Medical Image Computing and Computer-Assisted Intervention (MICCAI). Springer, p. 356-63, 2013.

S. Bauer, J. Wasza, F. Lugauer, D. Neumann, J. Hornegger
"Real-Time Rgb-D Mapping and 3-D Modeling on the Gpu Using the Random Ball Cover"
Consumer Depth Cameras for Computer Vision. Springer, p. 27-48, 2013.

A. Mendoza, **B. Baumgartner**, **N. Sprunk**, S. Schreiber, R. Eichhorn, R. Lange, A. Knoll
"Automation of a Portable Extracorporeal Circulatory Support System with Adaptive Fuzzy Controllers"
To be published in: Medical Engineering & Physics, 2013.

B. Baumgartner, K. Rodel, A. Knoll
"A Data Mining Approach to Reduce the False Alarm Rate of Patient Monitors"
Proceedings of the Annual International Conference of the IEEE Engineering in Medicine and Biology Society (EMBC), p. 5935-8, 2012.

B. Baumgartner, K. Rodel, U. Schreiber, A. Knoll
"A Web-Based Survey for Expert Review of Monitor Alarms"
Proceedings of the Computing in Cardiology (CinC), 2012, IEEE, p. 209-12, 2012.

A. Liedén, M.C. Winge, A. Saeaef, I. Kockum, E. Ekelund, E. Rodriguez, R. Foelster-Holst, A. Franke, T. Illig, M. Tengvall-Linder, **H. Baurecht**
"Genetic Variation in the Epidermal Transglutaminase Genes Is Not Associated with Atopic Dermatitis"
PloS one, 7(11), p. e49694, 2012.

M. Arnold, M.L. Hartsperger, **H. Baurecht**, E. Rodríguez, B. Wachinger, A. Franke, M. Kabesch, J. Winkelmann, A. Pfeufer, M. Romanos
"Network-Based Snp Meta-Analysis Identifies Joint and Disjoint Genetic Features across Common Human Diseases"
BMC Genomics, 13(1), p. 1-15, 2012.

A. Rebane, M. Zimmermann, A. Aab, **H. Baurecht**, A. Koreck, M. Karelson, K. Abram, T. Metsalu, M. Pihlap, N. Meyer
"Mechanisms of Ifn-I–Induced Apoptosis of Human Skin Keratinocytes in Patients with Atopic Dermatitis"
Journal of Allergy and Clinical Immunology, 129(5), p. 1297-306, 2012.

H. Stern, **H. Baurecht**, R. Luechinger, M. Schwaiger, J. Hess, S. Fratz
"Does the Amplatzer Septal Occluder Device Alter Ventricular Contraction Pattern?
A Ventricular Motion Analysis by Mr Tagging"
Journal of Magnetic Resonance Imaging, 35(4), p. 949-56, 2012.

C. Chen, A. Knoll, H.-E. Wichmann, A. Horsch
"A Review of Three-Layer Wireless Body Sensor Network Systems in Healthcare for Continuous Monitoring"
Journal of Modern Internet of Things, 2(3), p. 24-34, 2013.

A. Dias, **L. Gorzelniak**, R.A. Jörres, R. Fischer, G. Hartvigsen, A. Horsch
"Assessing Physical Activity in the Daily Life of Cystic Fibrosis Patients"
Pervasive and Mobile Computing, 8(6), p. 837-44, 2012.

M. Eder, M. Karl, A. Knoll, S. Riesner
"Compliant Worm-Like Robotic Mechanism with Decentrally Controlled Pneumatic Artificial Muscles"
Proceedings of the IEEE First International Conference on Innovative Engineering Systems, p. 263-8, 2012.

M. A. Nasseri, E. Dean, **S. Nair**, **M. Eder**, A. Knoll, M. Maier, C.P. Lohmann
„Clinical Motion Tracking and Motion Analysis During Ophthalmic Surgery Using Electromagnetic Tracking System“
Proceedings of the 5th International Conference on Biomedical Engineering and Informatics (BMEI), p. 1058-62, 2012.

S. Nair, **M. A. Nasseri**, **M. Eder**, C.P. Lohmann, A. Knoll
"Embedded Middleware and Hard Real-Time Based Architecture for Robot Assisted Ophthalmic Surgery"
Proceedings of the The Hamlyn Symposium on Medical Robotics, 2013.

M. Nasseri, **M. Eder**, **S. Nair**, E. Dean, M. Maier, D. Zapp, C. Lohmann, A. Knoll
"The Introduction of a New Robot for Assistance in Ophthalmic Surgery"
Proceedings of the 35th Annual International Conference of the IEEE Engineering in Medicine and Biology Society (EMBC), p. 5682-5, 2013.

M. Nasseri, **M. Eder**, D. Eberts, S. Nair, M. Maier, D. Zapp, C. Lohmann, A. Knoll
"Kinematics and Dynamics Analysis of a Hybrid Parallel-Serial Micromanipulator Designed for Biomedical Applications"
Proceedings of the IEEE/ASME International Conference on Advanced Intelligent Mechatronics (AIM), p. 293-9, 2013.

S. Fürst, J. Pulko, M. Hohberg, A. Mann, S. Ziegler
"Effects of Temperature and Bias Voltage on the Properties of a Pet Detector Module Based on the Individual Readout of 1× 1 Mm2 Lyso Crystals by Monolithic Arrays of Sipms"
Journal of Instrumentation, 7(08), p. P08002, 2012.

F. Gaertner, **S. Fürst**, M. Schwaiger
"Pet/Mr: A Paradigm Shift"
Cancer imaging: The Official Publication of the International Cancer Imaging Society, 13, 36-52, 2012.

F.C. Gaertner, A.J. Beer, M. Souvatzoglou, M. Eiber, **S. Fürst**, S.I. Ziegler, F. Brohl, M. Schwaiger, K. Scheidhauer
"Evaluation of Feasibility and Image Quality of 68ga-Dotatoc Positron Emission Tomography/Magnetic Resonance in Comparison with Positron Emission Tomography/Computed Tomography in Patients with Neuroendocrine Tumors"
Investigative Radiology, 48(5), p. 263-72, 2013.

M. Souvatzoglou, M. Eiber, A. Martinez-Moeller, **S. Fürst**, K. Holzapfel, T. Maurer, S. Ziegler, S. Nekolla, M. Schwaiger, A.J. Beer
"Pet/MR in Prostate Cancer: Technical Aspects and Potential Diagnostic Value"
European Journal of Nuclear Medicine and Molecular Imaging, p. 1-10, 2013.

J. Vogel, **T. Reichl**, **J. Gardiazabal**, N. Navab, **T. Lasser**
"Optimization of Acquisition Geometry for Intra-Operative Tomographic Imaging"
Medical Image Computing and Computer-Assisted Intervention (Miccai). Springer, p. 42-9, 2012.

J.I. Sperl, E.T. Tan, **T. Sprenger**, **V. Golkov**, K.F. King, C.J. Hardy, L. Marinelli, M.I. Menzel
"Phase Sensitive Reconstruction in Diffusion Spectrum Imaging Enabling Velocity Encoding and Unbiased Noise Distribution"
Proceedings of the International Society for Magnetic Resonance in Medicine (ISMRM), 2013.

V. Golkov, **T. Sprenger**, M.I. Menzel, E.T. Tan, K.F. King, C.J. Hardy, L. Marinelli, D. Cremers, J.I. Sperl
"Noise Reduction in Accelerated Diffusion Spectrum Imaging through Integration of Sense Reconstruction into Joint Reconstruction in Combination with Q-Space Compressed Sensing"
Proceedings of the International Society for Magnetic Resonance in Medicine (ISMRM), 2013.

T. Sprenger, B. Fernandez, J.I. Sperl, **V. Golkov**, M. Bach, E.T. Tan, K.F. King, C.J. Hardy, L. Marinelli, M. Czisch, P. Sämann, A. Haase, M.I. Menzel
„Snr-Dependent Quality Assessment of Compressed-Sensing-Accelerated Diffusion Spectrum Imaging Using a Fiber Crossing Phantom“
Proceedings of the International Society for Magnetic Resonance in Medicine (ISMRM), 2013.

V. Golkov, **T. Sprenger**, M.I. Menzel, D. Cremers, J.I. Sperl
"Line-Process-Based Joint Sense Reconstruction of Diffusion Images with Intensity Inhomogeneity Correction and Noise Non-Stationarity Correction"
Proceedings of the International Society for Magnetic Resonance in Medicine (ISMRM), 2013.

V. Golkov, **T. Sprenger**, A. Menini, M.I. Menzel, D. Cremers, J.I. Sperl
"Effects of Low-Rank Constraints, Line-Process Denoising, and Q-Space Compressed Sensing on Diffusion MR Image Reconstruction and Kurtosis Tensor Estimation"
Proceedings of the International Society for Magnetic Resonance in Medicine (ISMRM), 2013.

S. Haase, J. Hornegger, T. Kilgus, L. Maier-Hein, A. Schneider, M. Kranzfelder, H. Feußner
"Time-of-Flight Based Collision Avoidance for Robot Assisted Minimally Invasive Surgery"
Proceedings of the IEEE International Conference on Robotics and Automation, 2013.

S. Haase, C. Forman, T. Kilgus, R. Bammer, L. Maier-Hein, J. Hornegger
"Tof/Rgb Sensor Fusion for 3-D Endoscopy"
Current Medical Imaging Reviews, 9(2), p. 113-9, 2013.

S. Haase, J. Wasza, T. Kilgus, J. Hornegger
"Laparoscopic Instrument Localization Using a 3-D Time-of-Flight/Rgb Endoscope"
Proceedings of the IEEE Workshop on Applications of Computer Vision (WACV), p. 449-54, 2013.

T. Köhler, **S. Haase**, **S. Bauer**, J. Wasza, T. Kilgus, L. Maier-Hein, H. Feußner, J. Hornegger
"Tof Meets Rgb: Novel Multi-Sensor Super-Resolution for Hybrid 3-D Endoscopy"
Medical Image Computing and Computer-Assisted Intervention (Miccai). Springer, p. 139-46, 2013.

J. Wetzl, O. Taubmann, **S. Haase**, T. Köhler, M. Kraus, J. Hornegger
"Gpu-Accelerated Time-of-Flight Super-Resolution for Image-Guided Surgery"
Bildverarbeitung Für Die Medizin 2013. Springer, p. 21-6, 2013.

S. Haase, **S. Bauer**, J. Wasza, T. Kilgus, L. Maier-Hein, A. Schneider, M. Kranzfelder, H. Feußner, J. Hornegger
"3-D Operation Situs Reconstruction with Time-of-Flight Satellite Cameras Using Photogeometric Data Fusion"
Medical Image Computing and Computer-Assisted Intervention (Miccai). Springer, p. 356-63, 2013.

S. Haase, J. Hornegger, T. Kilgus, L. Maier-Hein, A. Schneider, M. Kranzfelder, H. Feußner
"Time-of-Flight Based Collision Avoidance for Robot Assisted Minimally Invasive Surgery"
Proceedings of the IEEE International Conference on Robotics and Automation (ICRA), 2013.

D.I. Shakir, A. Okur, A. Hartl, P. Matthies, S.I. Ziegler, M. Essler, T. Lasser, N. Navab
"Towards Intra-Operative Pet for Head and Neck Cancer: Lymph Node Localization Using High-Energy Probes"
Medical Image Computing and Computer-Assisted Intervention (Miccai). Springer, 430-7, 2012.

N.M. Hirsch, C. Preibisch
"T2* Mapping with Background Gradient Correction Using Different Excitation Pulse Shapes"
American Journal of Neuroradiology, 34(6), p. E65-E8, 2013.

C. Preibisch, **N.M. Hirsch**, V. Toth, H. Kooijman, C. Zimmer
"Influence of Cbv on Mr Based Measures of Hypoxia in Healthy Human Brain and Tumorous Tissue"
Proceedings of the European Society for Magnetic Resonance in Medicine and Biology (ESMRMB), 2012.

R. Li, S. Kramer
"Efficient Redundancy Reduced Subgroup Discovery Via Quadratic Programming"
Proceedings of the Discovery Science, Springer, p. 125-38, 2012.

S. Mandal, X.L. Deán-Ben, D. Razansky
"Automated Calibration of Temporal Changes in the Speed of Sound in Optoacoustic Tomography"
Proceedings of the European Conferences on Biomedical Optics, International Society for Optics and Photonics, p. 88000K-K-5, 2013.

M. Maier, **M.A. Nasseri**, D. Zapp, **M. Eder**, K. Kobuch, C.P. Lohmann, A. Knoll
"Robot-Assisted Vitreoretinal Surgery"
Proceedings of the Association for Research in Vision and Ophthalmology (ARVO), 2013.

J. Wu, **M.A. Nasseri**, **M. Eder**, M.A. Gavaldon, C.P. Lohmann, A. Knoll
"The 3d Eyeball Fta Model with Needle Rotation"
APCBEE Procedia, 3rd International Conference on Biomedical Engineering and Technology (ICBET), 2012.

D. Queirós, X.L. Déan-Ben, A. Buehler, D. Razansky, A. Rosenthal, V. Ntziachristos
"Modeling the Shape of Cylindrically Focused Transducers in Three-Dimensional Optoacoustic Tomography"
Journal of Biomedical Optics, 18(7), p. 076014-, 2013.

D. Queirós, X.L. Déan-Ben, A. Buehler, D. Razansky, A. Rosenthal, V. Ntziachristos
"Incorporating Geometric Detector Properties into Three-Dimensional Optoacoustic Tomography"
Proceedings of the European Conferences on Biomedical Optics, International Society for Optics and Photonics, p. 88000C-C-7, 2013.

A. Aichert, W. Wein, A. Ladikos, **T. Reichl**, N. Navab
"Image-Based Tracking of the Teeth for Orthodontic Augmented Reality"
Medical Image Computing and Computer-Assisted Intervention (Miccai). Springer, p. 601-8, 2012.

D.J. Scholz, **O. Khegai**, A. Otto, R.F. Schulte, M. Schwaiger, S. Ziegler, A. Haase, M.I. Menzel
"Quantitative Ph Analysis with Sodium 13c-Bicarbonate at Small Ph Variations"
Proceedings of the European Society for Magnetic Resonance in Medicine and Biology (ESMRMB), 2012.

D.I. Shakir, A. Okur, A. Hartl, P. Matthies, S.I. Ziegler, M. Essler, **T. Lasser**, N. Navab
"Towards Intra-Operative Pet for Head and Neck Cancer: Lymph Node Localization Using High-Energy Probes"
Medical Image Computing and Computer-Assisted Intervention (Miccai). Springer, p. 430-7, 2012.

N. Sprunk, M. Kaur, R. Bauernschmitt, G. Mendoza, A. Knoll
"System Design for Simultaneous Data Acquisition from Patient Monitor and Syringe Pumps in Intensive Care Unit"
Proceedings of the IEEE EMBS Conference on Biomedical Engineering and Sciences (IECBES), p. 878-82, 2012.

K. Thaler-Kall, F. Tusker, J. Hermsdörfer, **L. Gorzelniak**, A. Horsch
"Where to Wear Accelerometers to Measure Physical Activity in People?"
Studies in Health Technology and Informatics, 192, p. 1045-, 2012.

T. Hamp, R. Kassner, S. Seemayer, **E. Vicedo**, **C. Schaefer**, D. Achten, F. Auer, A. Boehm, T. Braun, M. Hecht
"Homology-Based Inference Sets the Bar High for Protein Function Prediction"
BMC Bioinformatics, 14(Suppl 3), p. S7, 2013.

P. Wucherer, P. Stefan, S. Weidert, P. Fallavollita, N. Navab
"Development and Procedural Evaluation of Immersive Medical Simulation Environments"
Information Processing in Computer-Assisted Interventions Lecture Notes in Computer Science, Volume 7915, 2013, p. 1-10, 2013.

M. Yigitsoy, S. Kirchhoff, M.F. Reiser, N. Navab
"Out-of-Plane Motion Compensation in Cine-Mri"
Abdominal Imaging Computational and Clinical Applications. Springer, p. 107-15, 2012.

P. Radivojac, W. Clark, T.R. Oron, A.M. Schnoes, T. Wittkop, A. Sokolov, K. Graim, C. Funk, K. Verspoor, A. Ben-Hur, G. Pandey, J.M. Yunes, A.S. Talwalkar, S. Repo, M.L. Souza, D. Piovesan, R. Casadio, Z. Wang, J. Cheng, H. Fang, J. Gough, P. Koskinen, P. Törönen, J. Nokso-Koivisto, L. Holm, D. Cozzetto, D.W. Buchan, K. Bryson, D.T. Jones, B. Limaye, H. Inamdar, A. Datta, S.K. Manjari, R. Joshi, M. Chitale, D. Kihara, A.M. Lisewski, S. Erdin, E. Venner, O. Lichtarge, R. Rentzsch, H. Yang, A.E. Romero, P. Bhat, A. Paccanaro, T. Hamp, R. Kaßner, S. Seemayer, **E. Vicedo**, **C. Schaefer**, D. Achten, F. Auer, A. Boehm, T. Braun, M. Hecht, M. Heron, P. Hönigschmid, T.A. Hopf, S. Kaufmann, M. Kiening, D. Krompass, C. Landerer, Y. Mahlich, M. Roos, J. Björne, T. Salakoski, A. Wong, H. Shatkay, F. Gatzmann, I. Sommer, M.N. Wass, M.J. Sternberg, N. Škunca,
F. Supek, M. Bošnjak, P. Panov, S. Džeroski, T. Šmuc, Y.A. Kourmpetis, A.D. van Dijk, C.J. ter Braak, Y. Zhou, Q. Gong, X. Dong, W. Tian, M. Falda, P. Fontana, E. Lavezzo, B. Di Camillo, S. Toppo, L. Lan, N. Djuric, Y. Guo, S. Vucetic, A. Bairoch, M. Linial, P.C. Babbitt, S.E. Brenner, C. Orengo, B. Rost, S.D. Mooney, I. Friedberg
"A Large-Scale Evaluation of Computational Protein Function Prediction"
Nature methods, 10(3), p. 221-7, 2013.

SUBMITTED PAPERS

O. Khegai, R. F. Schulte, M. A. Janich, M. I. Menzel, E. Weidl, A. M. Otto, S. J. Glaser, S. I. Ziegler, A. Haase, M. Schwaiger, F. Wiesinger
"*In vivo* Mapping of Metabolic Rate Constants with Hyperpolarized [1-13C]pyruvate"
Submitted to Magnetic Resonance in Medicine

P. A. Gómez Damián, J. I. Sperl, **O. Khegai**, S. Grott, E. Weidl, M. Janich, F. Wiesinger, S. J. Glaser, A. Haase, M. Schwaiger, R. F. Schulte , M. I. Menzel
"Multi-side kinetic modeling of 13C metabolic MR using [1-13C]pyruvate"
Submitted to NMR in Biomedicine

M. I. Menzel, E. V. Farrell, M. A. Janich, **O. Khegai**, F. Wiesinger, S. Nekolla, S. van Marwick, A. Otto, A. Haase, R. F. Schulte, M. Schwaiger
"Multimodal assessment of in vivo biochemistry: Hyperpolarized [1-13C]MRS and 18F-FDG-PET imaging in HCC tumor bearing rats"
Submitted to Journal of Nuclear Medicine

K. Thaler-Kall, A. Döring, A. Peters, B. Thorand, E. Grill, W. Koenig, A. Horsch, C. Meisinger
"Association between anemia and falls in community-dwelling older people: results from the prospective KORA-Age study"
Submitted to BMC Geriatrics

PARTICIPATION IN CONFERENCES

National Conferences I Oct. 2012 - Oct. 2013

Verbündetenkonferenz **Gesundheit im Alter**, Helmholtz Zentrum Munich, Germany, Oct. 15 – 16, 2012.

11th Annual Meeting of the German National Genome Research Network (NFGN), Heidelberg, Germany, Dec. 11 – 13, 2012.

Frühjahrstagung der Deutschen Physikalischen Gesellschaft (DPG), Jena, Germany, Feb. 25 – Mar. 01, 2013.

Bildverarbeitung für die Medizin (BVM 2013), Heidelberg, March 03 – 05, 2013.

Abschlussveranstaltung im Förderschwerpunkt **Gesundheit im Alter** des Bundesministeriums für Bildung und Forschung (BMBF), Hamburg, Germany, Oct. 17, 2013.

International Conferences I Oct. 2012 - Oct. 2013

15th International Conference on Medical Image Computing and Computer Assisted Intervention (MICCAI 2012), Nice, France, Oct. 01 – 05, 2012.

The 30th Annual Scientific Meeting of the European Society for Magnetic Resonance in Medicine and Biology (ESMRMB 2012), Lisbon, Portugal, Oct. 04 – 06, 2012.

5th International Conference on Biomedical Engineering and Informatics (BMEI 2012), Chongqing, China, Oct. 16 – 18, 2012.

The 23rd International Conference on Algorithmic Learning Theory (ALT 2012) and **15th International Conference on Discovery Science (DS 2012)**, Lyon, France, Oct. 29 – 31, 2012.

98th Scientific Assembly and Annual Meeting of the Radiological Society of North America (RSNA 2012), Chicago, USA, Nov. 25 – 30, 2012.

International Conference on Biomedical Engineering and Sciences (IECBES 2012), Langkawi, Malaysia, Dec. 16 – 19, 2012.

IEEE Workshop on the Application of Computer Vision (WACV 2013), Clearwater Beach, USA, Jan. 17 – 18, 2013.

1st International Symposium on BioMedical Applications of X-Ray Phase Contrast Imaging (IMXP), Garmisch-Partenkirchen, Germany, Jan. 24 – 25, 2013.

MedFys, Stockholm, Sweden, Feb. 04 – 05, 2013.

SPIE Photonics West 2013, San Francisco, USA, Feb. 02 – 07, 2013.

European Congress of Radiology (ECR 2013), Vienna, Austria, March 07 – 11, 2013.

International Conference on Nuclear Cardiology and Cardiac CT (ICNC 11), Berlin, Germany, May 05 – 08, 2013.

Annual Meeting of the Association for Research in Vision and Ophtalmology (ARVO 2013), Seattle, USA, May 05 – 09, 2013.

IEEE International Conference on Robotics and Automation (ICRA), Karlsruhe, Germany, May 06 – 10, 2013.

European Conference on Biomedical Optics (ECBO), Munich, Germany May 12 – 16, 2013.

International Conference on Biomedical Engineering and Technology (ICBET 2013), Copenhagen, Denmark, May 19 – 20, 2013.

Annual Meeting of the Society of Nuclear Medicine (SNMMI 2013), Vancouver, Canada, June 08 – 12, 2013.

14th World Congress on Medical and Health Informatics (Medinfo), Copenhagen, Denmark, June 20 – 23, 2013.

The Hamlyn Symposium on Medical Robotics 2013, London, GB, June 23 – 25, 2013.

European Foundation of Clinical Nanomedicine (CLINAM) and European Foundation of Clinical Nanomedicine (ETPN) Summit, Basel, Switzerland, June 23 – 26, 2013.

35th Annual International Conference of IEEE Engineering in Medicine and Biology Society (EMBC 2013), Osaka, Japan, July 03 – 07, 2013.

IEEE/ASME International Conference on Advanced Intelligent Mechatronics (AIM 2013), Wollongong, Australia, July 09 – 12, 2013.

The 6th Annual World Molecular Imaging Congress (WMIC 2013), Savannah, USA, Sept. 18 – 21, 2013.

16th International Conference on Medical Image Computing and Computer Assisted Intervention (MICCAI 2013), Nagoya, Japan, Sept. 22 – 26, 2013.

SHORT RESEARCH STAYS ABROAD

Sebastian Fürst:
Division of Imaging Sciences & Biomedical Engineering, School of Medicine, **Kings's College London**, UK, Feb. 25 – March 01, 2013.

Rui Li:
Imperial College London, UK, April 24 – June 28, 2013.

Johannes Scholz:
DTU Copenhagen, Denmark, September 1-14,2013.

Imprint

Publisher

TUM Graduate School of Information Science in Health (GSISH)
Technische Universität München
Boltzmannstr. 11
85748 Garching

http://gsish.tum.edu/

Editor
Katharina Lang
GSISH Project Manager

Dr. Petra Dorfner
GSISH Managing Director

Design and Layout
Katharina Lang
GSISH Project Manager

Print
RM - Robert Maier Druck und Kopie
FM Kopierbar GmbH, München

Photographs / Graphics
TU München / Photographs by Astrid Eckert, Andreas Heddergott, Uli Benz
TUM Klinikum rechts der Isar
www.istockphoto.com
www.freegreatpicture.com

All used graphics were provided by GSISH or the authors themselves.

Technische Universität München
Graduate School of Information Science in Health
Boltzmannstr. 11 · 85748 Garching

Tel +49.89.289.18142
Fax +49.89.289.10805
Mail gsish@tum.de
http://gsish.tum.edu